uni.lu

UNIVERSITÉ DU
LUXEMBOURG

DISSERTATION

Defence held on 05/05/2022 in Luxembourg

to obtain the degree of

DOCTEUR DE L'UNIVERSITÉ DU LUXEMBOURG

EN SCIENCES DE L'INGÉNIEUR

by

Jovan FODOR
Born on 4 July 1990 in Smederevo, (Republic of Serbia)

INVESTIGATION IN REUSABLE COMPOSITE FLOORING SYSTEMS IN STEEL AND CONCRETE BASED ON COMPOSITE BEHAVIOUR BY FRICTION

Dissertation defence committee

Dr Markus Schäfer, dissertation supervisor
Professor, Université du Luxembourg

Dr Christoph Odenbreit, Chairman
Professor, Université du Luxembourg

Dr Danièle Waldmann-Diedrich, Vice Chairman
Professor, Technical University of Darmstadt

Dr Christoph Czaderski
Senior researcher, Swiss Federal Laboratories for Materials Science and Technology (EMPA)

Dr Marko Pavlovic
Professor, Delft University of Technology

Acknowledgement

The presented doctoral work has been realized at the *Faculty of Science, Technology and Medicine* (at the start of the research project *Faculty of Science, Technology and Communication*) of the *University of Luxembourg* within the *ECON4SD* research project founded by the *European Regional Development Fund* (*FEDER)*. The work commenced on the 15th of January 2018 and is due to be completed on the 15th of April 2022.

At the first place, I want to express my sincere gratitude to my supervisor *Prof. Dr. Markus Schäfer* who provided me with the opportunity to engage myself in this academic endeavour and who supported me during the whole doctoral studies regarding the research work, academic and personal development. I'm looking forward to our further collaboration.

I would like to express my gratitude to the members of the *CET* committee, *Prof. Dr. Danièle Waldmann-Diedrich*, *Prof. Dr. Motavalli Masoud (EMPA)* and *Dr. Christoph Czaderski (EMPA)* who helped me to steer the direction of this research with their essential feedback.

I would like to offer special thanks to all the colleagues and supervisors, especially to *Ms. Arghavan Akbarieh* and *Ms. Marielle Ferreira Silva*, who were also engaged in the *ECON4SD* research project and who helped me to expand my knowledge not strictly related to the structural analysis and structural design.

I am particularly grateful to *Prof. Dr. Marko Pavlovic*, who was my former supervisor at the Faculty of civil engineering of the University of Belgrade and who was also lecturer during my attendance of the *SUSCOS-M Erasmus Mundus* master programme. Our academic interaction inspired me to continue with the academic formation.
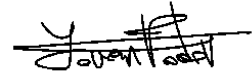
I am grateful to our external partners who committed their knowledge and material contributions regarding the test campaign. Here I want to express my sincere thanks to *Dr. Ferdinand Reif* of *Spannverbund S.A.*, to *Dr. Frank Häusler* of *Halfen GmbH* and *Mr. Rene Oly* of *Astron Buildings S.A.*

I would like to offer my special appreciations to the members of research support department of the Department of Engineering of University of Luxembourg, to *Mr. Gilbert Klein*,

Kirchberg, 07/3/2022   Jovan FODOR

Investigation in reusable composite flooring systems in steel and concrete based on composite behaviour by friction

Abstract

The steel-concrete composite systems proved to be very efficient structural solution in terms of material consumption and mechanical response regarding the construction of the structural floor systems whether in the case of industrial and residential buildings or especially in the case of car parks. However, their contemporary application that relies on the utilization of the welded headed studs as a mean to provide the shear connection between the steel section and the concrete chord renders the system unable to be disassembled (in the best case its steel and concrete parts are recycled). Considering the ongoing push from the linear to circular economical models and the application of 3R principle (Reduce, Reuse & Recycle) such systems are unable to furtherly improve their environmental and economic efficiency through reuse schemes.

The profound task in this research is development and the verification of the new demountable shear connector solutions that could allow modularity and demountability (hence reusability) of the steel-concrete composite floor systems while retaining their inherent structural advantages. Based on the previous investigations of the demountable shear connector systems (at the first-place bolted solutions) and investigations of mechanical components that were not strictly related to the shear connectors, four demountable shear connector devices were developed. Having in mind the drawbacks of the earlier solutions, adequate detailing and structural measures were applied and the ease of assembly and disassembly was proved on the constructed prototypes. Afterwards, the mechanical properties of devised demountable connector systems were investigated thoroughly through experimental campaign (push tests) and numerical investigation.

Based on the experimental and numerical results of the shear connector behaviour it is concluded that the proposed shear connector device Type B possess adequate strength and stiffness and might be considered ductile in accordance with the EN 1994-1-1 allowing for the application of existent design strategies in accordance with the same design code. The force-slip behaviour of the proposed shear connector is explained and adequate analytic model is proposed. Based on the force-slip behaviour model the applicability of the shear connector is verified on a range of composite beams that represent the demountable floor.

Keywords: Sustainability, Steel-concrete composite floors, Demountable shear connection, Friction based shear connection, Trilinear force-slip model, Composite beam behaviour

I. Contents

II.   Figures

III. Tables

IV. Abbreviations

3R - Reduce, Reuse & Recycle

CDP - Concrete damaged plasticity

CE - Conformité Européene

ECON4SD - Eco-Construction For Sustainable Development

GPC - Geopolymer cement

LCA - Life cycle assessment

LCCA - Life cycle coste assesment

LVDT - Linear variable differential transformer

OPC - Ordinary Portland cement

SLS - Serviceability limit state

UDL - Uniformly distributed load

ULS - Ultimat limit state

1. Introduction - Research project ECON4SD

The investigation in the reusable composite flooring systems in steel and concrete based on composite behaviour by friction is proceeded under the cover of ECON4SD research project led by *Institute for Civil Engineering and Environment* (INCEEN) [1].

This investigation is labelled as Work Package 2 of the ECON4SD research project.
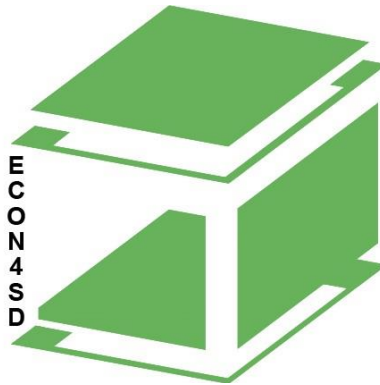
Figure 1.1 - ECON4SD logo [2]

ECON4SD project stands for *Eco-Construction for Sustainable Development*. The overall objective of the project is to provide design models, schemes and structural components for resource and energy efficient buildings.

The project is supported by *The European Regional Development Fund* (FEDER) [3] as it is in line with FEDER's *Priority Axis 1* which supports strengthening of the research, technological development and innovation.

In accordance with FEDER *Priority Axis 1*, project provides:

- 6 new *R&D* jobs

- Development and improvement of the R&D capacities by mutual funding by FEDER and the University of Luxembourg

- Improvement of energy efficiency in building sector

- New and smarter building materials

The project aims to increase the sustainability and resource efficiency in the building sector considering whole life cycle of the buildings and building components and by applying holistic approach to the problem by engaging several research fields represented by six Work groups:

- Work Package 1 – Architecture

- Work Package 2 – Slab structure in steel-concrete

- Work Package 3 – Slab structure in timber-concrete

- Work Package 4 – Concrete ageing

- Work Package 5 – Energy consumption

- Work Package 6 – Monitoring systems

- Postdoc position – Material Data-Bank
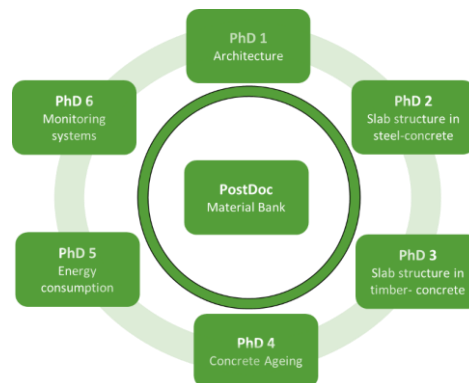
Figure 1.2 - ECON4SD Work Groups [2]

By providing new easily demountable connection systems regarding composite flooring structural systems made of materials steel, concrete and timber (Work groups 2 and 3) the focus shall lie on the reuse of their components. Multiple reuse of the components shall drastically reduce environmental impact of the further construction endeavours.

The reuse is the more potent way of reducing the environmental impact of construction industry than only recycling the material as the end of life scenario in 3R principle (Reduce, Reuse and Recycle). The potency depends on the number of reuse cycles of the particular component hence the importance of the durability of the components becomes important.

The promotion of the reuse of the structural components is expected also to rise the interest of the financial sector, as it will give additional economical value to the components that are at the best recycled or discarded in the common practice regarding their end of life scenario.
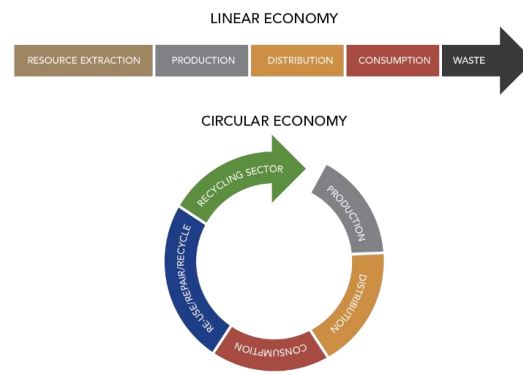
Figure 1.3 - Circular vs. linear economy [4]

Additional value added by the reuse possibility leads to the requirement of tracking of the well-being of the components intended for the reuse and their labelling as suitable for reuse option.

In order to reuse the components their material and mechanical properties have to be guaranteed. To be able to do so, numerical approach has to be devised (Work group 4) in order to estimate the material properties of the elements regarding their life cycle (aging), especially those made of concrete (load history, environmental exposure, etc.).

To be able to differentiate the elements, all have to be labelled and tracked during their life cycle (possibly by the application of BIM methods). The labelling would consider procedures similar to the CE labelling of the products. In this case, it requires application of the BIM methodologies and development of the digital library (Material Data-Bank) where the information regarding every single component shall be stored and updated (Work group 6 and Postdoc position).

As the proposed solutions are reusable, they have to be considered in the context of modular and flexible structural and architectural layouts. In order to benefit on this type of structural solutions new flexible and modular architectural schemes have to be devised within the research scope of the Work group 1.

In order to provide overall sustainability of the buildings throughout their whole life cycle, use phase is also considered. The energy efficiency of the buildings will be improved by optimization of the developed components and by means of modular design of technical installations (Work group 5).

During the research, the research package teams have to correlate and harmonize the undertaken work as the results of one group are often input for the others and vice versa (Figure 1.4).
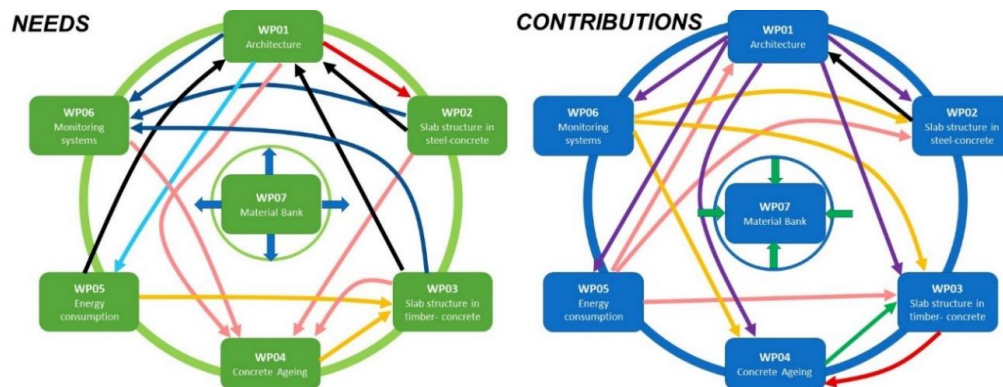
Figure 1.4 - Needs and contributions of the ECON4SD Work Package teams [2]

The project officially started on the 1st of October 2017 and shall last until the 30th September 2021.

The outcomes of the project shall be communicated to the:

- Industry – Via partnership with major stakeholders and dissemination at construction sector events

- Future civil engineers – Integration of the outcomes and principles in the teaching material

- Scientific community – All research results and theses shall be published through the UL's OrbiLu online platform [5]

- Wider public – Via press and media activities and web publications

2. Motivation and methodology

2.1 Motivation

Pursuing the sustainability in the construction industry and embracing the principles of the circular economy, new structural solutions which are at the same time modular, flexible, reusable and recyclable have to be devised. In order to achieve these requirements regarding steel-concrete composite flooring systems, it is crucial that these solutions are demountable and without damage infliction to its components during their life cycle.

Main aim of this research is to devise demountable longitudinal shear connection between the concrete slab and the steel beam, which shall be based on frictional behaviour, exploiting its superior ductility. This solution has to guarantee that elements will not be damaged during the assembly, reassembly and exploitation phases. Demountability shall allow for modularity and reusability of the proposed system. The applied solution should rely mostly on market available products what reduces construction time and cost.

Composite flooring systems based on concrete and steel materials are a highly efficient structural solution in building applications regarding structural, execution and economical aspects [6].

Compared to the steel-only solutions with concrete slab, clear mechanical advantages are observable in terms of:

- Stiffness

- Strength

- Fire resistance
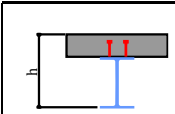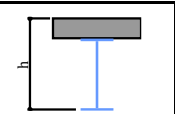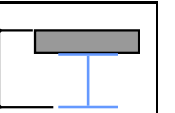
	Composite beam	Steel beam without any shear connection	
Steel cross section	**IPE 400**	IPE550	HE360B
Construction height [mm]	**560**	710	520
Load capacity	**100%**	100%	100%
Steel weight	**100%**	159%	214%
Construction height	**100%**	127%	93%
Stiffness	**100%**	72%	46%

Table 2.1 - Three beams with similar load capacity in bending [7]

Due to increase of mechanical properties compared to non-composite state it is possible to drastically reduce consumption of the virgin materials (Table 2.1).

Decrease of material consumption (smaller sections, slab thicknesses etc.) allows for:

- Decrease of structural height of the floor and whole building

- Decrease of the active seismic mass

- Decrease of the overall building volume (decrease of energy consumption for HVAC)

- Decrease of façade surface (decrease of energy loss)

Besides mechanical and architectural advantages, due to the similarity with steel structures, benefits also originate from the ease of fabrication, execution and quality control.

Contemporary steel-concrete composite flooring systems assume the use of the embedded mechanical connector devices (notably welded headed studs for which detailed rules are currently provided in EN 1994-1-1 [8]) as a mean to transfer longitudinal shear between the steel section and the concrete slab in order to achieve the composite action (Figure 2.1).

Figure 2.1 - Mounted steel beams with welded headed studs - Courtesy of UNI LU

After the concreting, they remain firmly bonded within the concrete slab what prevents the reuse of the structural elements, maintenance in form of the substitution of the structural elements comprising the composite floor and making future recycling resource intensive in terms of time, energy and finances.

Trying to implement the idea of the modularity in the execution of the steel-concrete composite flooring structures using precast slab elements or strengthening of the existing steel bridges by connecting the steel girder with the bridge concrete deck, several solutions which allow demountability had been investigated before in this context.

Prominent are the friction-grip bolt connectors and bolted shear connectors with preload force (which induces friction forces between components) or without.
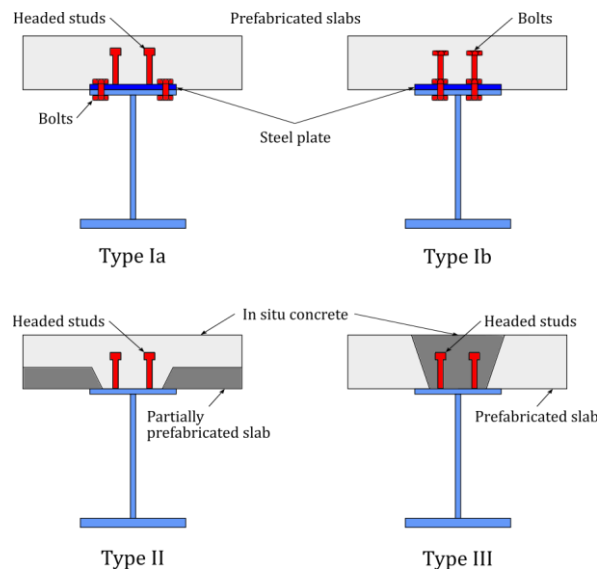
Figure 2.2 - Demountable (I) and modular (I, II and III) composite flooring systems by Hanswille [9]

These solutions fulfil all previously set requirements except that in order to attach the concrete slab to the steel section, the steel section has to be drilled hence damaged in order to accommodate the bolts what limits its reuse potential.

The further step in the development of the sustainable composite steel-concrete flooring systems in buildings is to devise a demountable connection between the steel beam and the precast concrete slab element which would leave these structural elements intact (possibly without drilling of the holes in steel section to accommodate the bolts etc.). This would give an opportunity for multiple reuse of the structural elements if standardized building grids were used.

This type of flooring solution would allow for further step in an effort to reduce the environmental impact of the construction industry. Compared to the previous practice, it is a step forward as the environmental benefit shall not only originate from the recycling of the consumed materials as an end-of-life scenario, but also from multiple reuses of the structural elements during their life cycle.
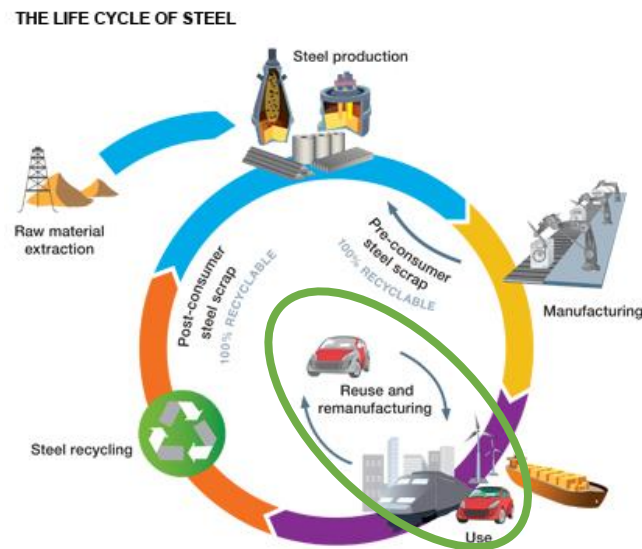
Figure 2.3 - The life cycle of steel structures [10]

In each reuse state, the same amount of resources required to produce reused elements shall be spared, hence greatly reducing the environmental impacts through reuse concept (Figure 2.3).

2.2 Methodology

The flooring system developed in this work is intended to be applied in office and residential buildings and possibly in the case of multi-storey carparks where its modularity and demountability shall be particularly beneficial. The system is comprised of modular concrete solid slab, devised using prefabricated elements, that is coupled with the steel beam by demountable shear connectors.

Methodology of the research may be briefly summarized in the following steps. The structure of the thesis follows the underlined workflow:

- State of the Art analyses

Investigation in existing demountable shear connector devices and devices that possess the favourable mechanical properties but are applied in assemblies that perform different mechanical purpose. The appropriate investigation and conclusions can be found in the chapter *3 State of the Art.*

- Elaboration of general details and definition of erection and dismounting technologies

Within the scope of this step, the typologies and detailing of the investigated shear connectors are defined. Based on the detailing of the shear connector, the sequencing of the shear

connection, composite beam and the composite floor itself is designated. The chapter representing this step of the work is the chapter *4 Structural concept*.

- Production of the prototype

Within the scope of this step the proposed connector devices are produced and their ease of assembly is tested. The work performed in this step predates the production of the test specimens for the push tests.

- Determination of the shear resistance by push tests

When the final detailing of the demountable shear connector solutions is defined and their prototypes approved, the mechanical properties of the shear connectors are experimentally determined by performing the standard push tests in accordance with EN 1994-1-1 Annex B [8]. Besides standard push tests that are the culmination of the experimental campaign, material tests shall be performed in order to obtain material properties of applied materials in the critical parts of the connector assembly and to build the reliable material models for the numerical analysis. In order to build reliable relationship between the bolt pretension force and the applied torque, the torque calibration tests are performed in accordance with EN-1090 Annex H [11]. The performed work and results within this research step may be found in the chapter *5 Experimental campaign*.

- Numerical simulation of the local behavior (push tests)

In this step the advance FEA model is built and benchmarked against the results of the material and push tests. Based on the reliable FEA model of the push tests the experimental results could be extrapolated and the mechanical behaviour of the demountable shear connector investigated in detail. This step of the work is represented by the chapter *6 Numerical analysis*.

- Optimization of shear connector form based on the FE analysis

Using the reliable FEA model of the push test the connector assembly is furtherly improved without the repetition of the experimental stage. This step of the work is represented by the chapter *7 Connector Type B behaviour and design model*.

- Determination of the mechanical force-slip model

Based on the experimental campaign results and FE analyses the force-slip model is proposed. This step of the work is represented also by the chapter *7 Connector Type B behaviour and design model*.

- Numerical simulation of the global (beam) behavior

In order to prove the applicability of the shear connector in the designated demountable steel-concrete composite floor system regarding its mechanical properties, the mechanical response of series of simply supported composite beams, where the shear connection is achieved using proposed shear connector, is investigated using appropriate FEA composite beam model. The investigation and conclusions of this step are represented by the chapter *8 Implications of the connector Type B behaviour on the demountable secondary composite beam response*.

- Proposal of the design methodology

Based on the conclusions of the previous step the design methodology is proposed. This step is as well represented by the chapter *8 Implications of the connector Type B behaviour on the demountable secondary composite beam response*.

3. State of the Art

3.1 Introduction

In this chapter, the most notable investigations regarding demountable shear connector typologies for steel-concrete composite beams are discussed. In addition, as the shear connection proposed by this research is partly or fully based on friction, investigations in frictional behaviour and friction-based connectors shall be reviewed. Besides the shear connectors some special joint assemblies that are not shear connectors in the narrow sense of view but fulfil very similar mechanical role shall be investigated as well.

The idea of demountable shear connection for composite beams is not new. First investigations had been proceeded at the start of the second half of the 20th century due to the need for retrofitting of the old steel bridges for ever increasing traffic load [12]. Nowadays the interest for demountable shear connections comes from the idea of reusability and overall sustainability of the composite structures [13].

Majority of solutions implement the use of high strength bolts, which are embedded or post installed in the concrete deck and connected to the flange of the steel girder. These bolts may or may not be preloaded. If preloaded they inflict clamping force between the bottom surface of the concrete slab and the top surface of the steel girder (friction grip connectors). Initially, the shear capacity in this case is provided by the friction between the surfaces in contact. After overcoming the friction resistance, additional capacity is provided by the bearing of the bolt (shear mechanism).

If not preloaded, the main mechanism for providing the shear capacity is by the bearing of the bolt against the bolthole (bolted shear connection). Bolts may be embedded or post installed in the concrete slab. In addition, they may have one or two embedded nuts or none.

Regarding previously stated, the demountable bolted shear connectors might be classified in following categories (Figure 3.1):

    A. Friction grip connection
    B. Bolted connection without embedded nut
    C. Bolted connection with one embedded nut
    D. Bolted connection with two embedded nuts
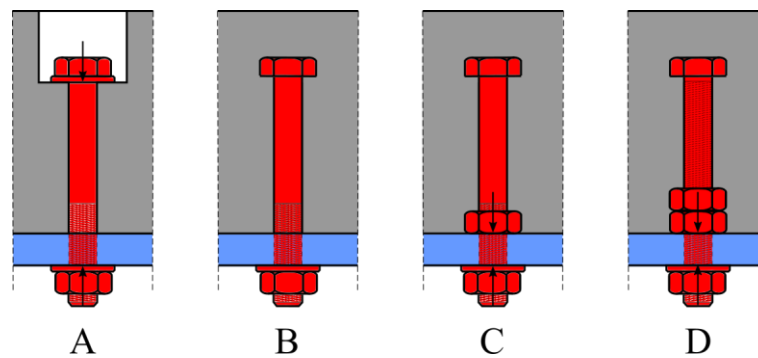
Figure 3.1 - Types of bolted demountable shear connectors by Pavlovic [14]

Particularly important for this research are friction grip connectors. Their capacity is as stated, partially based on the frictional behaviour. Due to this, the findings reported in the researches of the friction grip connectors, at the first-place findings regarding frictional behaviour and bearing mechanism shall be exploited and related.

Until today, there is only one investigation of demountable shear connection where the connector response was based solely on friction and was performed by Wang et. al [15]. In this case the shear connector is devised by using the Lindapter fixing clamps (Figure 3.2). The results obtained in this research were important source of information for the development of the shear connection device within the scope of this research work.
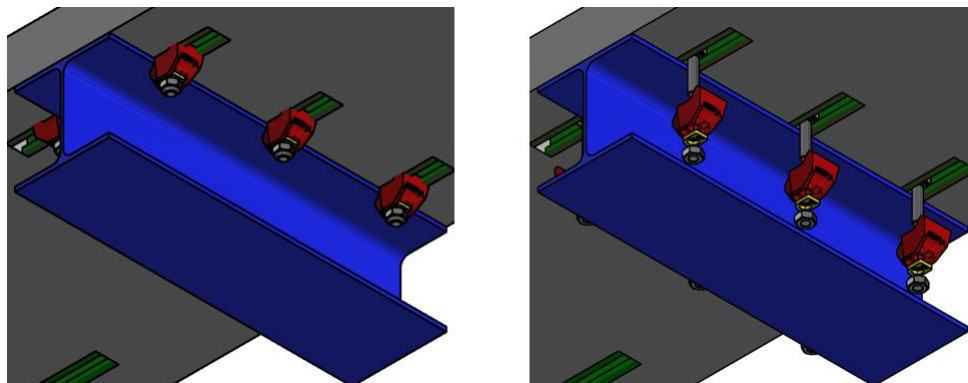
Figure 3.2 - Demountable shear connection based on friction [15]

3.2 Friction grip connectors

As explained before, the friction grip connectors provide shear capacity by combination of the friction and the bolt bearing. As the preload force is introduced through the thickness of the concrete, there is a significant problem with the preload loss due to the creep of the concrete in the vicinity of the pretension force introduction through the concrete slab. Usually around the bolthole, the helicoidal reinforcement is provided in order to receive and transfer the compressive stresses that originate from the bolt preload while relieving the concrete of the excessive compression.
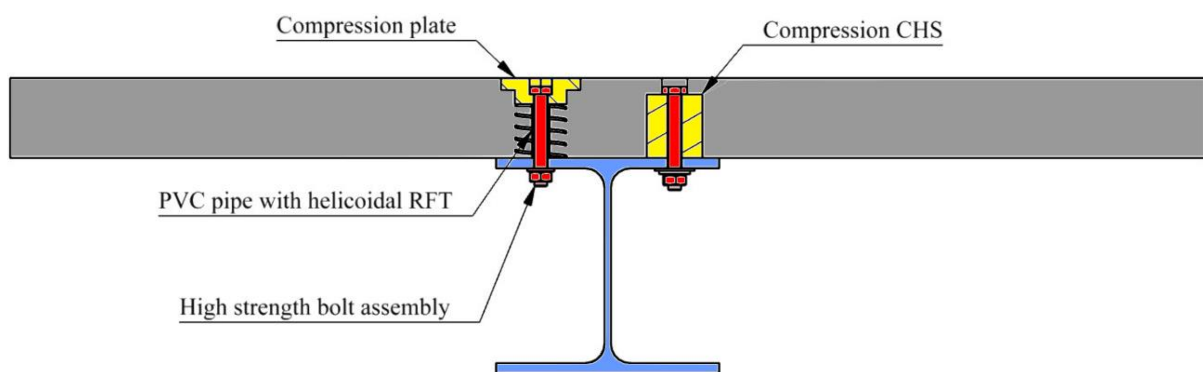
Figure 3.3 - Some layouts of friction-grip connectors

Dallam [16] investigated the behaviour of the embedded preloaded bolted shear connectors for composite beams. Objective was to obtain higher stiffness of the connection in comparison to the welded studs by using the high-strength preloaded bolts and to obtain connection that may be easily executed at the construction site by means of bolting.
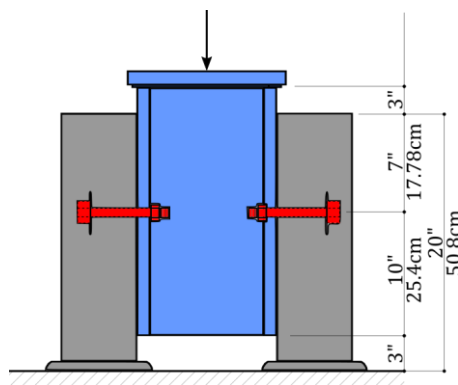
Figure 3.4 - Pushout test specimen and its steel section before concreting [16]

Twelve push tests were performed (Figure 3.4), four test specimens per each of three diameters of A325 high strength bolts (comparable to the bolt class 8.8).

The bolt diameters investigated were $\frac{1}{2}$" $(12.7mm)$, $5/8$" $(15.9mm)$ and $\frac{3}{4}$" $(19.1mm)$. The bolts were first fixed to the "snug tight" condition and then preloaded by the "turn of the nut" method applying ½ turn.

It was reported that the connection behaved almost perfectly rigid (Figure 3.5) until reaching the slip capacity what makes it ideal for the exploitation load levels and fulfilment of SLS requirements. The ultimate shear capacity was almost twice higher than the one obtained with the shear connection provided by studs with corresponding diameter what is attributed to the higher material strength of the bolts compared to the material strength of the welded headed studs.

Important finding is that no preload force loss was recorded, at least no decrease of the resistance if the bolt was preloaded earlier (effect of creep). This statement is indirect, as it was concluded from the comparison of the capacities. In addition, exact preload force was not measured and the "turn of the nut" method is rather inaccurate method of introduction of the preload force. This conclusion is also challenged in later investigations, for example by Hanswille [17], where significant preload loss (46%) was recorded after 8 months due to the creep of the compressed concrete around the bolt hole.
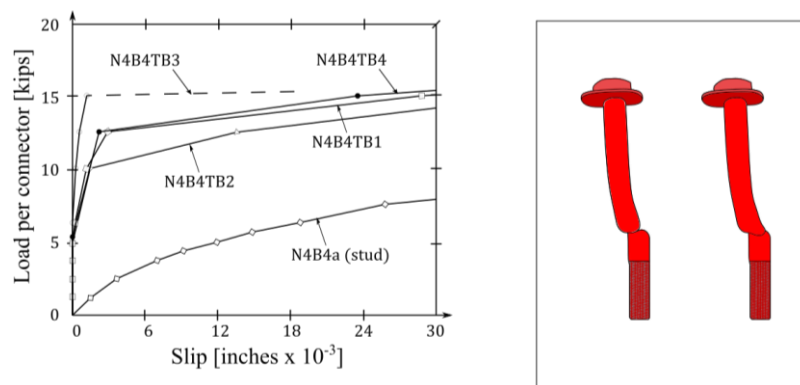
Figure 3.5 - Load slip curves and aftermath of the test [16]

Under the cyclic load-deload sequence of loading the friction resistance component increased (Figure 3.6). Due to the ductile behaviour after reaching the slip resistance and due to the increase of frictional resistance with the slip, the behaviour of the connector may be related to the yielding of the steel with strain hardening effect.
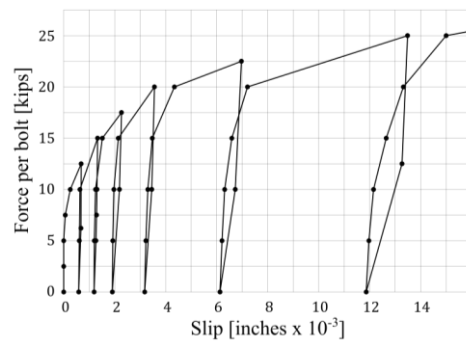
Figure 3.6 - Cyclic force-slip behaviour of the shear connector [16]

The investigation was expanded later by the full scale beam tests also by Dallam [12]. The objective was to confirm the elementary beam theory, to confirm the consistent behaviour of the connection between the push tests and the full-scale beam test and to confirm ultimate strength theory (plastic bending capacity of the cross section under the plastic distribution of longitudinal shear). All assumptions were satisfied or the behaviour exceeded the expectations. The shear capacity of the connector derived from the beam response was higher than the one obtained by the means of push tests.
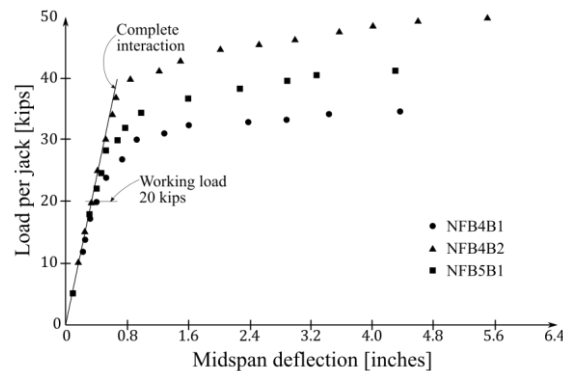
Figure 3.7 - Agreement between theoretical and experimental results in region of working loads [12]

Important finding was, as presented in the Figure 3.7, that in the region of the serviceability loads, the composite beam behaved in accordance with the complete interaction theory.

Marshall et al. [18] undertook investigation of the friction grip connectors as a continuation of the research work done by the Sattler [19]. Objective was similar as in researches of Dallam, [16] and [12], but in a more meticulous way regarding the frictional behaviour. In this research, the influence of the preload force on the shear capacity was investigated as the determination of the slip coefficients regarding the use of precast or cast-in-situ concrete slabs. In the first part of the investigation 12 pushout specimens were tested where method of casting and the preload force were variated (Figure 3.8).
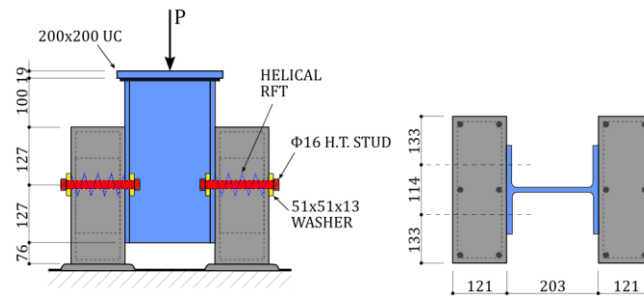
Figure 3.8 - Pushout test specimen [18]

It was reported that, as expected, with increase of preload force the capacity of the connector increases due to the increase of the frictional part of the total shear capacity (Figure 3.9).
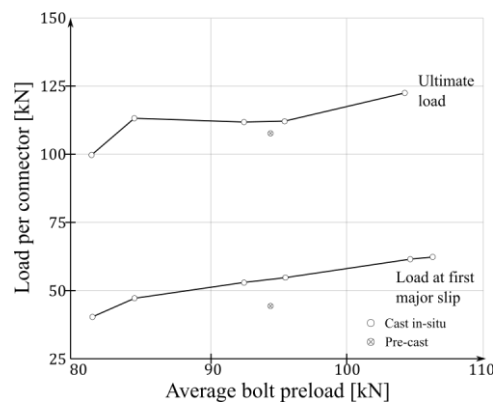
Figure 3.9 - Dependence of the shear capacity on the bolt preload [18]

Recorded slip coefficient was higher for the cast in-situ concrete slab ($\cong 0.6$) than in the case of precast slab ($\cong 0.5$) as there were no interfacial bedding materials (Table 3.1).

Table 3.1 - Slip coefficients [18]

Specimen	Load per connector [kN]		Type of failure	Bolt preload [kN]	μ
	First slip	Ultimate			
1/1	41.1	100.0	Bolt-shear	81.4	0.504
1/2	47.8	114.0	Bolt-shear	84.5	0.565
1/3	52.8	111.7	Bolt-shear	92.5	0.571
2/1	54.4	112.1	Bolt-shear	95.5	0.570
2/2	53.4	111.0	Bolt-shear	92.6	0.576
3/1	44.5	107.7	Bolt-shear	94.5	0.470
3/2	61.0	Not completed		105.0	0.583
3/3	63.2	122.0	Bolt-shear	104.5	0.613
4/1	44.5	120.0	Bolt-shear	94.5	0.470
4/2	45.3	122.0	Bolt-shear	94.5	0.470
4/3	48.9	121.0	Bolt-shear	94.5	0.475

*In situ
**Precast

The slip coefficient for the cast in-situ concrete $\mu_{c,is} \cong 0.55$ was slightly higher than the slip coefficient for the precast concrete slabs $\mu_{c,pc} \cong 0.47$. The concrete strength had no influence on the frictional (slip) capacity of the steel-concrete interface.

Under load-deload sequencing in the sliding region of the force-slip response, similar frictional "hardening" as reported in [16] was observed (Figure 3.10).
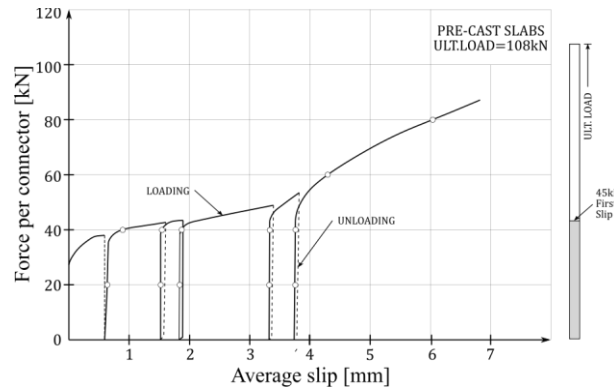
Figure 3.10 - Cyclic force-slip behaviour of the shear connector [18]

Later five full scale simply supported steel-concrete composite beam tests were performed where the casting method, load arrangement and span were variated. Investigation was performed in order to assess the effect of the slip on the behaviour of the composite beam by applying full interaction, Newmark partial interaction [20] and no interaction model. It was again confirmed that in the region of serviceability loads (elastic range) complete interaction theory may be applied with sufficient accuracy (Figure 3.11).
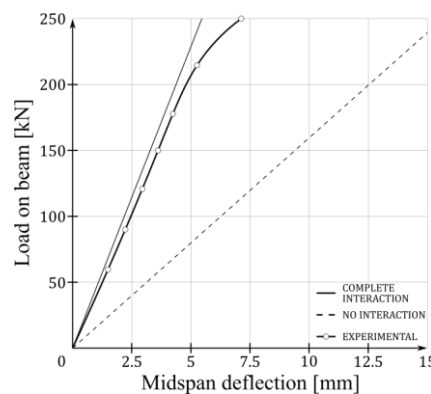
Figure 3.11 - Agreement between complete interaction and test results [18]

It was observed that the friction coefficients, based on the assumption of complete interaction, were higher in the beam tests than in the push tests (Table 3.2). The effect originates from the additional clamping force that the load applied on the beam inflicts on the slab-steel section top flange faying interface.

Table 3.2 - Slip coefficient of friction - Beam tests [18]

Beam	Bolt preload [kN]	No. of connectors	Load (P) at first slip	Shear load per bolt	μ
1/2	83.8	8	223.0	0.284P	0.75
1/3	83.8	8	250.0	0.284P	0.84
2/1	85.3	10	254.0	0.223P	0.67
2/2	70.7	10	214.0	0.223P	0.68
2/3	115.0	6	187.0	0.223P	0.62

Overall conclusion was that the friction grip connectors are suitable for the application in composite beams. If the shear connection is adequately provided, assuming the recommended slip friction coefficient of $\mu = 0.45$ by Satler [19], in the region of serviceability loads it is safe to assume that the behaviour is same as in the case of composite beam with complete interaction.

Dedic and Klaiber [21] investigated also the use of high strength bolts as shear connectors for rehabilitation works. Three push test series were performed of which the Series 2 was post-installed friction grip connection (Figure 3.12). After the drilling of the concrete slab and the steel flange, the hole in which the bolt head was placed was filled with grout and the bolt hole was filled with concrete-steel epoxy to provide even bearing surface for the bolt. Push out specimens consisted out of 4 A325 (8.8 grade equivalent) high strength bolts, which were tightened after positioning in the bolthole.
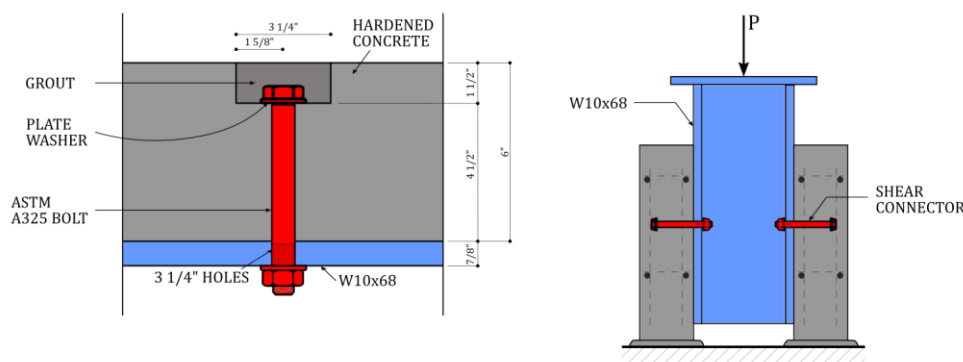
Figure 3.12 - Detailing of the post installed friction grip connector and push specimen [21]

Shear connection obtained this way was stiffer and stronger compared to the equivalent one devised using the headed studs.

Maybe the most comprehensive investigation of the behaviour of friction grip connectors was undertaken by Roik and Hanswille [17]. Eleven push test series, each composed of 5 test specimens were tested (Figure 3.13). Aim of the testing was to investigate the influence of the

bolthole tolerance, slip coefficient of friction, influence of the eccentric position of the bolt in the bolthole, influence of the fatigue on the slip friction coefficient and ultimate capacity and the loss of the preload force due to the creep and shrinkage of the concrete.
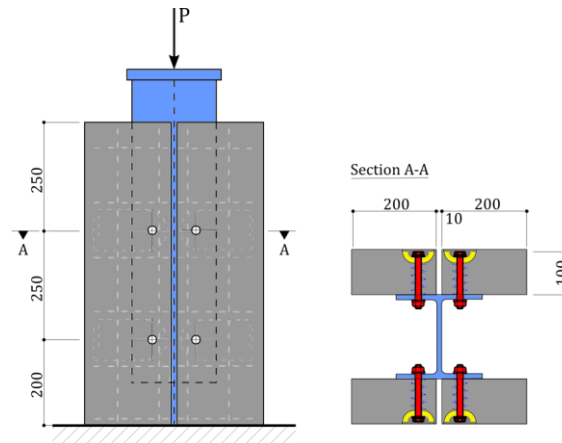
Figure 3.13 - Push test specimen [17]

Besides the force-slip model (Figure 3.14), for the first time the analytical expression for the evaluation of the ultimate shear capacity based on the combination of the friction and bearing was proposed:

$$P_u = P_R + P_A = \delta \cdot \mu \cdot V_0 + P_A$$

(3.1)

P_u – Shear capacity

P_R – Frictional capacity

P_A – Bearing capacity

δ – Reduction of preload force due to the bending of the bolt

μ – Slip factor

V_0 – Design preload force of the bolt
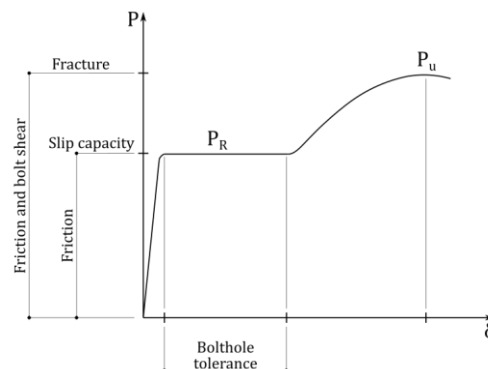
Figure 3.14 - Typical force-slip behaviour and resistance components of friction grip connector [17]

The reduction factor δ considers the loss of preload force due to activation of the bolt in the bending which leads to yielding of the bolt material and local destruction of the concrete. Reference value of $\delta = 0.6$ was reported. This will be very important for the shear connection proposed in this research, as similar phenomena will be observed. Increasing frictional contribution leads to the preload force loss, hence to decrease of the overall shear capacity of the connection. Therefore, in this research special attention was put on adequate design of connector detailing regarding bolt diameter, bolt material class and clamping length of the bolt assembly within the connector device.

Another important finding was the fact that measured slip before reaching the slip capacity is very small ($0.3\ mm$), providing almost rigid-like behavior until slip capacity is reached. This allows for complete interaction assumption for the serviceability load levels.

The different force slip models were defined depending on the bolthole tolerance (Figure 3.15). If the bolts were almost fitted, no displacement plateau was observed as the bearing starts immediately after the friction resistance is reached. However, this is hardly possible in reality due to the fact that certain tolerance is necessary in the construction phase.
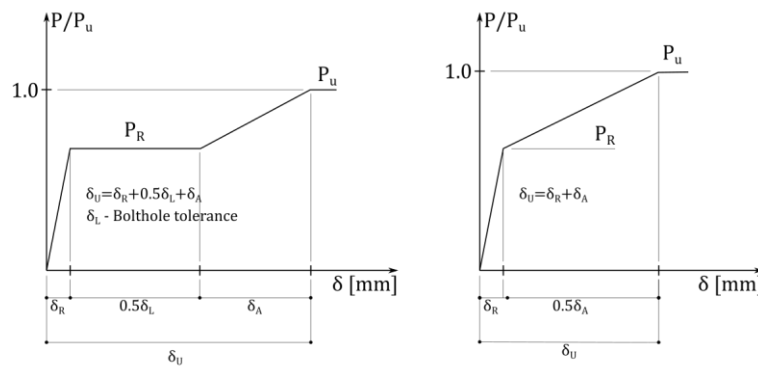
Figure 3.15 - Different force slip behavior regarding bolt hole tolerance
Normal vs. fitted bolt hole [17]

Important finding was also that due to the high compressive stresses around the bolthole, as a consequence of the preloading of the bolt, there is significant creep of the surrounding concrete material (Figure 3.16). Measured loss of preload force was in average 46%. Analytical model according to at that time current code for the design of prestressed concrete structures, DIN 4227, estimated the bolt preload loss of 26%. This result rendered code approach unsafe, as corresponding friction related shear capacity would also be overestimated.
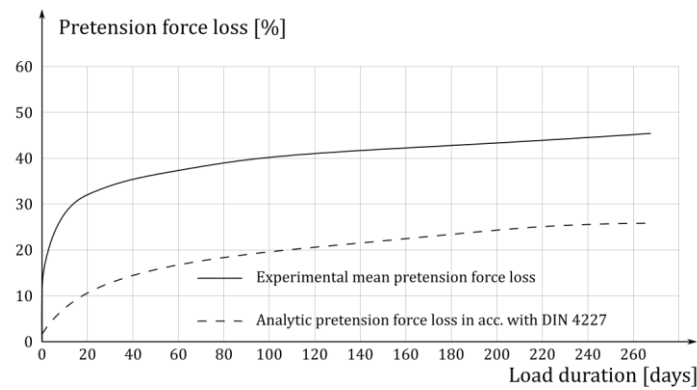
Figure 3.16 - Preload loss due to the creep
Test results vs. analytical model [17]

Bradford and Lee [22] investigated the use of the preloaded M20 8.8 bolts in combination with GPC precast concrete slabs as a substitution for OPC concrete. The use of GPC concrete would increase the sustainability of the structure further as its production has drastically lower environmental impacts than the OPC concrete counterpart. In total 5 push tests were performed where influence of the pretension force, clearance of the bolt hole, diameter of the bolt and number of the bolts in the connection were investigated (Figure 3.17).
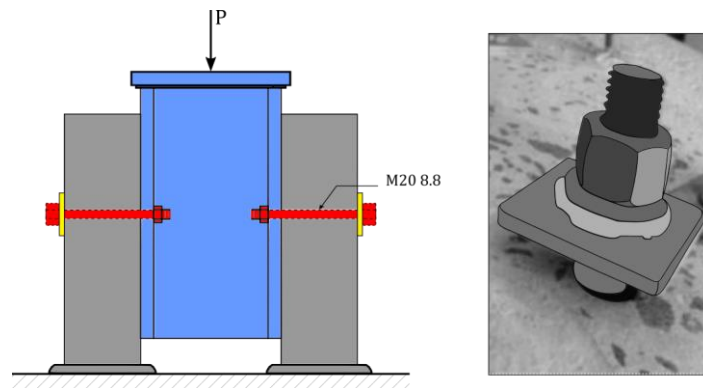
Figure 3.17 - Test specimen and the slab top with square washer [22]

Similarly to the research of Marshal [18], the slip friction coefficient for the precast elements was obtained as $\mu_c \cong 0.5$. As in previous investigations, similar three-stage force-slip behavior was reported. This behavior was idealized with trilinear curve and theoretical beam bending model was developed (Figure 3.18).
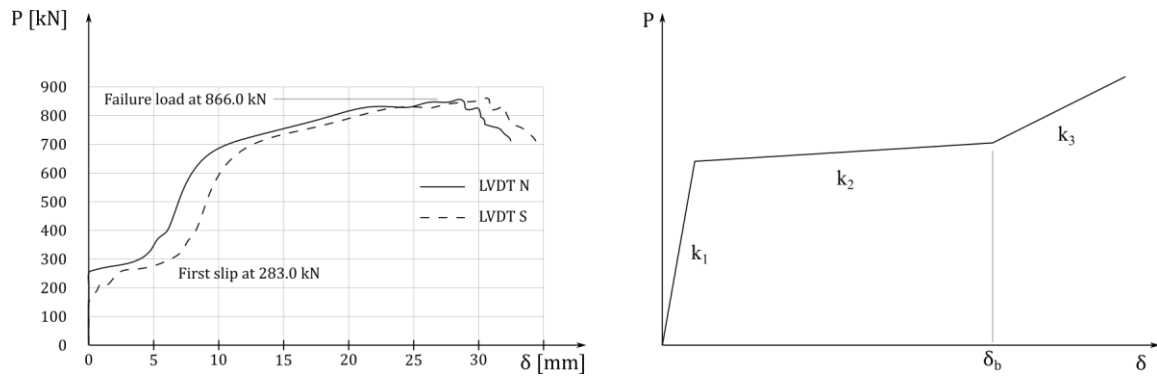
Figure 3.18 - Experimental and idealized force-slip curves [22]

Increase of pretension led to the increase of capacity. After slip capacity was reached, the final failure was obtained by shearing of the bolts. Again, although it is not explicitly reported, similar phenomena of the preload loss may be concluded as in [17].

If compared are the slip capacities and ultimate capacities of the specimens with full and half bolt preload force it may be observed that the slip capacity when full preload force is used is higher than the case with the half, as expected, but the difference between ultimate capacities is significantly lower (Figure 3.19). This must be attributed to the preload loss which eventually decreased friction contribution, hence the difference in ultimate capacities.
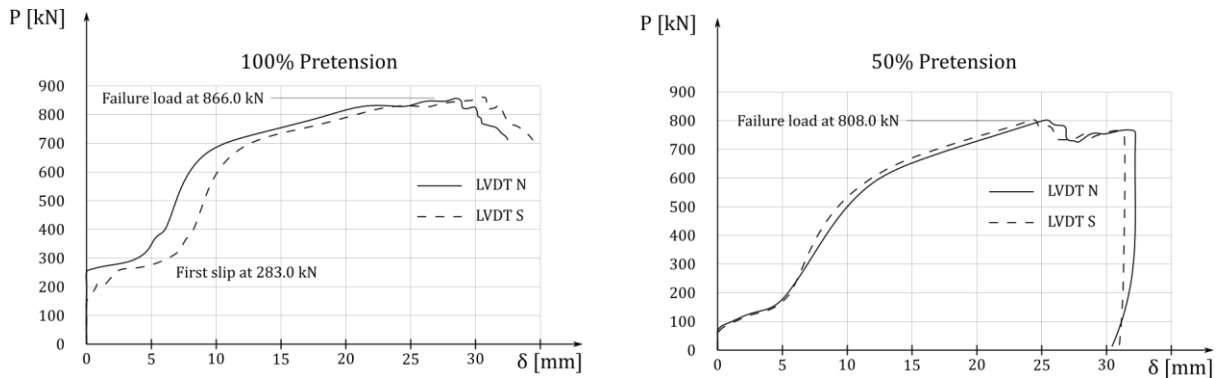
Figure 3.19 - Difference between friction contribution at first slip and at ultimate shear capacity [22]

Same phenomena may be observed from the following figure where it is shown that the benefit from pretension increase is much higher for slip capacity rather than in the case of ultimate shear capacity (Figure 3.20).
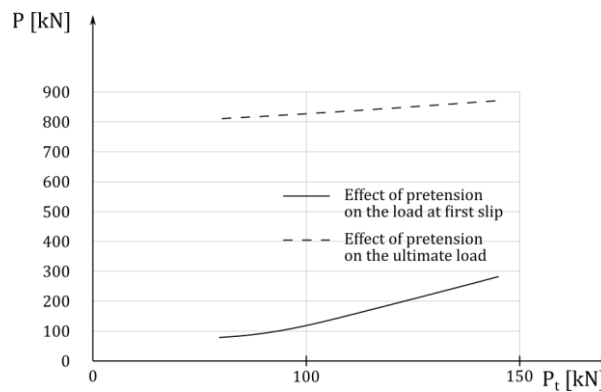
Figure 3.20 - Dependence of ultimate and slip capacity on level of bolt pretension [22]

Within the REDUCE multilateral research project, demountable coupler system was investigated by Kozma at the University of Luxembourg [13]. The solution provides a from-the-bottom demountable shear connector system. The coupler element M20 10.9 welded on the edge L profile is embedded in the concrete matrix of the modular slab element. It provides an anchor point for the bolt M20 8.8 that is also embedded in the concrete and acts like a stud and also for the demountable M20 8.8 bolt that is tightened through the bolt hole of the flange into the coupler element (Figure 3.21).
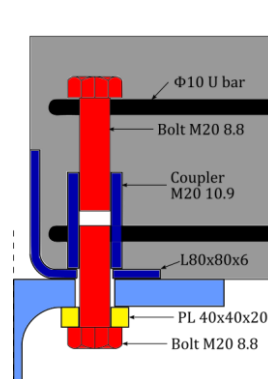
Figure 3.21 - Coupler connector system [13]

The M20 8.8 bolt is then preloaded hence providing a friction-grip type demountable shear connector. The component is tested using 3 test specimens in accordance with the Annex B of EN 1994-1-1 [8]. The obtained tri-part force-slip curve is the typical force-slip curve of the friction-grip connectors. The slip capacity of $50kN$ per connector is recorded (Figure 3.22). Afterwards the bolt hole tolerance is closed, the bearing of the bolt leads to the brittle failure by the shearing of the bolt shank at $F_u \cong 140kN$.
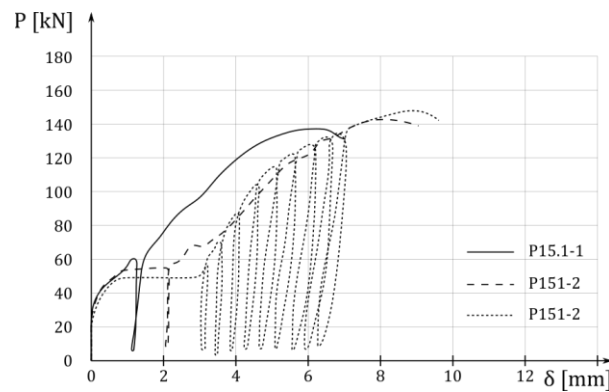
Figure 3.22 - Force-slip curves of the coupler shear connector [13]

Due to the robustness of the embedded coupler element there were no concrete related failure modes, it was possible to dismount and reassemble the test assembly proving that the proposed system indeed has a reuse potential. However, the question arises whether the durability of the threads of the embedded coupler element is adequate so the slab may be actually reused multiple times as the damage to the threads would prevent the assembly of the shear connection and the reuse of the modular slab element.

3.3   Bolted shear connectors

3.3.1   Without embedded nut

Hawkins [23] investigated the behaviour of cast-in-place anchor bolts by conducting testing on 27 specimens. The investigation was performed in two stages. Fifteen tests were firstly performed in order to investigate the shear capacity and later twelve in order to investigate pull-out behavior of the anchors.
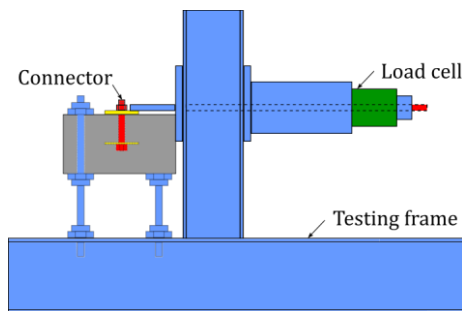
Figure 3.23 - Horizontal push test layout [23]

Fifteen push test specimens (Figure 3.23) were tested in horizontal push test arrangement. The parameters varied were bolt diameter, embedment depth, thickness of the washer inserted beneath the bolt head, size of the concrete specimen and concrete strength. The results were compared to the results previously obtained by the same author for corresponding headed studs.
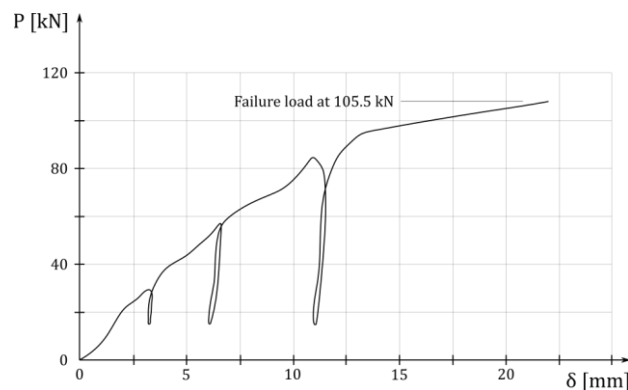
Figure 3.24 - Typical force-slip curve of cast-in-place anchor [23]

Obtained failure modes were concrete cone pull out failure for low embedment lengths or by radial cracking of concrete. Force-slip behaviour was recorded to be linear up to 80% of the ultimate load P_u as may be observed in Figure 3.24. In case of failure by radial cracking, the capacity is close to the shear capacity of the anchor, but in all cases significant bending deformation of the bolt was observable.

(a) Cone Pullout   (b) Radial cracking   (c) Bolt shape
at failure
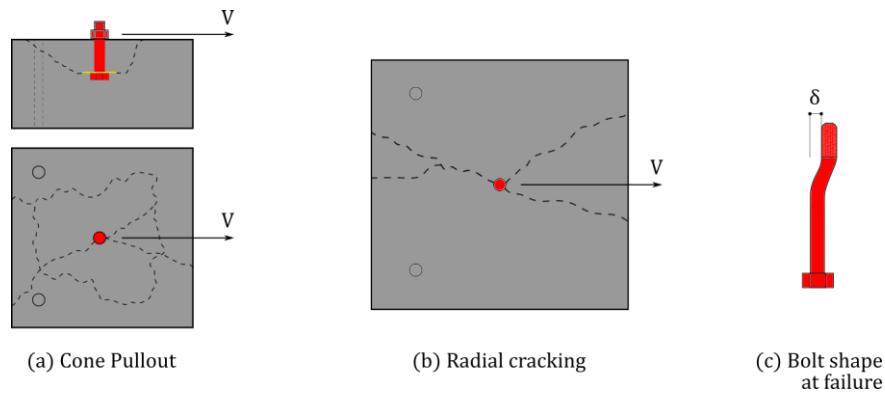
Figure 3.25 - Modes of failure [23]

The stiffness of the anchor was significantly lower than of the corresponding stud (Figure 3.26).
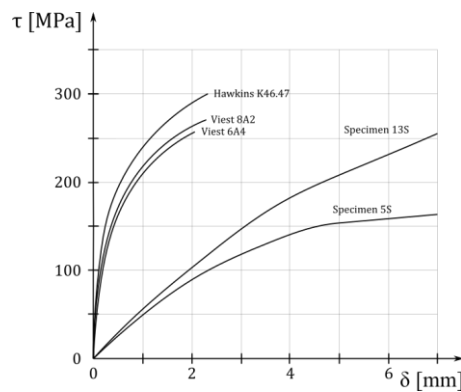
Figure 3.26 - Difference in stiffness and strength of shear studs and anchor bolts [23]

This is attributed to the flexible rotational restraint of the end of the anchor compared to the almost double end fixed restraint condition of the headed stud (Figure 3.27). In later case, additional catenary axial forces are developed which clamp the elements and produce friction what increases the stiffness of the connection further.
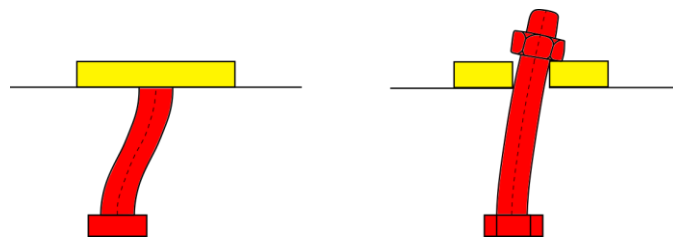
Figure 3.27 - Different support boundary conditions for stud and anchor bolt [23]

As may be observed in Figure 3.26, the ultimate capacity was lower. However, the limit of embedment length to diameter of the anchor where transition between cone pull-out failure to the shear failure of the connector or radial cracking of the concrete was similar.

Lam and Dai [24] investigated the use of threaded shear studs embedded in the concrete slab in order to achieve demountable shear connection (Figure 3.28). The research was proceeded with the aim to increase sustainability and provide reusability of composite structures.

Figure 3.28 - Anchor bolt derived by treading of the Nelson headed stud [24]

In total 8 push tests were performed in accordance with the Annex B of EN-1994-1-1 [8]. The variable parameters were concrete strength and stud diameter. Obtained failure modes are either by shearing of the stud or by crushing and splitting of the concrete with later being more ductile (Figure 3.29).
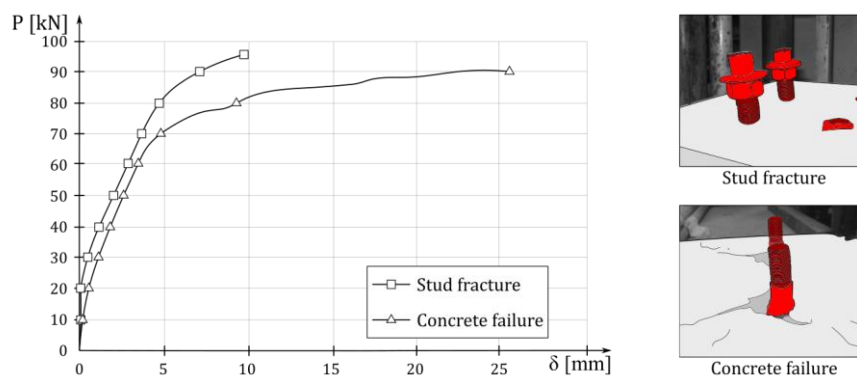
Figure 3.29 - Force-slip curves and failure modes in case of failure by shearing of the anchor and by failure of the concrete [24]

It was reported that specimens which experienced failure by concrete crushing had no damage of the threaded part of the shank and that the specimen was easily demounted.

The capacity of the anchor stud and the corresponding welded stud from which the anchor was milled were comparable. However, the threaded anchor provided higher ductility but significantly smaller initial stiffness. Authors comment that due to the similar capacities the application of the threaded anchor bolt won't be impaired in comparison to the comparable welded headed stud solutions regarding both SLS and ULS, however this statement is

questionable due to the smaller initial stiffness (Figure 3.30), especially in the case of serviceability load levels.
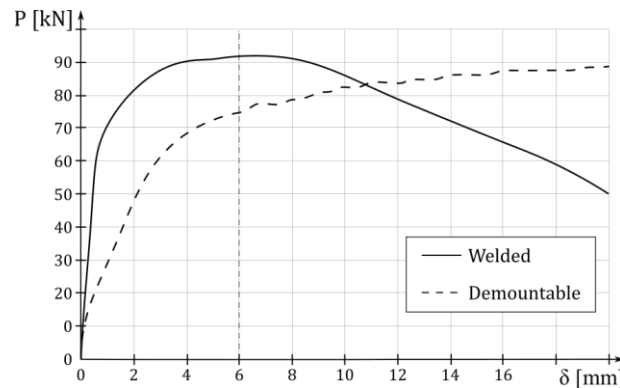
Figure 3.30 - Force-slip curves - Headed stud vs. threaded stud anchor [24]

3.3.2 With embedded nut

In the work of Dedic and Klaiber [21] one test series was dedicated to the post-installed, double-nutted (one embedded nut) bolted shear connection (Figure 3.31). This connection was tested along the previously mentioned friction grip solution and specimens with corresponding diameter headed studs.

The concrete slab was drilled first and later the top flange of the steel beam as well in order to accommodate the post-installed bolt. The bolt was positioned with a nut against the steel flange inside the slab and the nut on the bottom side of the flange was tightened. After positioning of the bolt, the slab hole was grouted with non-shrink grout.
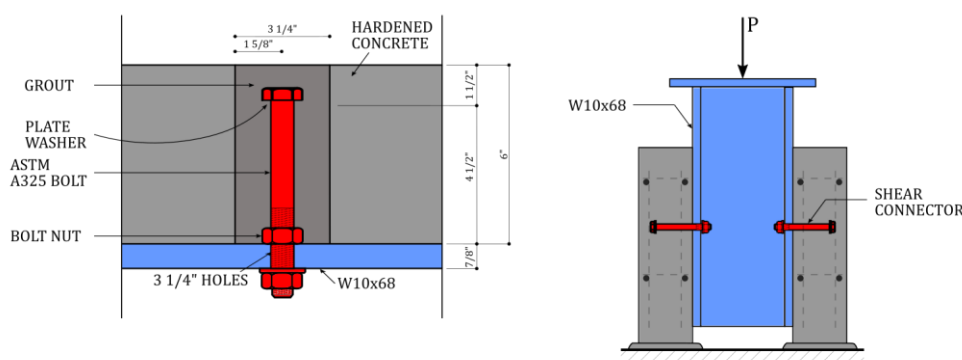
Figure 3.31 - Detailing of the post-installed, double-nutted bolted connector and push specimen [21]

Same as in the case of the friction grip specimen, obtained failure was by shearing of the bolt. The double nutted connector was also stiffer than corresponding welded stud but in the initial loading region, stiffness was lower than in the case of epoxied friction grip connector. In the

higher load regions, the exhibited stiffness was higher than in the case of friction grip solution (Figure 3.32).

The higher stiffness is contributed to the larger bearing surface in concrete slab provided by the embedded nut. The lower initial stiffness is contributed to the setting of the bolt in the bolthole and deformation of threads under bearing. Due to the use of concrete epoxy in the friction grip connector, there is no setting, hence higher stiffness.

Overall, the both types of connectors exhibited similar mechanical behaviour in terms of strength, stiffness and ductility.
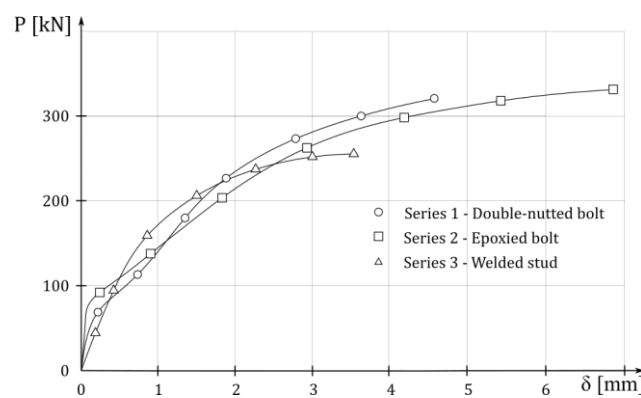
Figure 3.32 - Force-slip behaviour of double-nutted, friction grip bolt and welded stud [21]

Compared to the epoxied post-installed bolted connection, this solution is found as preferable as there are less operational steps for almost same mechanical response.

Hanswille [9] investigated two demountable, bolted solutions and two solutions by using partially prefabricated concrete slabs with headed studs and prefabricated concrete slabs with headed studs in a group. Motivation was to implement the use of partially or fully prefabricated concrete slabs regarding composite beams and the use of bolted shear connections regarding substitution of the concrete decks of composite bridges and for the application in temporary composite bridges. The solution type I_b represents preinstalled, bolted shear connection with two embedded nuts. In total 3 push test specimens were tested of which one was tested applying fatigue load (Specimen 3) after which it was statically loaded until the failure (Figure 3.33).
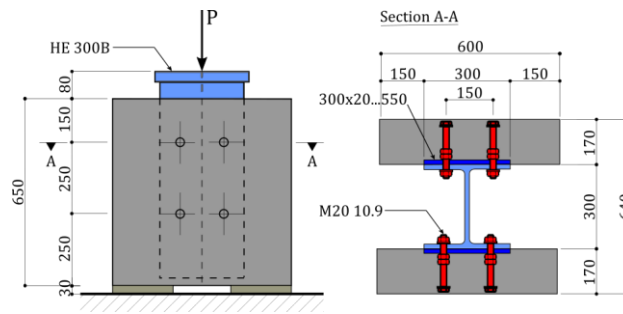
Figure 3.33 - Test specimen I_b [9]

Obtained failure in all cases was by the shearing of the bolts on the concrete slab - steel flange interface. The fatigue behaviour was assessed as good as no fatigue related failure occurred. After the fatigue load sequence, static push test was performed using the same specimen (Specimen 3). No significant difference was observed compared to the static load only specimens confirming the good fatigue behaviour (Figure 3.34).
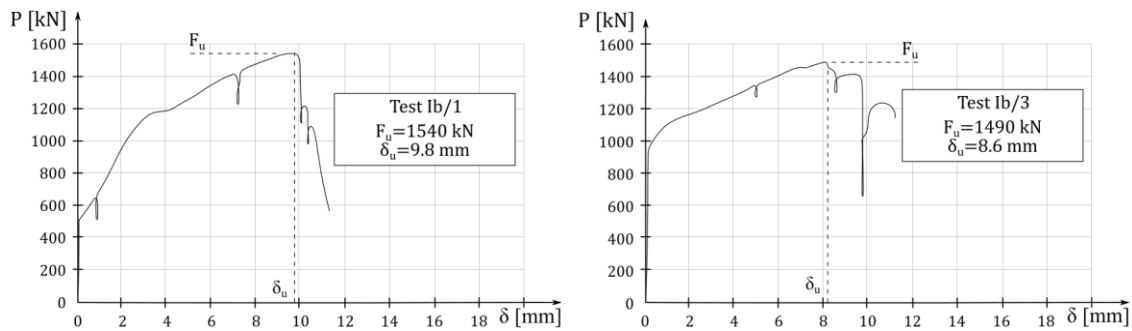
Figure 3.34 - Static force slip curves for static only and fatigue specimen [9]

Analytical model was provided for the assessment of the shear capacity of bolted connector with two embedded nuts. Similarly to the headed studs, two failure modes were proposed, one by shearing of the bolt and one by the crushing of the concrete due to the bearing.
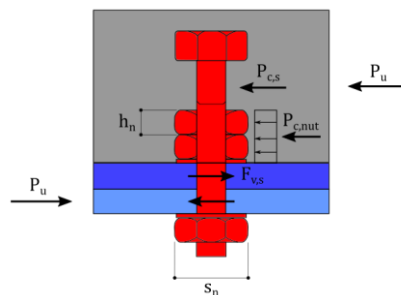
Figure 3.35 - Shear resistance model of bolted connector with two embedded nuts [9]

Difference in models is that for calculation of concrete failure the contribution of the embedded nuts was added (Figure 3.35). Good agreement with test results (failure by shearing of the bolt) was obtained.

- Mode 1 – Concrete crushing

$$P_u = n_b(P_{c,s} + 2 \cdot P_{c,nut})$$

(3.2)

P_u – Connector strength

n_b – Number of bolts

$P_{c,s}$ – Concrete strength contribution of bolt

$P_{c,nut}$ – Concrete strength contribution of nut

- Mode 2 – Shearing of the bolt

$$P_u = n_b F_{vs}$$

(3.3)

$F_{v,s}$ – Shear strength of the bolt

Pavlovic et al. [25] investigated the behaviour of the bolted shear connection with one embedded nut in combination with prefabricated concrete slabs (Figure 3.36). The prefabricated concrete slab was provided with a square hole where the space was reserved for bolt placement. After the placement of the bolts, the hole was grouted and the nuts on the bottom side of the flange were tightened, hence bolts preloaded. The investigation was performed in line with efforts of Spremic [26] who was researching the behaviour of grouped welded headed studs, which were in a similar way combined with prefabricated concrete slabs. In total 32 standard push specimens were tested (8 bolted and 24 with welded headed studs).
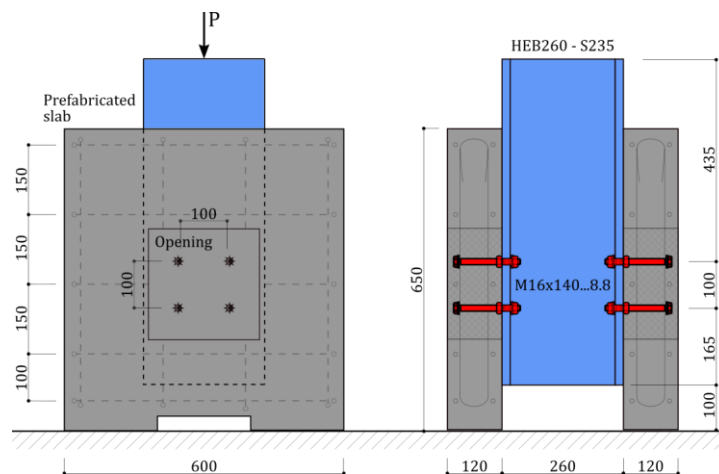
Figure 3.36 - Push test specimen [25]

As currently there are no detailed rules provided for the application of these solutions in the common design, they are not exploited in practice. Hence, the investigations were performed in accordance with EN 1994-1-1 [8] and EN 1990 [27] so the obtained results are suitable for code implementation. Both endeavours were motivated by similar intentions, to provide enhanced modularity and ease of construction of composite slab systems for buildings, car parks and small span bridges. The bolted solution also provided demountability option.

In the research of Pavlovic et al. [25] for the first time extensive numerical analyses and development of analytical solutions of failure modes of bolted shear connections with one embedded nut were performed. The FEM material model was calibrated to the material testing results, corresponding material damage models were developed and the final FEA model was calibrated to the obtained experimental push test results. Good agreement was observed compared to the test results (Figure 3.37). After calibration, parametric study was performed by variating the embedment depth of the bolt.

Obtained failure mode was by the shearing of the bolt and not by the failure of concrete by crushing or by cone-pull-out failure. In addition, the influence of the reinforcement was negligible.
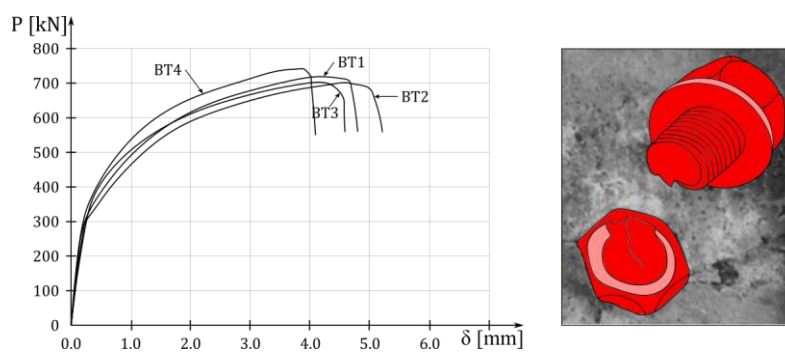
Figure 3.37 - Experimental force-slip curves and observed failure mode [25]

Similarly to the findings of Hawkins [23], obtained shear capacity was comparable to the equivalent stud connector, but the stiffness and ductility were quite different. The bolt resistance in shear was 20% higher than provided by EN 1993-1-8 [28]. Source of additional resistance were friction at the nut-flange interface and catenary effect of the bolt. Bolted connector exhibited smaller initial stiffness due to the bolthole tolerance and penetration of the threads onto the bolthole. The stiffness was 50% of the corresponding welded stud.

Ductility was expressed as the slip at the ultimate load δ_u. Obtained value in case of bolted connectors was lower $\delta_u = 4\ mm$, compared to the results of the corresponding headed stud. In accordance with EN 1994-1-1 [8] this implies that aforementioned bolt connector may not be considered as ductile. Consequence is that even distribution of shear connectors along the beam half-span while assuming the plastic distribution of the longitudinal shear force may not be considered. The reduced ductility comes from the obtained failure mode by pure shearing of the bolt at the flange-slab interface beneath the nut. This is the main source of lower performance in terms of ductility compared to the welded studs where the failure is obtained by combination of bending and shear above the weld collar.
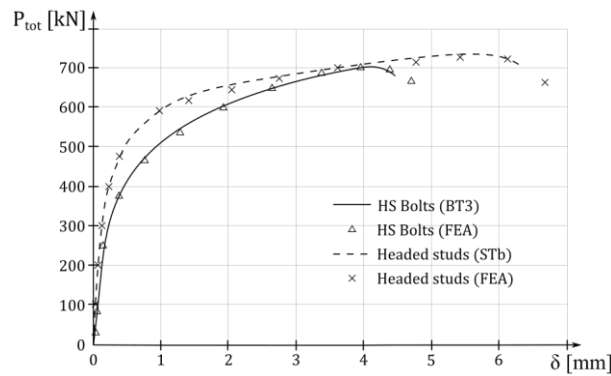
Figure 3.38 - Test vs. FEA results of bolted and welded stud connection [25]

If the ratio of embedment depth to bolt diameter is kept bellow $\frac{h_{sc}}{d} \leq 2.5$, the failure mode transitions to the failure by concrete cone pull-out. In that case, the slip at failure is higher and if the characteristic slip capacity is equal or higher than $\delta_{uk} \geq 6\ mm$, the connector may be considered as ductile. The whole research in detail may be found in the doctoral thesis of Pavlovic [14].

3.4   Friction behaviour

In this chapter frictional behavior between concrete slab and steel section is reviewed. Investigations considered were performed as initial research of the application of friction grip connectors.

Sattler [19] investigated the slip friction coefficient between the steel and concrete and the behavior of the high strenght HV bolts in friction grip connections by performing push tests and by applying the same solution in full scale beam tests.

In the first test series, the concrete slab was pressed by two steel plates in the horizontal push layout. The aim of the test was to estimate slip friction coefficient between the steel and concrete. The slip friction coefficient was meassured for two normal stress ranges, $\sigma_{n,1} = 2.45\ MPa$ and $\sigma_{n,2} = 9.81\ MPa$. The recorded slip friction coefficients were respectively $\mu_{c,1} = 0.60$ and $\mu_{c,2} = 0.45$.

It was found that the slip friction coefficient was higher in the case with smaller normal stress. The friction was tested also by meassuring the friction angle where the recorded value was $\mu_c = 0.55$ what is equal to recommended slip coffeicient value by ENV 1994-1-1 [29]. These results were considered as reference values for further push test stage.
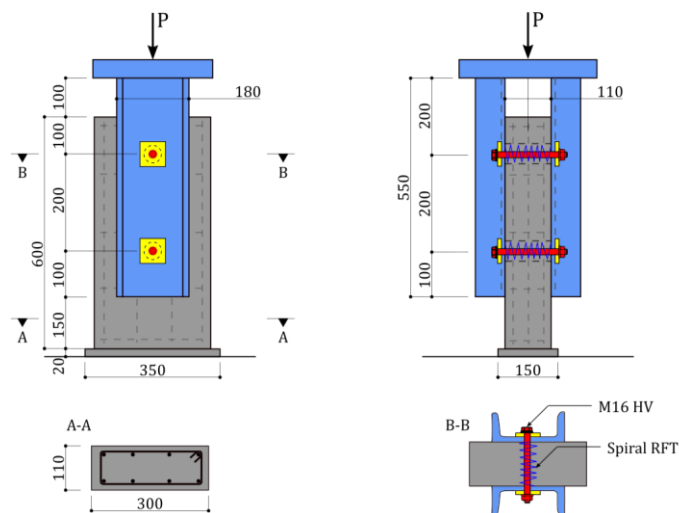
Figure 3.39 - Push test layout [19]

In the second test series, push test specimen (Figure 3.39) wass assembled. It consisted of the two steel U profiles with concrete slab in between. Steel sections and the slab were connected by high strenght preloaded HV bolts that form the friction grip connection. Helicoidal reinforcement secured the concrete bolt hole.

Corresponding to the load at the first slip, meassured slip friction coefficient was $\mu_c = 0.488$. Specimen with lower cube concrete strength exibited slightly larger friction coefficient $\mu_c = 0.55$. The connection had substantial reserve capacity due to the bolt bearing mechanism, but in order to prevent the crushing of the concrete author states that helicoidal reinforcement has to be provided in the concrete surounding the bolt hole. Also, due to the high compressive contact stresses between the bolt head and the concrete slab, steel washers have to be provided in order to distribute the contact load. The conclusion was that in the range of serviceability loads, the slip capacity of double sided bolted friction connection may be expressed as:

$$P_{zul} = 2 \cdot \mu_c \cdot P_V$$

(3.4)

P_{zul} – Friction component of the shear capacity

2 – Double-sided connection

μ_c – Slip friction coefficient

P_V – Clamping (preload) force

The lower limit of slip friction coefficient may be assumed as $\mu_c = 0.45$. Secondly, after the frist slip, the connection still posses considerable reserve capacity (due to the bolt bearing).

Beam tests confirmed that in the serviceability load range, after deloading, deformation is completely elasticly reversed and no damage of the bolt hole occurred. Until the first slip, the composite beam behaved in complete interaction manner.

The most extensive investigation of friction behavior of friction grip based shear coonnections was performed by Roik and Bürkner [30]. In total 103 test specimens were tested. Tests were divided in 4 test series groups:

- Group I – Tests of $t_{pl} = 10\,mm$ steel plates preassured between two concrete prisms (Figure 3.40)

- Group II – Same as group I with steel plastes $t_{pl} = 15\,mm$ thick

- Group III – Push test specimen with IPE300 section, four concrete slabs with 3 high strength preload bolts M16

- Group IV – Dynamic test specimen with $n = 3 \cdot 10^6$ cycles, specimen same as group I

Variables in test series were thickness of the steel plates, treatment of the formwork (with or without oil), number of preload points, intensity of the preload force, influence of the bolt hole tolerance and the load duration.
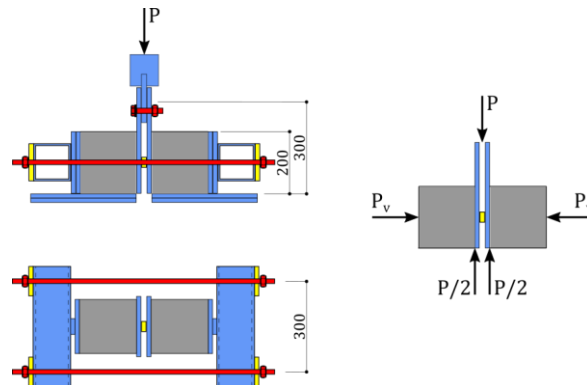
Figure 3.40 - Test specimens of groups I-II-IV [30]

For the first time beside meassured and mean values of the slip friction coefficient, characteristic values based on the 5% fractile value were determined what is suitable for later code implementation.

From the test series groups I and II, it was concluded that thicker steel plate in conntact provides higher friction. Similarly to the finding of Satler [19], lower contact presure exibited higher friction. In case with thicker plates (15mm) due to the larger effective load area the interface normal stresses were lower than in case of (10mm) plate. Similar phenomenae was observed if the preload force was variated. In the case of lower preload force (lower contact presure) meassured friction was higher.

In test series where concrete was casted in oiled formwork, the friction coefficient was lower on average 10%. Important finding is that long term load exposure provided no significant deviation of the friction coefficient value in comparisson to the short term loading.

Important finding in the Groups I,II and III was also that after reaching slip friction resistance the capacity did not drop, the friction resistance plateau was observed (Figure 3.41). This finding is crucial as it confirms rigid-perfectly plastic like behavior at large slips which is laster assumed regarding proposed connection solution of this research.
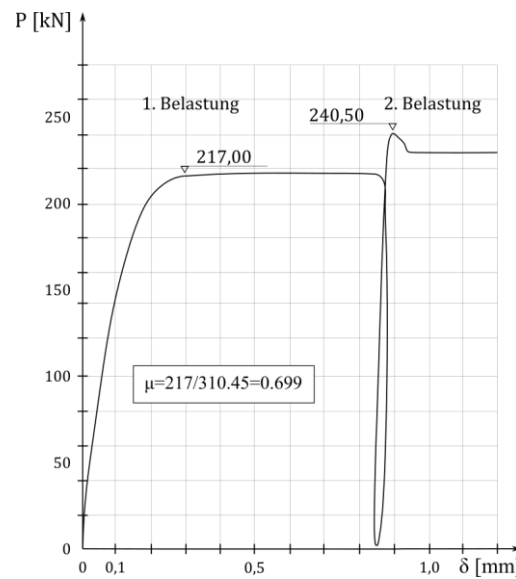
Figure 3.41 - Stable load plateau and increase of friction due to the reapplication of the load [30]

Similarly to the previous investigations, if the specimen was deloaded and subsequently reloaded, the increase of the friction slip coefficient was observed. In the test Group III characteristic friction-grip three part force-slip curve was obtained (Figure 3.42).
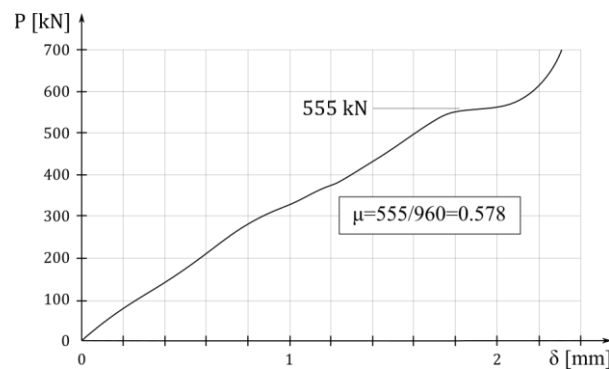
Figure 3.42 - Three-part force-slip curve [30]

Dynamic test was performed by cycling the applied shear load between $20 kN$ and 80% of expected shear capacity ($182\ kN$). After cycling, the specimen was staticly loaded up to the failure. The slip resitance recorded was higher than expected, this proved good frictional behavior under dynamic loading what is especialy important in the case of bridges.

3.5 Friction based connectors

Bagon [31] presented a new type of demountable and modular solution for composite bridges in urban zones. Bridges designed to serve in urban zones usually have to be built quickly without disturbing the ongoing traffic of nearby communications. On the other hand, their lifespan is meant to be short as they serve in urban zones which are quickly expanding, thus the possibility of easy deconstraction is especially important.

The static solution chosen was continuous composite girder due to the higher stiffness and bearing capcity. Solution for splice joints of steel girder was provided by original "simplified continuity" joint (Figure 3.43) achieved by the use of bolts and web side-plates.
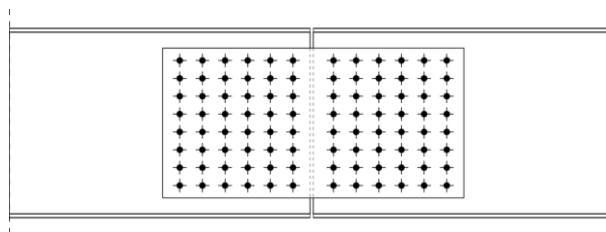
Figure 3.43 - "Simplified continuity" joint [31]

However, greater importance has the joint between the girder and the precast concrete slab. It was composed by the sleeper clips, preload bolt assemblies and neopren plates between the concrete slab and girder flange in order to provide tolerance for the conntact surface of the steel and concrete. In this manner, using the demountable friction based shear connection, composite action between the bridge concrete slab and the steel girder was achieved (Figure 3.44).
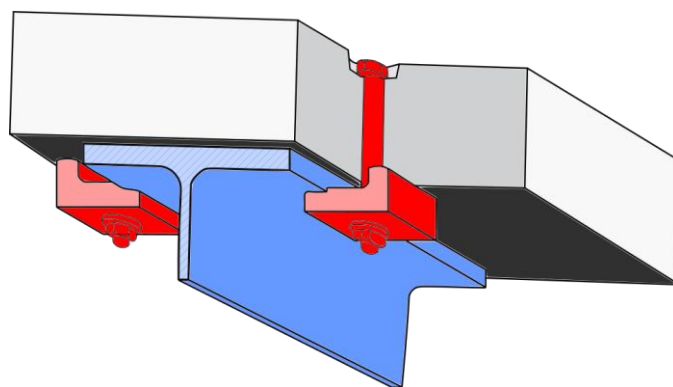
Figure 3.44 - Slab to girder connection [31]

Wang, Webster and Hajjar [15] investigated friction based demountable shear connectors. The motivation was to enhance the resuability and sustainability of composite flooring systems.

The system comprises precast concrete slabs with embedded rails coupled with the steel beam by Lindapter clamping devices and T bolt preload assemblies (Figure 3.45).
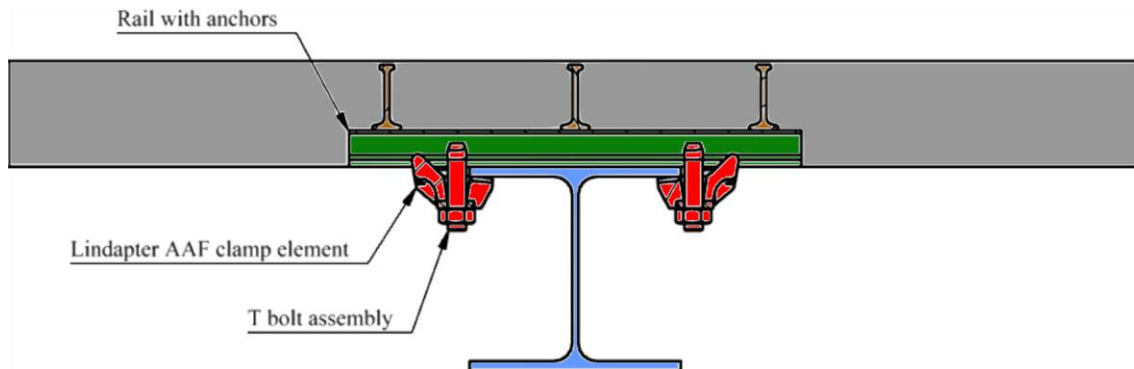
Figure 3.45 - Friction-based shear connector layout Wang et al. [15]

The longitudinal shear force arising between concrete and steel of composite section is transmitted by the friction between the underside of the precast concrete slab and the top surface of the top steel flange and bottom surface of the steel flange and clamping device.

Experimental study comprised push tests and full scale beam tests. In total 5 push test specimens and 5 beam specimens were tested. The first test specimen of push test investigation provided connection between the angle of nut turning (after snug tight condition) and the pretension force in the bolt. In push tests (Figure 3.46) variables were diamater of the bolt, number of the bolts, reinforcement layout (light or heavy), placement of shims between the clamp and the steel flange and number of nut turns after the snug tight condition (pretension).
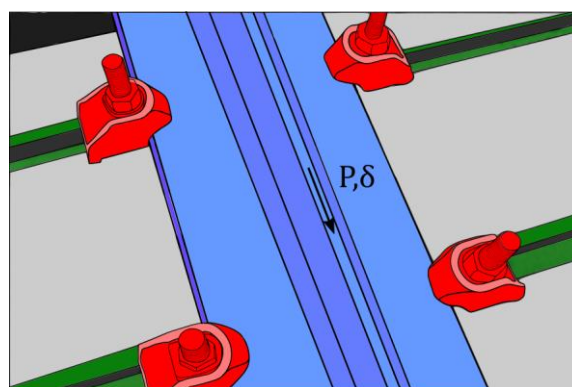
Figure 3.46 - Layout of the horizontal push test [15]

Obtained force-slip behavior (Figure 3.47) was highly ductile $\delta_u \gg 6\ mm$. Obtained ductile displacements were multiple times higher than required by EN 1994-1-1 [8] in order to clasify the connector as ductile ($\delta_{uk} \geq 6\ mm$).

Use of shims between clamp and flange exagerated stick-slip behavior and resistance oscilation. Due to this the use of shims between the clamp and the beam is highly unrecommended. Bolts M20 experienced preload and capacity loss due to the clamp rotation under the shear load. It is recommended to restrain the clamp from the rotation by detailing. This might be done by the fitting of the clamp tail in the socket of the embedded rail channel which was applied when the layout of the friction type shear connector Type A was developed within the chapter *4.2.1 Connector Type A*.
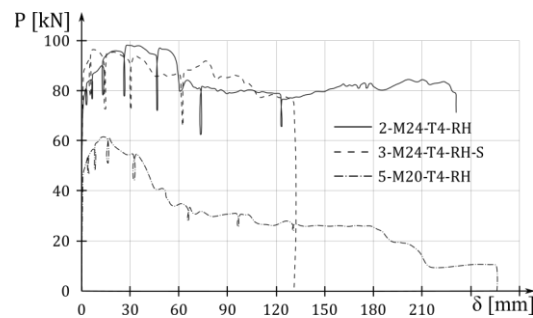
Figure 3.47 - Static force-slip behaviour of the friction based connection [15]

Cyclic push test specimen exibited preload loss due to the embedment at the friction interfaces (Figure 3.48). Degradation at the friction surfaces between the flange and concrete led to the relaxation of the bolt support conditions and pretension release. This preload loss could be accounted for in the design. After some number of cycles, stable ductile cyclic behavior was obtained making this connection also applicable as a dissipator in the seismic applications.
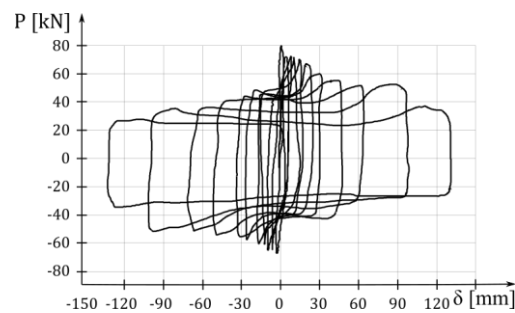
Figure 3.48 - Cyclic specimen - Capacity drop due to preload loss and stable dissipative behaviour [15]

Beside the push test investigations, four full beam tests were performed using previous solution. Various degrees of shear connection were implemented. Obtained plastic capacities agreed with the plastic design model provided by codes ([32], [8]).

As expected, stiffness increased with increase of the degree of shear connection what is governed by the Section I3.2 of AISC [32]. However, the meassured stiffness was higher than

the lower bound stiffness I_{LB} provided by AISC [32]. Explanaition is that the formula was calibrated for welded headed studs while the friction connection provides higher initial stiffness.

Conclusion was that this typology of shear connection, where the behaviour is based on friction is suitable for the application in composite beams. The efficiency may be increased further if tailored elements were developed for this particular problem. This way the problem of clamp rotation could be solved and the use of shims could be excluded.

3.6 Axial brace-type symmetric friction dumpers

Similar mechanical structural component to the friction-based shear connector that is also based on the frictional behaviour and is utilized for the seismic design of the dissipative steel structure solutions is the axial (symmetric) friction dumper.

The axial dumper is a lap joint with two faying surfaces formed on the interface between the inner steel plate and the outer plates. In order to initiate the clamping force, high strength pretension bolts are utilized. Compared to the classical lap joints, here the inner plate bolt holes are very long (they are outside the scope for long slotted holes in acc. with EN 1090-2 [11]). Instead of normal washers, coned disc springs are used beneath the nut. In the solution of Tano et al. [33] (Figure 3.49) the geometry of the disc springs does not conform to the geometry of the applied high strength bolts (i.e. DIN 6796 [34]) so special steel part (guide bush) is responsible for the transfer of the clamping force between the bolt nut and the springs.
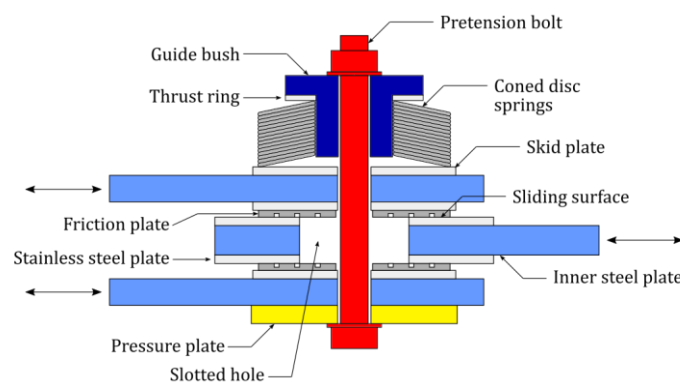
Figure 3.49 - The layout of the axial dumper Tano et al. [33]

To control the friction properties of the faying surfaces, the faying surface is formed by inserting a friction pad made of a special material (composite fibres mixed with phenolic resin).

The important element of the assembly are the disc-springs (Figure 3.50) packed in series. The main goal of the application of disc springs is to reduce the stiffness of the bolted assembly package making it far less susceptible regarding pretension loss originating from the contraction of the package due to abrasion of the friction surface under cyclic load or manufacturing errors [35].

Consequential benefit of the application of the disc springs is that the pretension force may be measured quite precise by measuring the vertical displacement of the guide bush relative to the top surface of the outer steel plate (knowing the stiffness of the springs).
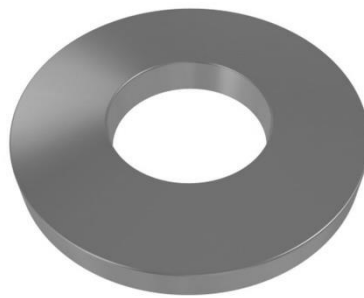
Figure 3.50 - Disc spring DIN 6796

The aimed performance of such a mechanical component is that under the normal exploitational loads (SLS) the component behaves rigid without developing slip in the joint under the axial load of the brace. However, at the seismic design situation (ULS), the component is meant to dissipate the seismic energy by sliding friction in a stable hysteretic manner. These requirements are similar if not the same in the case of the demountable shear connector developed within the scope of this work as well.

To test the concept, the test assembly comprised M27 high-strength pretension bolts paired with 13 disc springs stacked in series, inner plate $t_{ip} = 22mm$ and outer plates $t_{op} = 16mm$ and two friction plates of thickness $t_{fp} = 4.3mm$ (Figure 3.49).

The obtained force-displacement (force-slip) response (Figure 3.51) was extraordinarily stable. The obtained hysteretic curve was stable under the large slips and constant axial force. This was surely possible by conserving the pretension (clamping) force by applying the disc springs in the bolted assembly and by taking care of the friction properties of the faying surfaces with the application of the special friction materials.
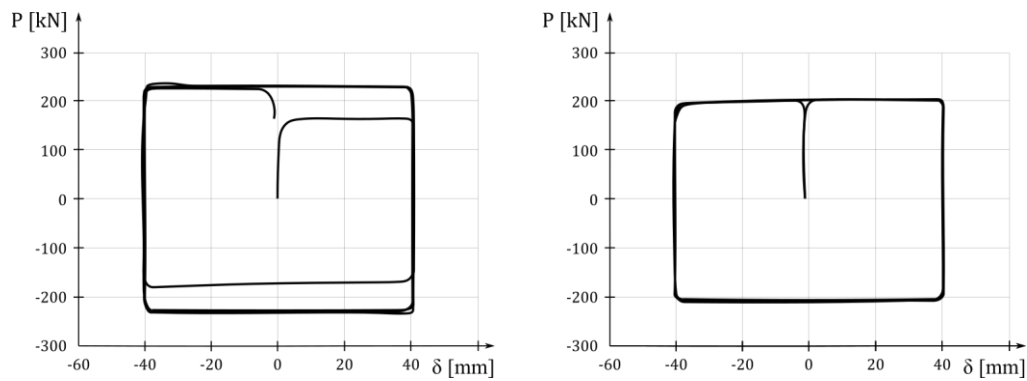
Figure 3.51 - Force-slip response under the cyclic load [33]

The same mechanical response is highly favourable in the case of shear connector as well regarding initial stiffness (rigid) and ductility.

Having in mind the problems of the pretension force loss regarding friction grip connectors due to the concrete creep in the vicinity of the bolt hole and the abrasion of the faying surfaces under large slips what has been identified in the chapters *3.2* and *3.5* it is advantageous to consider the application of the disc springs as it was done later in this work when the novel friction-based shear connector was conceived.

3.7   Moment frame-type asymmetric friction dumpers

The friction dissipation principle was also applied for the dissipative seismic design of beam to column joints in the case of steel moment frames. The dissipative action is also based on sliding friction but the assembly is asymmetric due to the absence of one cover plate in comparison to the case of lap joint. The layout of the connection proposed by Ramhormozian et al. [36] may be observed in the following figure (Figure 3.52).
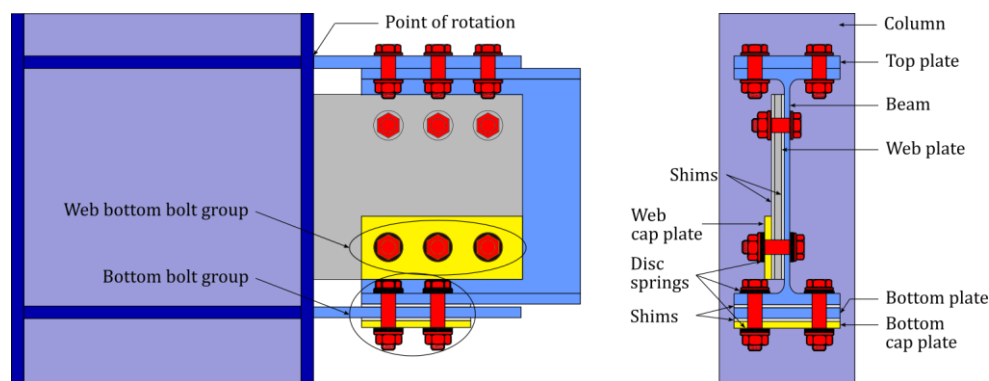
Figure 3.52 - Asymmetric friction-dissipative beam-column joint [36]

Two faying surfaces are formed, the first between the bottom flange of the beam section and the bottom flange plate of the column and the second between the bottom flange plate of the column and the additional cap plate (Figure 3.52). Here the bolt holes in the bottom flange of the column are slotted, hence the point of rotation of the assembly is located at the joint between the column and the top plate.

Compared to the axial dissipative friction component the behaviour is more complex. Under the rotation of the joint (moment) the first slip occurs after reaching the slip capacity of the first faying surface (point B).
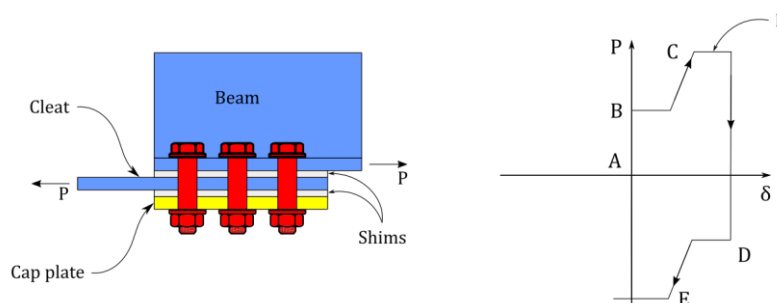
Figure 3.53 Double curvature stress-strain state of the bolt after slip at the first faying surface [36]

Afterwards, the second faying surface is activated. The friction force generated at the second faying surface is transferred into the beam section flange by shear and bending of the bolt

bringing it into combined M-V-P stress state (double curvature state) presented in the Figure 3.54.
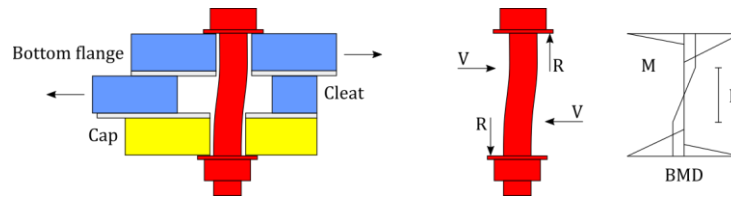
Figure 3.54 - Double curvature stress-strain state of the bolt after slip at the first faying surface [36]

This second part is characterized as a finite-stiffness branch in the force-slip diagram (B-D) and it is attributed to the bending stiffness of the bolt and its support boundary conditions. After reaching the friction capacity at the second faying surface (point C) the sliding should occur in ductile manner at the ultimate capacity of the component.

The contribution of the second faying surface (resistance) is directly dependent on the pretension force F_{pc} and the coefficient of the friction at the same faying surface. As this force is transferred through the bolt that is already highly utilized by the bolt preload ($0.7f_{ub}$ in acc. with EN 1090-2 [11]), the additional stresses lead to the yielding of the bolt material and significant drop of the pretension force ($\cong 40\%$) hence to the drop of the resistance of the component as whole.

The most effective measure to mitigate the effects of this phenomena and to allow for better predictability of the component behaviour is to decrease the applied pretension ($0.3 - 0.6\ f_{ub}$) regarding the design one ($0.7f_{ub}$) what provides large elastic reserve in the bolt material in order to avoid pretension loss due to combined M-V-P state.

The preload loss as in the case of symmetric friction component is not restricted only to the mechanics of the component. The preload loss is also inflicted due to the surface abrasion, creep of the faying surfaces and vibration induced loosening of the pretension assembly. Hence, in this case as well, it is highly recommended to apply the disc springs in the preload assembly in order to mitigate the sources of the pretension loss.

4. Structural concept of novel demountable steel-concrete composite floor

4.1 Structural layout

The structural layout of the demountable composite flooring system investigated within the research work of Work package group 2 of ECON4SD project performed at the Department of engineering (research area structural engineering and composite structures) of the University of Luxembourg is devised applying the principles of modularity and demountability.

The concrete slab is composed of a series of one-way concrete slab elements (simply supported and continuous) which are placed in horizontally offsetted layout on to the top of the simply supported grillage of secondary steel beams (Figure 4.1). The horizontally offsetted layout is applied in order to improve the inplane behaviour of the floor system and the distribution of the load among the secondary beams. The secondary composite beams are supported by the primary steel beams by the means of simple, pinned joints [28].
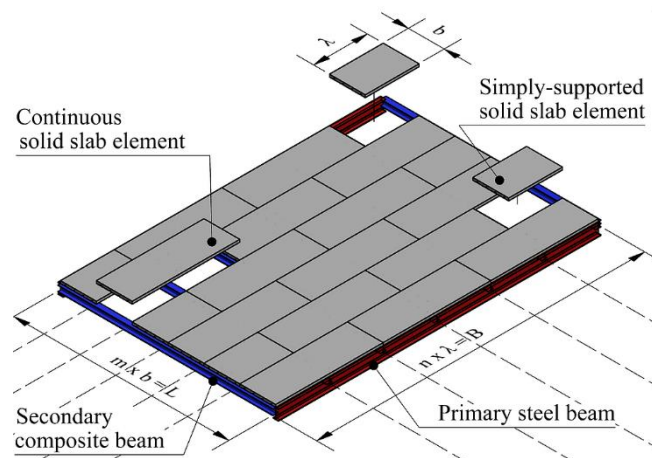
Figure 4.1 - The layout of the demountable composite floor

The floor system is erected in the unpropped condition decreasing resource demand at the construction stage. The steel sections are precambered in order to negate the deflection of the steel section under the self-weight load of the concrete slab and the steel section of the secondary beams.

After the placement of the slab elements what deflects the beams and floor in flat state (counters the designated self-weight precamber) the shear connection is initiated providing the composite response of the floor (beam) system. During the mounting of the modular elements and

assembly of the connector devices the steel sections are laterally braced in order to exclude the lateral instability of the secondary beams during the construction stage.

The modularity of the slab system is related to the following modular dimensions:

1. Width of the slab element – b

2. The span of the solid slab element (spacing of the beams) – λ

3. The spacing of the connectors (rails) along the width of the slab element – e

4. The span of the steel section – L

5. The width of the floor – B

These dimensions have to be related to the standardized architectural grids for the contemporary office and residential building where the distances are based on the basic grid distance λ $(2.5m\,;2.7m\,;3.0m)$ that are a product of unit length $(1.25m\,;1.35m\,;1.5m)$ [6].

Depending on the position of the concrete solid slab element in the horizontal offsetted layout, the elements are divided into two groups (Figure 4.2):

- Simply supported – Supported by two steel beams
- Continuous – Supported by three steel beams (one mid-support)
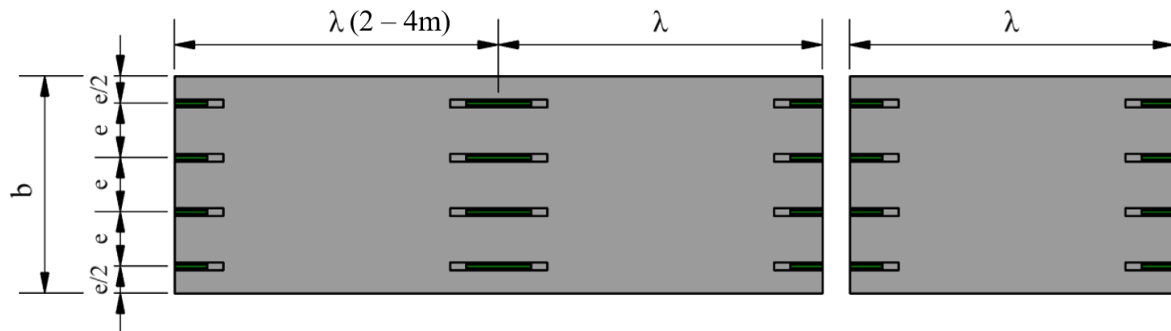
Figure 4.2 - Continuous and simply supported slab element

The one-way solid slab is characterized by its span λ, width b and its slab depth h_c. Along its width (b) embedded rails with anchors serve as an anchor point for the application of the demountable shear connector. The concrete recess allows access for the installation of the shear connector.

Especially important is the spacing between the rails (e) along the width of the modular element (Figure 4.3). As the requirement of the modularity of the slab element is that the spacing of

rails (e) is uniform along its width, hence the spacing of the shear connectors is uniform along the span of the composite beam (L). These bears consequences for the mechanical model of the composite beam behaviour as well.

As the distance between connectors is uniform, in order to fully utilize their strength along the span of the composite beam, it would be highly recommended that the shear connector may be classified as ductile ($\delta_{u,k} \geq 6\ mm$). Allong the additional requirements defined by chapter 6.6 of EN 1994-1-1 [8] the plastic moment capacity M_{pl} at the midspan shall be reached with uniform distribution of the longitudinal shear V_L (ideal plastic redistribution) along the span of the composite beam ([37], [38], [8]) when fulfilling the bending capacity criteria.
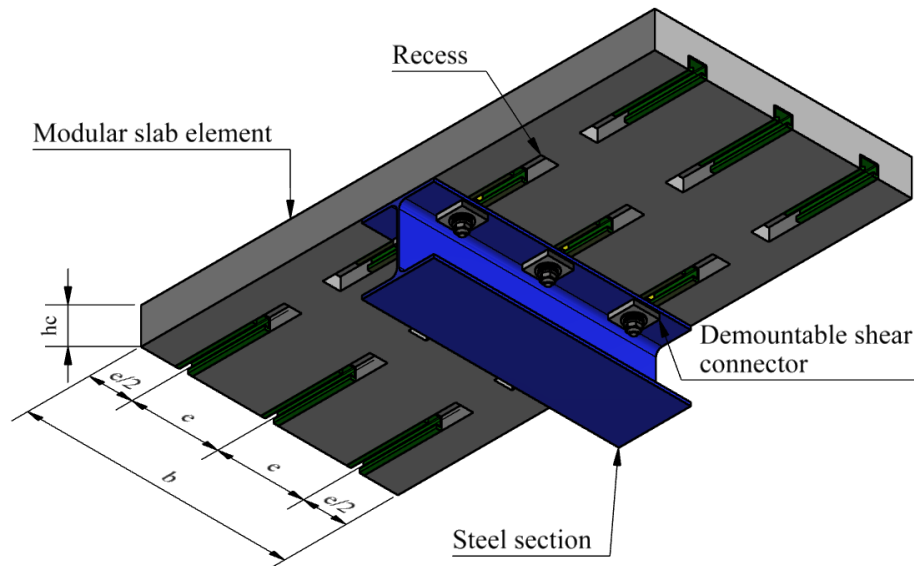
Figure 4.3 - Modular slab element with integrated shear connectors

The stiffness of the shear connector at the serviceability load levels should be enough for the complete interaction behaviour ([37], [38], [8]). This is partially solved applying the unpropped construction method where the connectors are relieved of the effects produced by the self-weight of the floor. However, this includes precambering of the steel section as well.

Second measure is the application of the full degree of shear connection $\eta = 1.00$ what is optimal regarding the composite beam bending capacity as the complete potential of the composite cross section is utilized (full plastic capacity $M_{pl,rd}$). Having this in mind the optimal spacing of the shear connectors (e) is related to the shear capacity of one shear connector (P_{rd}) and the axial capacity of the steel cross-section (assuming that the plastic neutral axis is within the thickness of the concrete slab as it is the most common case for economic design).

During the placement of the slab elements, besides the geometrical imperfections and the tolerances regarding the production of modular slab elements, the steel section experiences certain deformation (inclination and deflection). In order to successfully place the bolts, the bolt holes along the span of the steel section have to have a certain degree of tolerance (large diameter or slotted bolt holes) if the bolts are placed through the flange of the steel section.
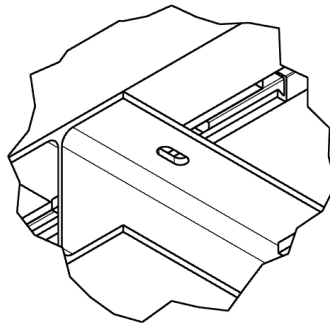
Figure 4.4 - Slotted bolt holes and the rail

As the concrete embedded HTA CE 72/48 rails [39] are parallel to the primary beams that support the secondary composite beams, the primary beams may not be connected with the slab hence remain pure steel beam elements.

The layout of all connector typologies is devised in a way that the pretension force introduction is realized by the steel parts (rail plate, rail channels and clamps or back plates). The benefit of this technology is the mitigation of the pretension loss due to the introduction of the pretension force through the thickness of the concrete deck related to the high compressive stress localization in the surrounding concrete explained in the chapter *3.2 Friction grip connectors*.

The connector systems devised within the course of this work were of two typologies, friction and friction-grip. Two connector devices were devised per each typology (in total four connector devices were investigated).

In the case of connector types B,C & D the thickness of the clamping package was reduced compared to the friction-based solution presented in the chapter *3.5 Friction based connectors*. Therefore, the pretension loss effects related to the bolt bending are limited.

4.2   Friction based connectors

The friction-type connectors rely completely on the friction response as a mean for the provision of the connector stiffness, shear resistance and ductility. In order to provide the clamping force, preloaded high strength HV 10.9 bolt assemblies were applied.

4.2.1   Connector Type A

Connector Type A is a friction-based connector. It is composed out of the clamp assembly made out of S355 JRG steel material, M24 EN 14399-4 HV [40] high strength pretension bolt with the corresponding M24 DIN 6796 disc spring, oversized outer diameter washers M24 ISO 7093 [41] and the rail plate that conforms to the Halfen HTA 72/48 rail channel in order to accommodate the M24 HV bolt into the rail channel socket and block its rotation during the application of the torque (Figure 4.5). The exact geometry of the assembly parts of connector system Type A are provided in the *Annex A - Geometry of custom-built connector assembly parts* of the manuscript.
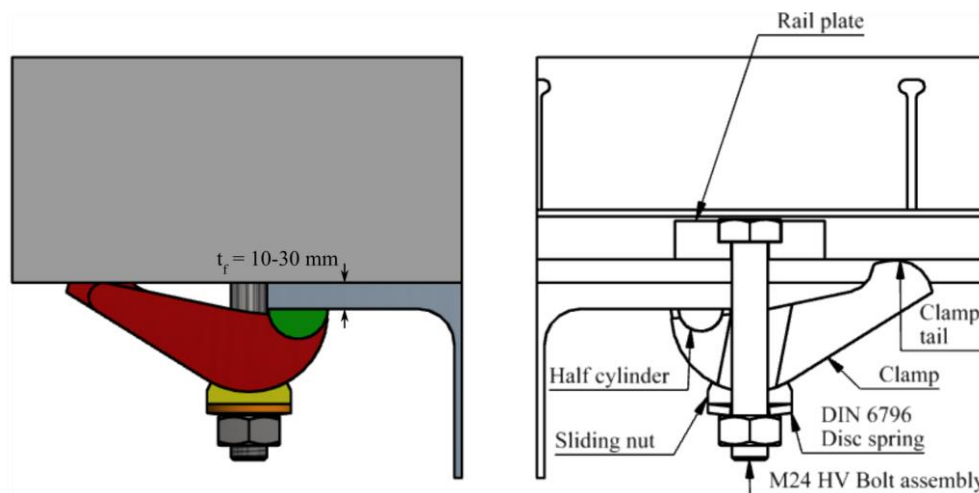
Figure 4.5 - Connector Type A cross section

As the bolt is offset regarding the edge of the steel flange, there is no need for having bolt holes along the steel flange. This also mitigates problems at construction stage that could arise from manufacturing tolerances.

After the placement of the connector the bolts are preloaded to the designated pretension level and the clamping force is introduced at the two distinctive interfaces. The top faying surface is formed between the concrete modular element and the top of the steel flange while the bottom

is formed between the clamp and the bottom surface of the steel flange. The faying surfaces in the later experimental stage for this connector type are sand blasted.

Regarding the previous friction-based solutions as demonstrated by Hajjar et. al [15] and Baggon [31], the clamp element is made specifically for this role and its tail fits into the rail socket of the rail channel preventing free rotation under the lateral (shear) load (Figure 4.6).
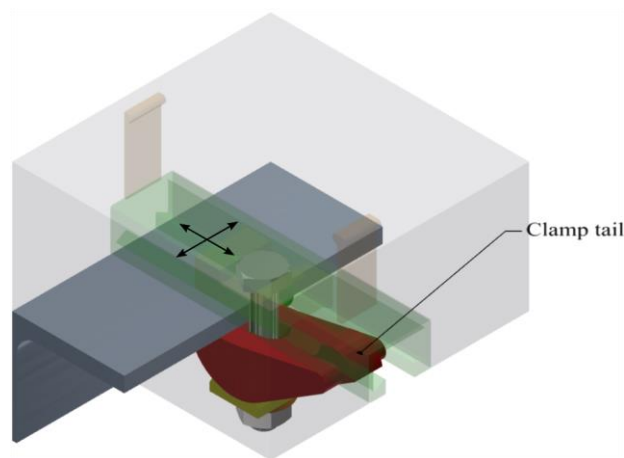
Figure 4.6 - Connector Type A

The sequencing of the shear connection is the simplest in comparison to the later solutions (Figure 4.7). After the placement of the concrete one-way modular solid slab elements the clamp connector is independently post-installed connecting the slab and the steel section. This allows for ease of construction and for practically no limitations regarding the execution tolerances.
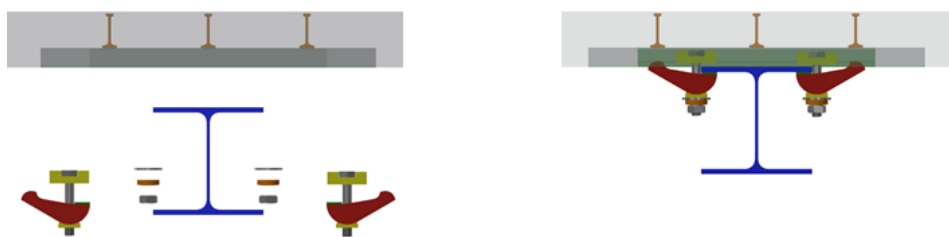
Figure 4.7 - Connector Type A sequencing

The clamp is provided with a sliding nut that is in contact with the disc spring and a rotating half-cylinder that forms the second faying surface. This layout allows for the clamp to cover different clamping heights (flange thicknesses in range of HEA200 – HEA800 sections) by the rotation movement of the aforementioned parts. Before the milling of the assembly components, the pieces were 3D printed and fitted as in the test assembly.

Due to the geometry of the clamp the clamping reaction is not equivalent to the pretension force.
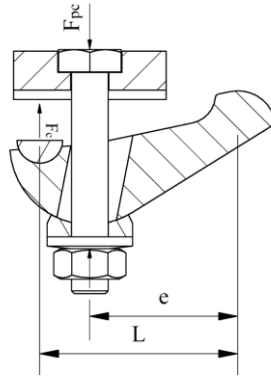
Figure 4.8 - Clamping device Type A

The amount of pretension transformed into the clamping force at the two interfaces depends on the clamp geometry (Figure 4.8), eccentricity (e) and length (L). Hence the clamping force is only a fraction of the pretension force:

$$F_c = \frac{F_{pc}e}{L} = F_{pc}a$$

(4.1)

The eccentricity e may not be indefinitely increased in order to increase the effectiveness of the pretension force as the clamping element itself is being bent under the pretension force. The custom designed clamping assembly produced for the needs of this research (Figure 4.9) has a reaction coefficient of $a = 0.75$ and its geometry was numerically optimized in order that it remains completely elastic under the design pretension force of M24 HV pretension bolt ($F_{pc} = 247kN$).

Figure 4.9 - Clamp assembly

The disc springs are provided in order to mitigate the issues of pretension loss related to the embedment of the clamping package, temperature differences and the sliding action [35]. As well, the pretension force in the later experiments due to the expected M-V-P interaction explained in the chapter *3.7 Moment frame-type asymmetric friction dumpers* will be fraction of the design pretension force F_{pc} related to $0.7f_{ub}$ stress level [11]. This is the case with both shear connectors based on friction that were investigated within the scope of this work.

The number of the applied disc springs (in this case in series) has to be devised regarding the applied pretension force F_p. In order to provide highest redundancy of the pretension assembly, the springs should elastically deform as much as possible when reaching the designated pretension F_p [35], [36].

4.2.2   Connector Type B

Connector Type B is the shear connector composed out of zinc-galvanized S355 JRG friction backplate, M24 EN 14399-4 HV high strength pretension bolt assembly with the corresponding DIN 6796 disc springs, oversized outer diameter washers M24 ISO 7093 and the rail plate in order to accommodate the bolt into the rail channel socket and prevent its rotation during the application of the torque (Figure 4.10). The assembly is similar to the moment frame-type assymetric friction-dumpers (Chapter 3.7) where the back plate provides additional faying surface besides the one at the intefrace of the concrete slab and the top flange, but for the first time it is furtherly developed as a shear connector.
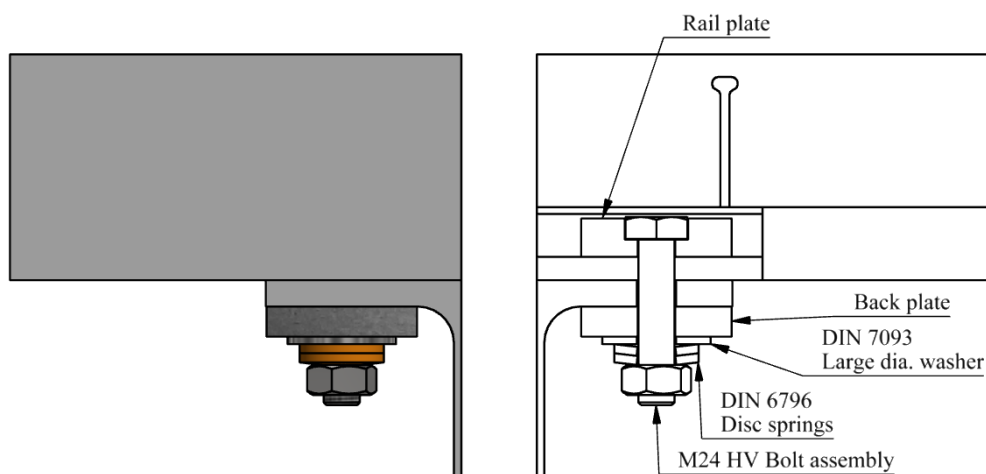
Figure 4.10 - Connector Type B cross section

The rail plate element allows for application of standard M24 HV high-strength pretension bolt assemblies that are stiffer (unthreaded bolt shank portion) compared to the channel complying

HS T bolt and provide better boundary conditions leading to the overall stiffer response of the assembly under the shear load. It also allows for better distribution of the contact stresses between the bolt head and the rail channel which mitigates the later pretension loss due to the embedment phenomena at the contact surfaces. The thickness of the rail plate is derived from the requirement that the plate material remains elastic at the design pretension force of M24 HV high-strength bolt ($F_{pc} = 247kN$). The rail plate geometry in the case of connector Type B is provided within the *Annex A - Geometry of custom-built connector assembly parts*.

The backplate has a normal diameter round hole, it is positioned flush regarding the bottom surface of the steel section top flange, hence the appropriate bolt holes along the steel section are required. In order to provide necessary execution tolerance and the shear response by friction only, the slotted holes (Figure 4.11) with the maximum slot length are chosen in accordance with EN 1090-2 [11].
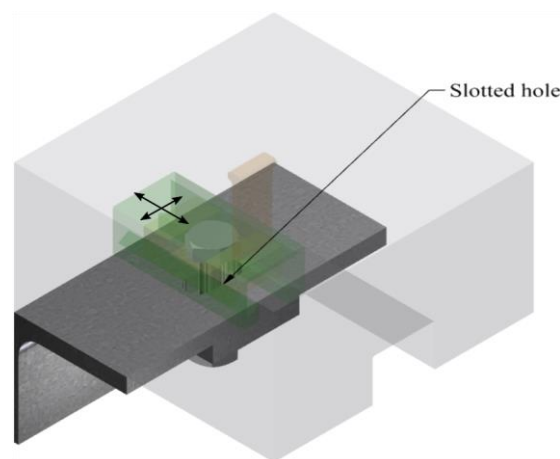
Figure 4.11 - Connector Type B

In the similar manner the two faying surfaces are formed, one between the concrete modular element bottom surface and the top surface of the top flange and one between the bottom surface of the top flange and the top surface of the back plate. In the later experimental campaign, the steel section and the back plate were hot-dip zinc galvanized.

Figure 4.12 - Connector Type B sequencing

The sequencing of the floor system composed using the connector Type B assembly is slightly more demanding (Figure 4.12). Before placing the slab onto the steel section, the bolts that are previously placed into the rail plates have to be slid first into the rail channel. This method seems demanding but there is large tolerance in both directions (along the slotted hole and transversely along the rail channel) which allows for easy installation of the connector system.
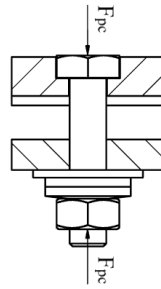
Figure 4.13 - Clamping device Type B

The complete pretension force is transformed into the clamping force (Figure 4.13). The shear capacity of this shear connector is based on the clamping force and the frictional properties at the mentioned faying surfaces. Compared to the connector Type A, the second faying surface is the surface between the back plate and the bottom of the steel section. The adequate disc springs are applied in the connector assembly due to the same reasons explained in the chapter *4.2.1 Connector Type A*.

4.3   Friction-grip type connectors

The friction-grip type connectors rely partly on the friction generated resistance (slip capacity) followed by the bearing of the bolt shank until the shear failure. In the scope of this research two connector layouts were considered, one applying standard EN 14399-3 HR 8.8 [42] pretension bolt assemblies and one applying the Halfen HS T 8.8 bolts [39].

4.3.1   Connector Type C

Connector Type C is the shear connector composed out of the friction backplate S355 JRG, M20 EN 14399-3 HR 8.8 high strength pretension bolt assembly with the corresponding M20 DIN 6796 disc springs, oversized outer diameter washers M20 ISO 7093 and the corresponding rail plate in order to accommodate the bolt into the rail channel socket and prevent its rotation when the torque is applied (Figure 4.14). The rail plate geometry in the case of connector Type C is also provided within the *Annex A - Geometry of custom-built connector assembly parts*.
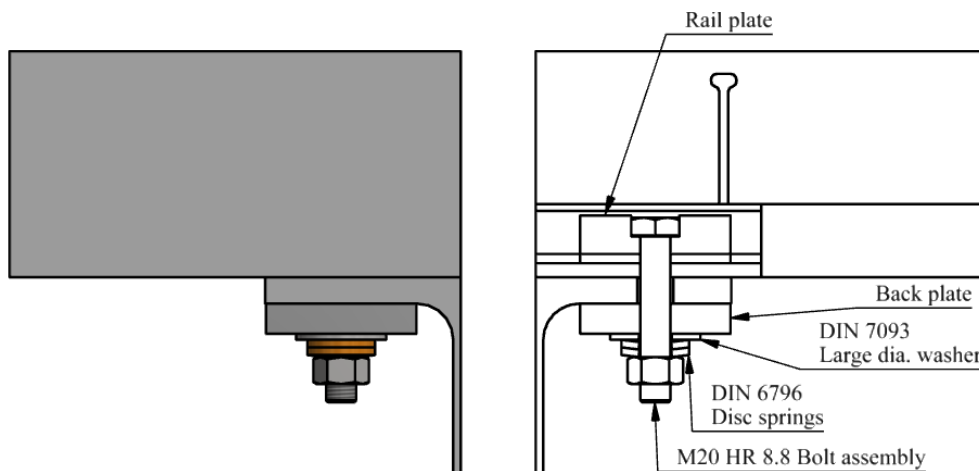
Figure 4.14 - Connector Type C cross section

The backplate has also in this case normal diameter round hole and it is positioned flush regarding the bottom surface of the steel section top flange. The bolt holes along the steel section are oversized round bolt holes (Figure 4.15) in accordance with EN 1090-2 [11] allowing for the bearing response after the bolt hole is closed (friction-grip connectors).

Similarly to the connector Type B, two faying surfaces are formed on the top and the bottom surface of the steel section top flange. In the course of the experimental campaign both the steel section and the back plate were hot dip zinc galvanized.
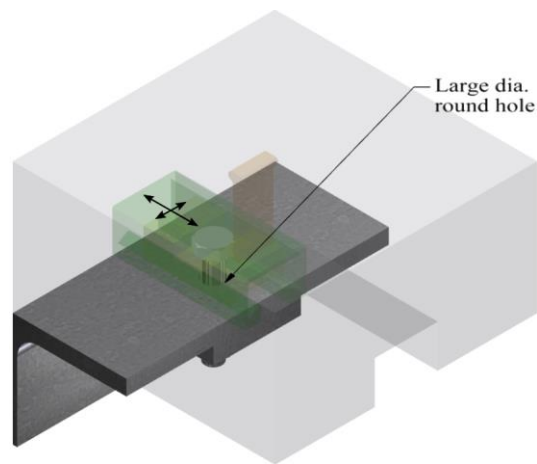
Figure 4.15 - Connector Type C

The sequencing of the shear connection is similar to the sequencing in the case of shear connector Type B (Figure 4.16). The difference is that as the bolt hole is round there is limited tolerance in the direction of the beam span (in the perpendicular direction the rail channel still provides adequate geometrical tolerance). However, the application of oversize round holes allows for sufficient geometrical tolerance in the direction of the beam span as well.

Figure 4.16 - Sequencing of the connector Type C

The pretension force applied to the high strength bolt is directly transformed into the clamping force at the faying surfaces (Figure 4.17) providing the initial frictional restraint (slip capacity).
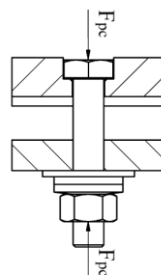
Figure 4.17 - Connector device Type C

After surpassing the slip capacity, the sliding friction provides the shear capacity until the bolt shank touches the bolt hole of the flange. Later, the bolt loaded in axial force, shear and the

corresponding moment is providing transfer of the shear force between the steel section and the concrete slab.

4.3.2   Connector Type D

Connector Type D is the shear connector composed out of friction backplate, Halfen HS T 8.8 M20 bolt assembly [39] with the corresponding M20 DIN 6796 disc springs and oversized outer diameter washer M20 ISO 7093. The rail plate is omitted as the T bolt which is used in conjunction with the HTA CE 72/48 rail channel is applied (Figure 4.18).
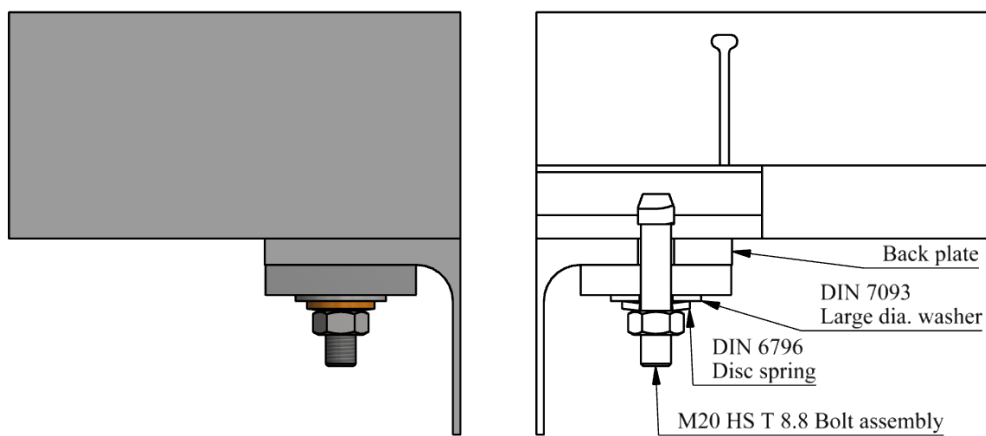
Figure 4.18 - Connector Type D cross section

The shear connector Type D corresponds to the connector Type C in layout and behavior. The only difference is that there is no requirement for the rail plate due to the application of the corresponding T bolt (Figure 4.19). In the later experimental investigation, the steel section and the back plate are as well hot dip zinc galvanized.
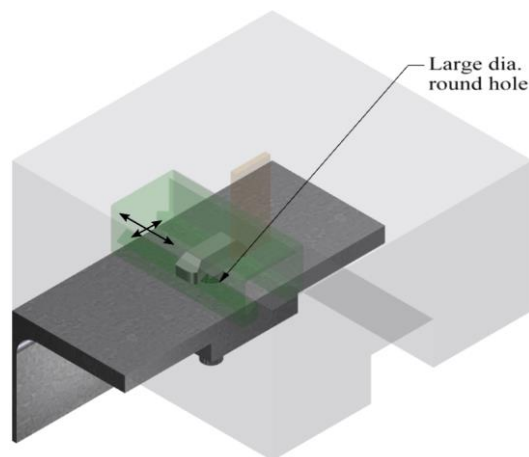
Figure 4.19 - Connector Type D

The sequencing is similar to the sequencing order of the shear connection Type C, however the fitting of the bolt assembly is quite simpler as the T bolt fits the geometry of the Halfen HTA/CE 72/48 rail channel (Figure 4.20).

Figure 4.20 - Connector Type D sequencing

The pretension force generated by preloading the T bolt is directly transferred into the clamping force (Figure 4.21) that acts at the two distinctive aforementioned faying surfaces.
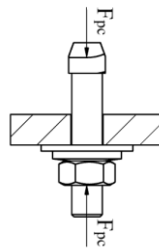
Figure 4.21 - Connector device Type D

The benefit of this solution is that all the parts are market available. However, the solution with the rail plate has advantages in terms of application of high strength pretension bolt assemblies (EN 14399-3 HR and EN 14399-4 HV), better transfer of the pretension force between the bolt head and the rail lips (contact embedment) and stiffer boundary conditions regarding the bolt.

5. Experimental campaign

5.1 Push tests

5.1.1 Procedure

In order to investigate the mechanical behaviour of the previously defined shear connectors (stiffness, strength and the ductility) the set of push tests were performed in accordance with the Annex B of EN 1994-1-1 [8]. For each connector typology a series of 3 push specimens were tested (minimum number of test specimens per series).

The steel section HEB 260 is connected to the concrete slabs by the means of shear connectors. It is pushed from the top by the hydraulic jack of the test frame. The applied force per connector and the displacement at the position of each connector row (slip) are measured and plotted forming the force-slip curve of the test specimen (Figure 5.1).
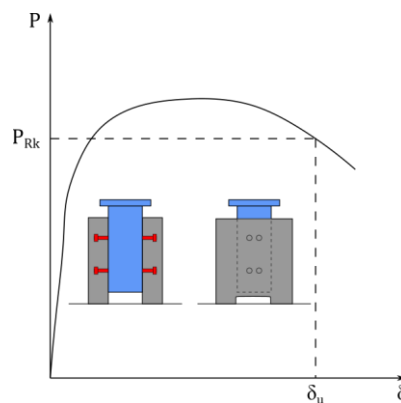
Figure 5.1 - Force slip curve and characteristic values [8]

The first specimen is tested monotonically in displacement-controlled mode up to the ultimate capacity. In the displacement-controlled mode, the application speed was also adjusted for quasi-static response of the system with the hydraulic jack speed of $0.25\ mm/s$. In this manner the failure was always reached after the minimum of $t_{min} = 15min$.

Subsequent two specimens are tested firstly in cyclic manner in the load range between $5 - 40\%$ of ultimate capacity $F_{u,1}$ obtained in the first monotonic test. The application speed of $6\ kN/s$ in cyclic test step is low enough to simulate quasistatic load application. The number of harmonic cycles was set as per code to $n = 25$. After the completion of the cycling load sequence, the test is continued in displacement control mode until failure.

5.1.2 Layout

The solution with recess in the slab was chosen for the test specimen (Figure 5.2). The test specimens were composed out of two concrete slabs (with long or short rail channels), HEB 260 steel section (hot-dip zinc galvanized except for the connector Type A that was sandblasted) and the lateral-restraint assembly composed out of four L sections and four M20 8.8 threaded rods that were snug tightened. To distribute the load uniformly between the slabs and floor, the slabs were placed on the grout that was cured for $24h$.
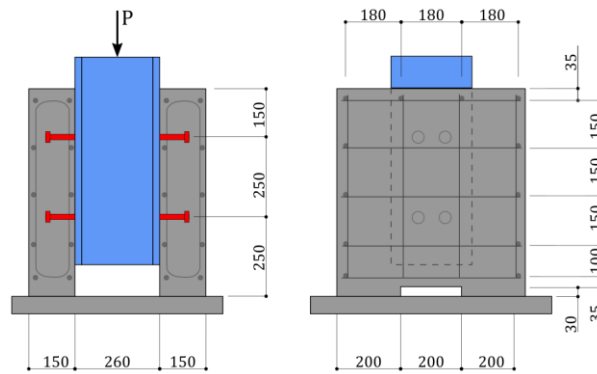
Figure 5.2 - Layout of the standard push test assembly with recess [8]

The slabs were provided with two embedded HTA-CE rails with anchors (Figure 5.3). In the case of Type A connector system, they were $600mm$ long while in the case of connectors Type B, C and D they were $300mm$ long and centrally positioned. To access the rail for the installation of the connector assembly, the concrete recess was provided. After the placement of the connector assembly, the bolts were preloaded using torque method in cross sequence to the target pretension level. In order to obtain uniformized pretension results Molycot G Rapid bolt lubricant was used.
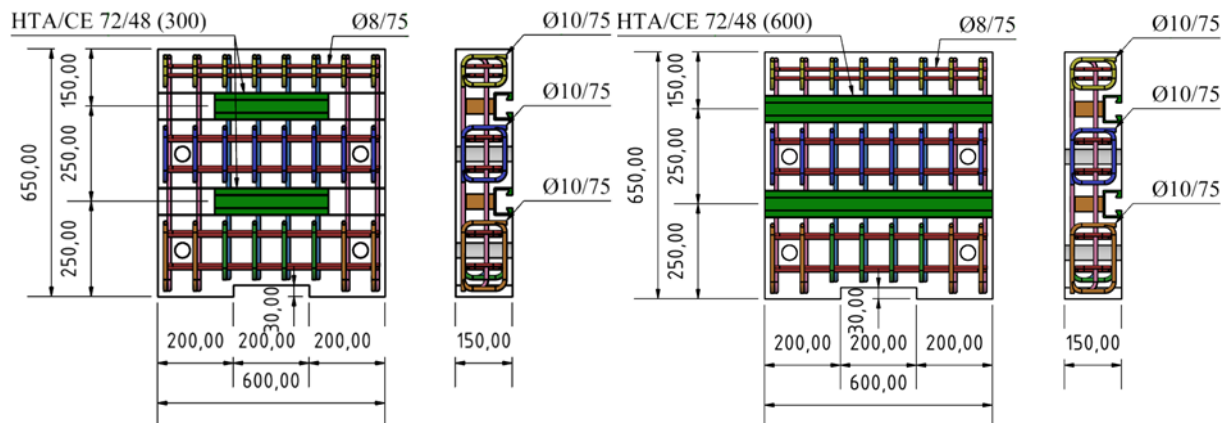
Figure 5.3 - The push specimen slabs (short and long rail)

In contrast to the provisions of EN 1994-1-1 Annex B the interface between the steel section and the concrete slab was not greased as the capacity is partially or completely based on friction.

The reinforcement of the slab elements was slightly denser than in the code provisions (ϕ10/75) in order to eliminate concrete related failure modes (Figure 5.4). This is acceptable as the modular concrete elements are meant for multiple reuse.

Figure 5.4 - The casting of the slab elements

The longitudinal reinforcement was represented by hooks ϕ8/75 while the transversal reinforcement was provided in form of stirrups ϕ10/75. The transversal reinforcement in actual application may be gradually reduced moving away from the point of the load introduction (shear connector). The exact layout of the test specimen concrete slab is provided within the *Annex B - Layout of the concrete slab* of the manuscript.
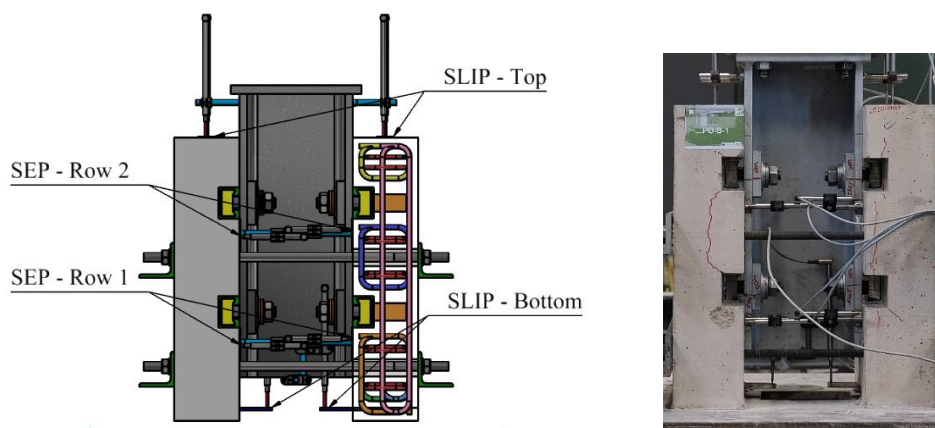
Figure 5.5 - The measurement layout

The force measurement was obtained directly from the readings of the hydraulic jack and divided by the number of connectors to obtain the force per connector. The displacement

measures were obtained from 14 LVDT sensor units (Figure 5.5). The slip displacement sensors had a range of $50mm$ while the separation measuring sensors $10mm$.

For the measurement of slip displacement four units were positioned at the top of the slab elements. The remaining two units were placed at the bottom. Especially these two are of significance as they were measuring the slip displacement without severe influence of the concrete deformation between the measuring points. Besides slip, eight LVDT units were measuring the separation displacement at the point of each connector and they were grouped by rows.

5.1.3 Schedule

The first performed push tests were for friction type (A&B) shear connectors followed by the friction-grip (C&D) typologies (Table 5.1). The tests were performed using the testing frame in campus Kirchberg and newly established laboratory facility in campus Belval of the University of Luxemborug. Test frames of $1MN$ and $4MN$ capacity were utilized for the execution of the push tests where the later were used for friction-grip type connector specimens.

Table 5.1 - The push test schedule

Series	Specimens	Connector type	Bolt	Disc springs DIN 6796	Pretension force [kN]	Faying surfaces
PO-A	3 (1+2)	Friction	M24 HV	M24 (1)	160 (65%)	As rolled
PO-B	3 (1+2)	Friction	M24 HV	M24 (2)	175 (70%)	Zinc-Galva
PO-C	3 (1+2)	Friction-grip	M20 HR 8.8	M20 (2)	140 (102%)	Zinc-Galva
PO-D	3 (1+2)	Friction grip	M20 HS T 8.8	M20 (2)	130 (95%)	Zinc-Galva

The designated pretension force F_p was less than the design one F_{pc} for the friction-based shear connectors (65% and 70%) compared to the full design pretension force in the case of the friction grip-connectors. This allowed for certain elastic reserve in the bolt material in the case of earlier. This reserve is not necessary for the friction-grip connectors as in the final phase of the response they rely on the shear capacity of the bolt shank.
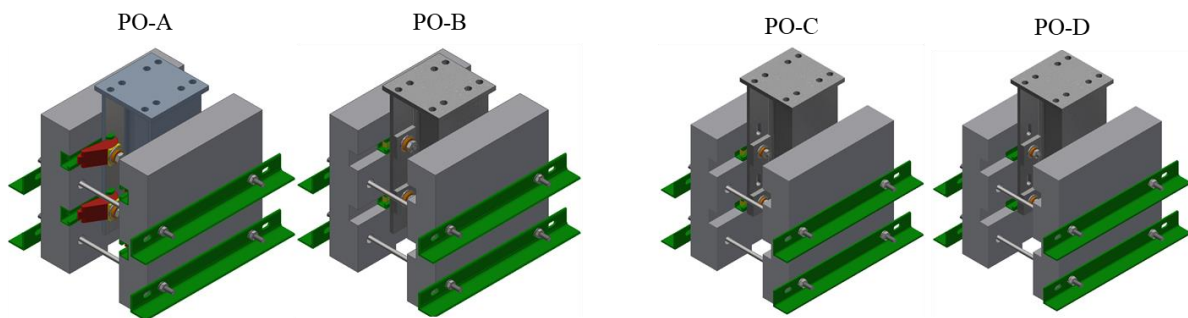
Figure 5.6 - Push test series

Each test series (Figure 5.6) was composed out of 3 identical specimens where the first was tested only in the displacement control mode. Based on the results of the first specimen the force levels for the cycling step were devised and applied to the following two specimens of the same series. After the cycling sequence the same specimens were tested until failure in the displacement-controlled mode.

5.2   Pretension tests

5.2.1   Procedure

In order to create a reliable relation between the torque that has to be applied using torque method and the target pretension force set in the previous chapter, the torque calibration tests in accordance with EN 1090-2 Annex H [11] were performed (Figure 5.7).
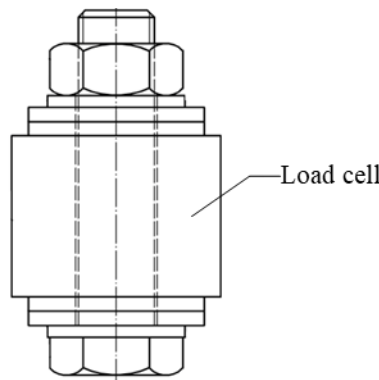
Figure 5.7 - Torque calibration test assembly [11]

The pretension assembly in the torque calibration tests was designed to recreate as close as possible the one in the push test. In order to uniformize the torque results Molykote G Rapid Plus bolt lubricant was applied at the faying surfaces of the pretension bolt assembly (threads and washer contact surfaces).

The bolts were preloaded gradually in steps using the torque wrench and the pretension force was recorded via the load cell. Every series consisted of 8 pretension bolts except in the case of connector Type A (7). Based on the established relationship between the torque M_t and pretension force F_p, the pretension force could be estimated based on the applied torque with allowable coefficient of variation up to $V_M \leq 6\%$.

When the design torque was determined, it was applied in the push test assembly in two steps. In the first step $M_{t,1} = 0.75 M_t$ and in the following step $M_{t,2} = 1.1 M_t$. This way the additional 10%

of the torque remedies the short term pretension losses between the torqueing and the execution of the push test [11].

5.2.2 Connector Type A

In the case of the connector Type A there was not enough space to use load cell in the torque calibration assembly directly. Firstly, the strain gauges were applied on the surface of the bolts at the midpoint of the shank length (Figure 5.8). In the tensile machine ZWICK 400 the bolts were axially loaded in tension.
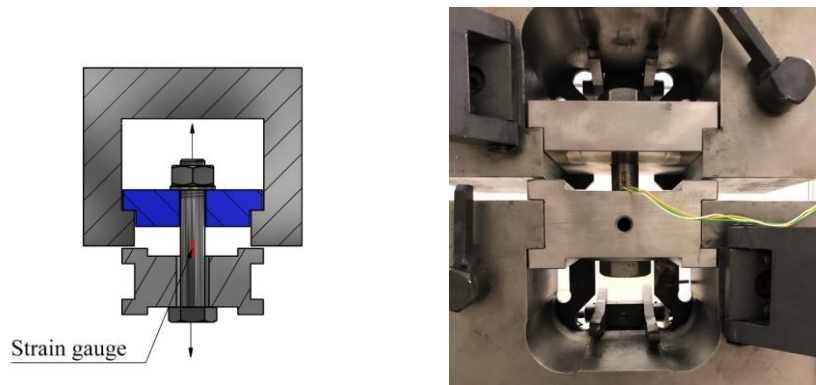
Figure 5.8 - Force vs. strain correlation test assembly

Based on these results for each bolt the relationship between the strain gauge measurement and the bolt force was created. If the mean modulus of elasticity obtained from the tensile tests for HV M24 bolts $E_{HV} = 210.667 GP_a$ is assumed, the experimentally obtained correlation between the strain and the bolt force matches the theoretical values.
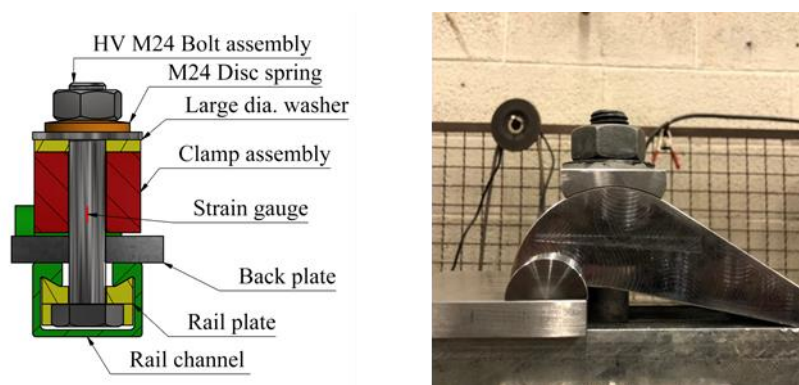
Figure 5.9 - Torque calibration assembly Type A

In the next step the torque calibration assembly was exploited (Figure 5.9). The assembly closely represents the actual bolt assembly in the push test series PO-A. The bolts were gradually torqued and the pretension force was extracted on the basis of strain gauge readings

and the previously established correlation between the bolt force and the strain. The following obtained curves represent the relationship between the preload torque and the pretension force (Figure 5.10).
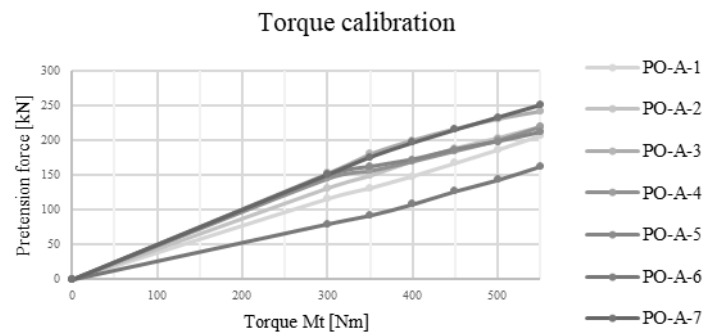
Figure 5.10 - Torque vs. pretension force - Assembly Type A

Based on these results the torque of $M_t = 350Nm$ gives the target pretension force $F_p = 160kN$ with the coefficient of variation of $V_M = 10.6\%$. Obtained accuracy does not fulfil the requirements of EN 1090-2 Annex H. This is the consequence of quite complicated geometry of the connector assembly. The following push tests of the series Type A were performed with the designated torque of $M_t = 350Nm$.

5.2.3 Connector Type B

In the case of the connector Type B there was enough space to use load cell KMR M24 directly in the torque calibration assembly. The torque calibration assembly is as close to the actual layout of the push test specimen of series Type B (Figure 5.11).
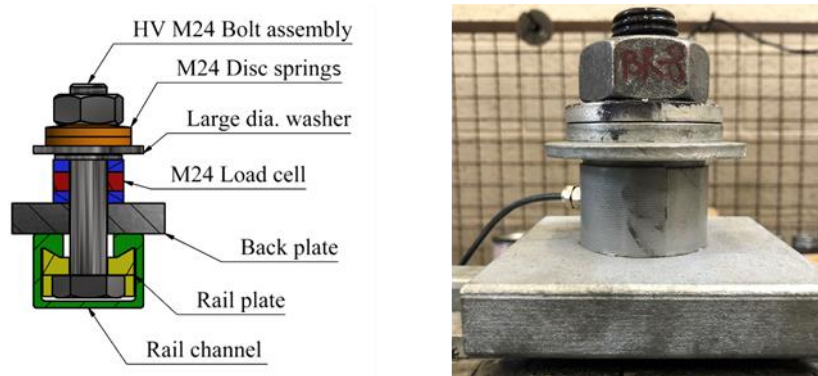
Figure 5.11 - Torque calibration assembly Type B

The bolts were stepwise torqued and the pretension force was measured directly by the means of the integrated load cell. The force-torque relationship was established for the required 8 M24

HV bolts. The following obtained curves represent the relationship between the preload torque and the pretension force (Figure 5.12).
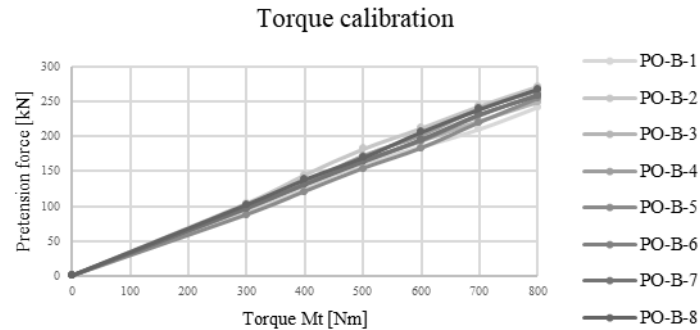
Figure 5.12 - Torque vs. pretension force - Assembly Type B

Based on the established relationships the torque of $M_t = 525 Nm$ gives the target pretension force $F_p = 170 kN$ with the coefficient of variation of $V_M = 5\%$. Obtained accuracy fulfils the requirements of EN 1090-2 Annex H. The following push tests of the series Type B were performed with the designated torque of $M_t = 525 Nm$.

5.2.4   Connector Type C

Connector Type C torque assembly was developed in the similar manner as in the case of Type B. This time KMR M20 load cell was applied in conjunction with HR M20 8.8 pretension bolt assembly (Figure 5.13).
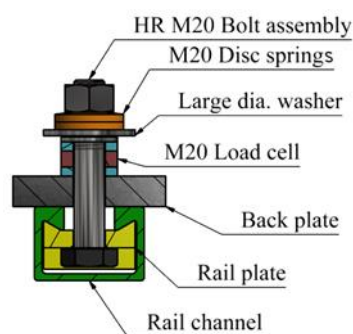
Figure 5.13 - Torque calibration assembly Type C

The bolts were torqued in a stepwise manner and the relationship between the torque and the pretension force was built for 8 HR M20 8.8 pretension bolt assemblies.

Based on the established torque-pretension force relationship, the torque value of $M_t = 325Nm$ was designated in order to reach the target pretension force of $F_p = 140 \, kN$ with the coefficient of variation of $V_M = 4.9\%$ what fulfils the requirement of EN 1090 Annex H (Figure 5.14).
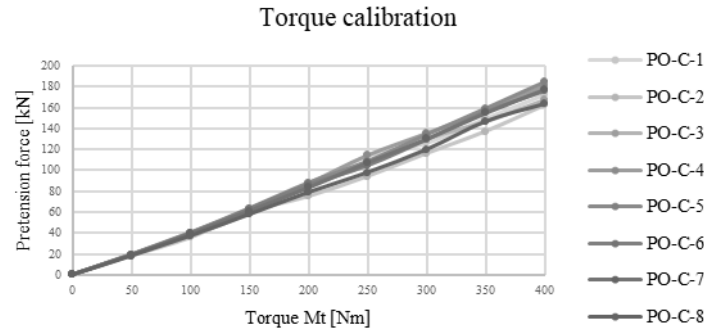
Figure 5.14 - Torque vs. pretension force assembly Type C

The following push tests of the series Type C were performed with the designated torque of $M_t = 325Nm$.

5.2.5   Connector Type D

Type D torque calibration assembly is the simplest of all (same as the connector assembly Type D). The KMR M20 cell was applied in conjunction with the HS T M20 8.8 pretension bolt assembly that fits the Halfen HTA/CE 72/48 rail channel (Figure 5.15).
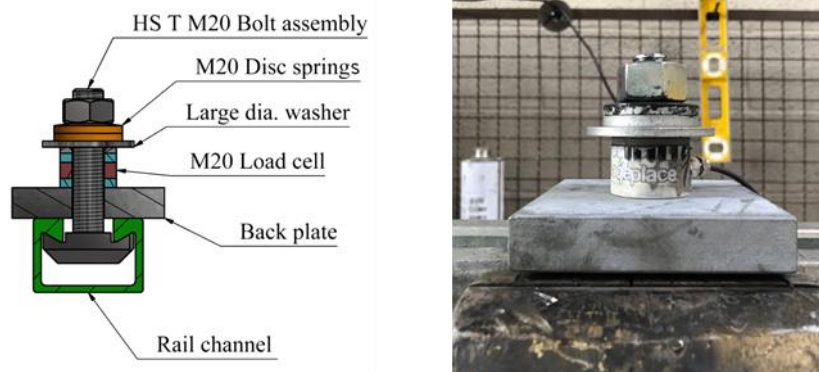
Figure 5.15 - Torque calibration assembly Type D

The bolts were torqued in a stepwise manner and the relationship between the torque and the pretension force was built for 8 HS T M20 8.8 pretension bolt assemblies.

Based on the established torque-pretension force relationship (Figure 5.16), the torque value of $M_t = 275Nm$ was designated in order to reach the target pretension force of $F_p = 130 \, kN$ with the coefficient of variation of $V_M = 5.1\%$ what fulfils the requirements of EN 1090 Annex H for 8

tested bolts. The following push tests of the series Type D were performed applying the torque of $M_t = 275Nm$.
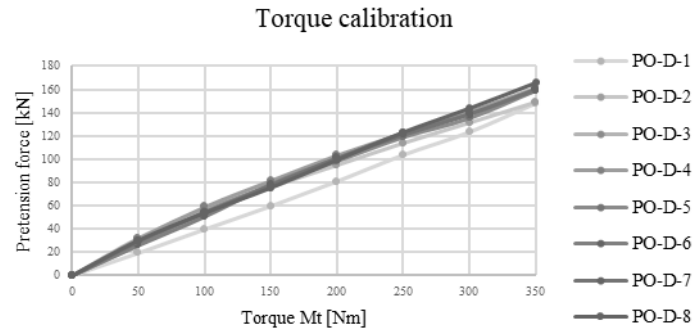
Figure 5.16 - Torque vs. pretension force assembly Type D

The corresponding torque values M_t leading to target pretension forces F_p for all push test series are summarized in the following table (Table 5.2).

Table 5.2 - Summarized results of pretension tests

Series	A	B	C	D
Bolt	HV M24	HV M24	HR M20	HST M20
M_t (Nm)	350	525	325	275
F_p (kN)	160	170	140	130

5.3 Material tests

5.3.1 Compression tests of hardened concrete material

The standard compressive tests of hardened concrete material on standard cylindric specimens were performed in accordance with EN 12390-3 [43] in order to assess the material properties of the concrete used for casting of the push test slabs. Based on these properties the adequate material model is later built for the application in the FE analysis of the connector systems.

Figure 5.17 - Casted push test specimen slabs and compression test samples

All the specimens were casted at the time of the casting of push test specimen slabs (Figure 5.17). The specimens FC 1-4 were stored in climatic chamber and tested $t = 28d$ after the day of casting. All other specimens were stored adjacent (in the same conditions) to the actual slab elements and tested on the day or within the week of the corresponding push test series.

Secant modulus of elasticity E_c and the compressive strength f_c of the hardened concrete material (Figure 5.18) were investigated in accordance with EN 12390-13 [44] and EN 12390-3 [43] respectively.
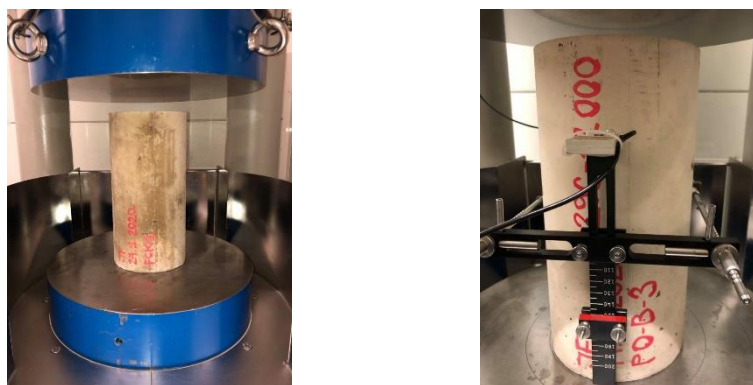
Figure 5.18 - Concrete compressive strength and modulus test assemblies

The mean value of the compressive strength after 28 days was $f_{cm,28} = 51.95 MPa$ with quite low scatter of the results (Table 5.3). The summary of the concrete compressive test results is provided in the *Annex C - Concrete compression test results* of the manuscript.

Table 5.3 - Compressive test results (t=28d)

Specimen	f_c [MPa]
FC-1	51.4
FC-2	53.04
FC-3	51.85
FC-4	51.51
	51.95

The mean compressive strength in the case of push test slab representative specimens (Table 5.4) was lower due to the fact that the FC specimens had better curing conditions during the maturing ($f_{c,p,m} = 50.83 MPa$).

Table 5.4 - Compressive test results (t=t$_{push}$)

Specimen	f_c [MPa]	E_{cm} [GPa]	$^*E_{cm}$ [GPa]
PO-A-1	49.26	36.071	
PO-A-2	52.12	36.916	
PO-A-3	52.26	37.571	
	51.21	**36.853**	**35.912**
PO-B-1	47.83	38.735	
PO-B-2	47.72	37.465	
PO-B-3	48.25	37.397	
	47.93	**37.866**	**35.206**
PO-C-1	48.62	34.410	
PO-C-2	49.40	37.542	
PO-C-3	46.87	36.246	
	48.3	**36.066**	**35.286**
PO-D-1	49.58	39.510	
PO-D-2	54.03	36.902	
PO-D-3	51.82	38.811	
	51.81	**38.408**	**36.037**
	50.83	**37.298**	**35.614**

The measured secant modulus of the elasticity (E_c) of the concrete was also slightly higher than the one predicated by the formula of the EN 1992-1-1 ($^*E_{cm}$) that is based on the concrete mean compressive strength f_{cm}.

Due to the limited number of test specimens and on the basis of the mean concrete compressive strength of $f_{cm} \approx 50 MPa$, the assigned concrete class of the concrete material is designated as C40/50 as the mean compressive strength of the class C40/50 is $f_{cm} = 48 MPa$ (EN 1992-1-1 [45]). The later concrete material models built for the FE analysis conform to the material properties of the concrete class C40/50.

5.3.2 Steel material tensile tests

The standard tensile tests of the metallic material were performed in accordance with the ISO 6892-1 [46] (Method A1 - Strain rate control). The properties of the metallic material (steel) were evaluated for the critical steel components of the connector assembly for all connector typologies. The designated critical components in the connector assemblies are HTA CE 72/48 rail channels and anchors and the bolt assemblies (HST 8.8, HR 8.8 and HV 10.9).

For the rail and anchor parts, standard flat test assemblies with dimensions $b_0 = 4mm$ and $a_0 = t = 3mm$ ($S_0 = 12mm^2$) were machined from the relevant steel parts (Figure 5.19). The original gauge (clip) length of the specimen was $L_0 = 20mm$.

HTA CE 72/48
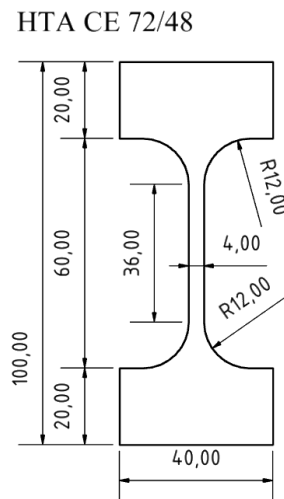
Figure 5.19 - Flat tensile test specimen - Rail and anchor

For the bolt assemblies, standard cylindrical test assemblies with the diameter $d_0 = 5mm$ ($S_0 = 19.635mm^2$) were machined from the relevant bolts (Figure 5.20). The original gauge (clip) length of the specimen was also $L_0 = 20mm$.
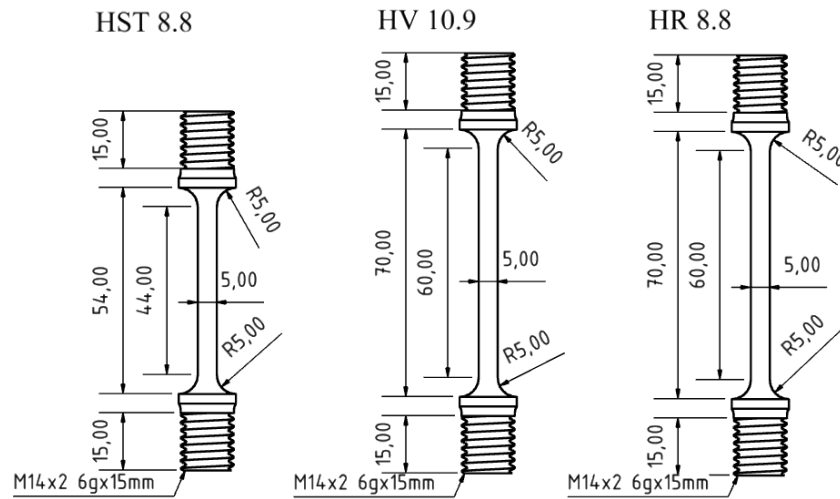
Figure 5.20 - Cylindric test specimens (bolts)

In each series 3 specimens were tested, 15 in total (Table 5.5). All test specimens were machined by the mechanical laboratory of the University of Luxembourg while the actual tensile tests were performed externally by the external partner Mistras Group [47]. The respective experimentally obtained stress-strain diagrams are provided in the *Annex D - Steel tensile test results*.

Table 5.5 - Tensile test schedule

Series	Specimens	Material
Rail	3	S235JRG
Anchor	3	S235JRG
HST	3	8.8
HR	3	8.8
HV	3	10.9

The results obtained for the rail and anchor specimens (Figure 5.21) correspond to the properties of mild steels as the basic material of the parts is designated by the producer as S235JRG (Table 5.6).

Table 5.6 - Tensile test results - Rail & Anchor

Specimen	$S_0\ [mm^2]$	$A\ [\%]$	$R_{eH}\ [MPa]$	$R_{eL}\ [MPa]$	$R_m\ [MPa]$	$E\ [GPa]$
HTA-CE Rail	12.14	28.0	380	364	443	211.2
HTA-CE Anchor	12.18	41.0	299	277	374	212.8

Figure 5.21 - Aftermath of the tensile tests - Rail & Anchor

The results obtained for the bolt specimens (Figure 5.22) correspond well to the bolt material
properties of class 8.8 (HST and HR bolt assemblies) and 10.9 (HV assemblies) bolt material
class (Table 5.7). The raw stress-strain data of the tensile tests are provided in the
Annex D - Steel tensile test results.

Table 5.7 - Tensile test results - Bolts

Specimen	S_0 [mm^2]	A [%]	$R_{p0.2}$ [MPa]	R_m [MPa]	E [GPa]
HST M20	19.635	20.5	823	938	211.4
HR M20	19.635	17	822	933	215
HV M24 Bolt	19.635	17.5	966	1055	210.7

Figure 5.22 - Aftermath of the tensile tests - Bolts

5.3.3   Steel material shear tests for bolts

The bolt shear tests were performed in order to calibrate the steel material model of the bolt concerning the shear behaviour for the application in the push FEA local models. The assembly is built around two-plane shear layout of the bolt assembly (Figure 5.23). Two support plates that accommodate the bolt holes with $1mm$ tolerance are bolted to the base plate. Two inner plates serve as a load introduction part transferring the compressive force of the jack into the shear force by bearing that shears the bolt in two distinctive shear planes. The inner plates as well have the bolt holes with $1mm$ tolerance.
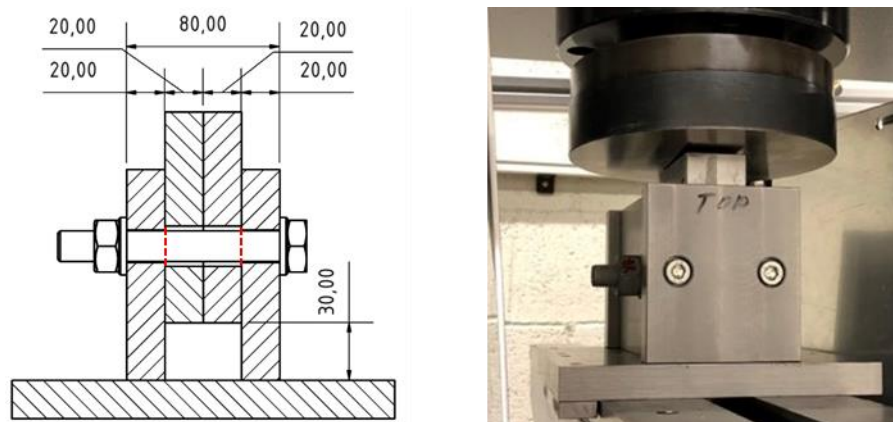
Figure 5.23 - General layout of shear test assembly

Every bolt type (series) were represented by 3 specimens (Table 5.8). The actual layout (shear plane through threaded or unthreaded shank portion) conforms to the one of the push test.

Table 5.8 - Shear test schedule

Series	Specimens	Material	Bolt	Shear area A_s [mm^2]	Shear plane
HST	3	8.8	M20 HS	245	Threaded
HR	3	8.8	M16 HR	201.06	Unthreaded
HV	3	10.9	M16 HV	201.06	Unthreaded

All plates are fabricated out of S355JRG steel material. The measurements (slip and total shear force) are obtained directly from the acquisition of the hydraulic press ZWICK400. During the test the bearing of the bolt holes and the deformation of the bolt threads produced additional bolt shank displacement that has to be addressed when the material model is assessed. For each bolt assembly 3 tests were performed.

Figure 5.24 - Aftermath of the shear tests

The sequencing of the test consists of positioning of the assembly in the "touch" position in order to reduce force-free displacement. Afterwards, the test is performed in the displacement-controlled mode with the actuator displacement speed that equals the one from later push tests $v = 0.25 \frac{mm}{min}$ recreating the quasi-static response of the system. The aftermath of the bolt shear tests is presented in Figure 5.24.

Due to the initial strain hardening around the bolt hole the response of the first specimen is delayed compared to the latter two (Figure 5.25). The ultimate shear capacity (two shear planes) is comparable to the bolt shear capacity provided by EN 1933-1-8 for the case of shear plane that runs through the threaded (HST 8.8 bolts) or unthreaded part of the bolt shank (HR 8.8 and HV bolts) if the ultimate strength f_{ub} obtained from the tensile material tests is applied:

$$F_u = 2F_v = 2 \cdot (0.6 \cdot A_s \cdot f_{ub}) = 2 \cdot 0.6 \cdot 245 \cdot 936.7 = 275.4 \; kN$$

(5.1)
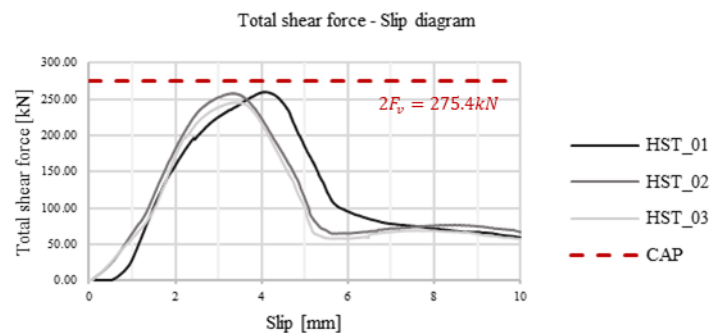
Figure 5.25 - Shear test results - HST series

In the case of HST bolt series, after the shear failure of the bolt shank in the position of two shear planes the displacement increases with almost constant force. This unexpected "ductile"

response of the assembly comes from the fact that after brittle failure in shear, the separated bolt threads are bearing onto the support and inner plate material (Figure 5.26).

Figure 5.26 - Thread embedment - HS T bolts

In the case of M16 bolts HR 8.8 and HV slightly higher capacity (Figure 5.27 & Figure 5.28) is obtained compared to the equation (5.1). This is due to the unavoidable bending action in the bolt during the course of test. The same effect was recorded in the bolt shear experiments of Pavlovic [14].

The reference shear capacity in the case of the M16 HR 8.8 bolts is:

$$F_u = 2F_v = 2 \cdot (0.6 \cdot A_s \cdot f_{ub}) = 0.6 \cdot 201 \cdot 924.66 = 214.68 \; kN$$

(5.2)
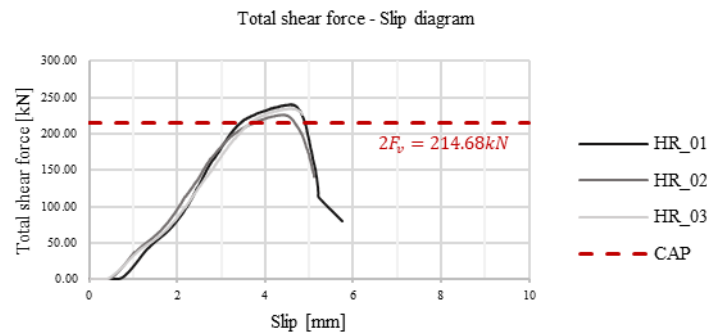
Figure 5.27 - Shear test results - HR series

The reference shear capacity in the case of the M16 HV bolts is:

$$F_u = 2F_v = 2 \cdot (0.6 \cdot A_s \cdot f_{ub}) = 0.6 \cdot 201 \cdot 1050.66 = 253.5 \; kN$$

(5.3)
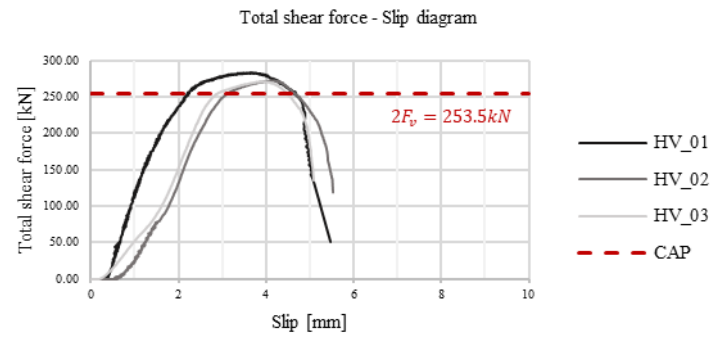
Figure 5.28 - Shear test results - HV series

The obtained force-slip behaviour of the bolt assemblies in shear will be later exploited for the assembly of the steel material model that will be applied to the steel bolt parts in the chapter *6 Numerical analysis*.

5.4 Push test results

5.4.1 Connector Type A

The connector Type A series was composed out of 3 test specimens. The steel parts surfaces were sandblasted (the rail channel is zinc-galvanized as produced). The target pretension force applied was $F_p = 160kN$ what is 65% of the design pretension force ($F_{pc} = 0.7f_{ub}A_s$ [28]) for M24 HV 10.9 bolt providing high elastic bolt material reserve. The clamping force achieved at the faying surface was $F_c = 0.75F_p = 120kN$. Due to the limited capacity of the test frame $F_{max} = 800kN$, four shear connectors Type A were placed in the bottom row only (Figure 5.29).

Figure 5.29 - Connector Type A test specimen

The first specimen was tested only in displacement-control mode with the displacement ratio of $v = 0.25 \frac{mm}{min}$. Based on the ultimate capacity of the first specimen $F_{u,A,1} \cong 200kN$ ($P_u \cong 50kN$), the parameters for the cycling step for later two specimens were defined. The latter two specimens were firstly cyclically loaded 25 times in harmonic manner between total force levels $F_{min} = 10kN$ and $F_{max} = 80kN$ with the force ratio of $v_F = 3\frac{kN}{s}$ what gives a cycle period of $T = 46.6s$.
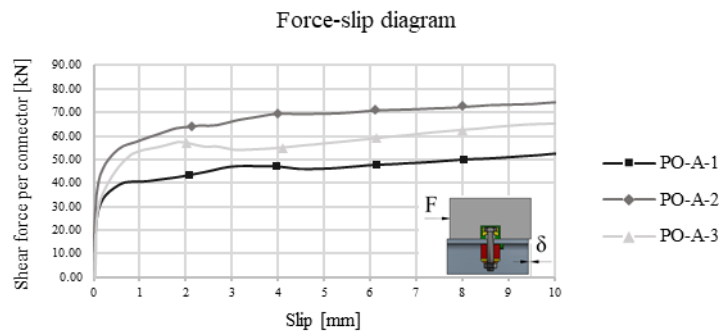
Figure 5.30 - Connector Type A force-slip curve

The initial response is characterized by the high stiffness due to the slip capacity at the slab-steel section faying interface (Figure 5.30). The slip capacity obtained in this way was $F_{1,A} \cong 35kN$ what corresponds to the slip capacity of $\mu_{1,A} = 0.29$. This is lower than the expected value of $\mu_1 \cong 0.4 - 0.5$.

The second part of the force-slip curve is characterized by the activation of the secondary faying surface and combined M-V-P action in the bolt shank. At the slip of $\delta = 2mm$ the ultimate capacity is reached by sliding at the both faying interfaces. The deviation of the ultimate capacity results from the mean value is higher than 10%. The scatter of the results is strongly influenced by the uncertainty of the application of the pretension force at the first place observed in the chapter *5.2 Pretension tests*.

The maximum obtained capacity per connector at slip of $6\ mm$ was $P_{u,A,2} = 75kN$. This is only a fraction (26.2%) of the expected M24 HV bolt shear capacity of $F_v = 286.36kN$. Coupled with the relatively large spacing between the connectors (compared to $e_{min} \geq 5d = 120mm$ for headed studs [8]) and relatively lower shear capacity the connector Type A does not provide sufficient capacity. On the other hand, the behaviour after reaching the ultimate shear capacity of the connector is exceptionally ductile ($\delta_u \gg 6mm$). The experiments were stopped at maximum connector slip of $\delta_{max} = 10mm$.

The separation in this type of shear connectors is prevented as the capacity is provided as a consequence of clamping effect. The measured separation between the slab and the steel section was negative. This is expected as in the case of the friction-grip connectors the sliding action damages the surfaces in touch. During the course of the test the limited embedment was recorded in the vicinity of the shear connector ($\delta_{s,min} = -0.088mm$).
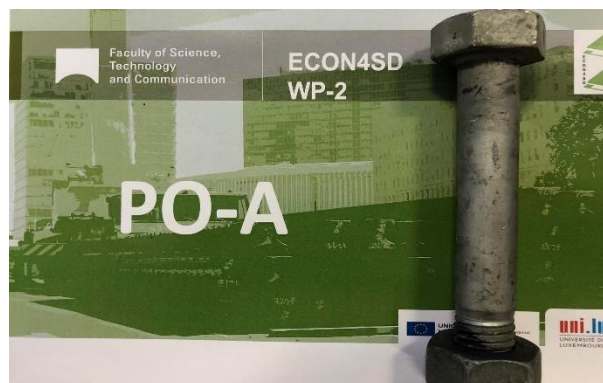
Figure 5.31 - Push test connector Type A aftermath

After the end of the push tests no permanent plastic deformation of the connector assembly was observed (Figure 5.31). The stable sliding response was guaranteed by the high elastic reserve of the bolt material and by the application of the disc springs.

5.4.2   Connector Type B

The connector Type B series was also composed out of 3 test specimens. The steel parts surface treatment was hot-dip zinc galvanized (steel section and the back plates). The section bolt holes were long-slotted. The target pretension force applied was $F_p = 175kN$ what is 70% of the design pretension force for M24 HV 10.9 bolt providing high elastic bolt material reserve. The clamping force achieved at the faying surface is equal to the bolt pretension force $F_c = F_p = 175kN$ as the complete pretension force acts as a clamping force at the both faying surfaces.

Due to the limited capacity of the test frame only bottom row of connectors was preloaded (active). The top row is present in the assembly but its bolts are loosely tightened and do not provide the shear capacity in the assembly (Figure 5.32).
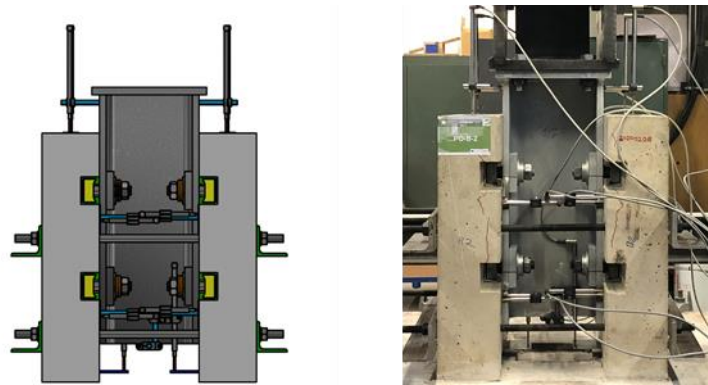
Figure 5.32 - Connector Type B test specimen

The first specimen was tested only in displacement-control mode with the displacement ratio of $v = 0.25 \frac{mm}{min}$. Based on the ultimate capacity of the first specimen $F_{u,B,1} \cong 590kN$ $(P_u \cong 147.5kN)$, the parameters for the cycling step for latter two specimens were defined.

The next two specimens were firstly cyclically loaded 25 times in harmonic manner between total force levels $F_{min} = 30kN$ and $F_{max} = 236kN$ with the force ratio of $v_F = 6\frac{kN}{s}$ what gives a cycling period of $T = 68.68s$.

The obtained response per connector is characterized by stiff initial response (slip capacity at the first faying surface) followed by activation of the second faying surface after the slip capacity is achieved at $F_{1,B} \cong 75kN$ (Figure 5.33). This corresponds to the coefficient of friction of $\mu_{1,B} \cong 0.43$ what corresponds well to the expected values discussed in the chapter *3.4 Friction behaviour*.

The first specimen behaved stiffer until reaching ultimate capacity due to the imperfect geometry of the steel section slotted holes what led to the bearing of the bolt. The ultimate capacity of $P_u \cong 140kN$ was reached at $\delta_u \cong 2.5mm$. Between the slip capacity and ultimate capacity linear relationship between shear force and slip may be established as it depends on the bending stiffness of the bolt shank and the actual boundary condition of the bolt assembly.
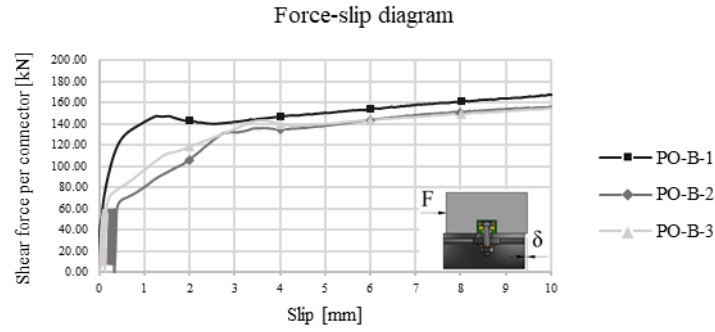
Figure 5.33 - Connector Type B force-slip curve

In this case the shear connector capacity P_u is considered as the ultimate force per connector generated solely due to the frictional resistance at the relevant faying surfaces. It should not be related to the ultimate capacity of the assembly as it is reached when the ultimate shear capacity of the bolt is achieved. Due to the application of the long-slotted holes, the bolt shear failure $P_{u,b}$ would happen at very large slips ($\delta_{u,b} \gg 6mm$) after the closure of the long-slotted bolt hole tolerance δ_2, hence could not be considered as the capacity of the shear connector.
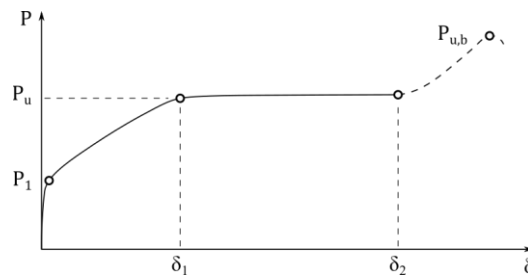
Figure 5.34 - Definition of the friction connector capacity

The maximum deviation of the connector shear capacity $P_{u,m} = 147kN$ at the slip of $\delta = 6mm$ is less than 5% ($CV = 4.28\%$). The obtained force-slip results were consistent and predictable. Similar "stiffening" effect in sliding was observed as discussed in the chapter *3.2 Friction grip connectors.* The force-slip response was highly ductile in all specimen cases. The experiments were stopped after reaching the maximum slip of $\delta = 10mm$.

Figure 5.35 - Push test connector Type B aftermath

The maximum recorded embedment at the vicinity of the shear connector was $\delta_{s,min} = -0.15mm$. No permanent plastic deformation of the connector assembly was recorded (Figure 5.35).

5.4.3   Connector Type C

The connector Type C series was also composed out of 3 test specimens. The steel parts surface treatment was hot-dip zinc galvanized (steel section and the back plates). The steel section bolt holes are enlarged round holes with $2mm$ of bolthole clearance. The target pretension force applied was $F_p = 140kN$ what is 102% of the design pretension force for M20 HR 8.8 bolt. The full pretension force ($0.7f_{ub}A_s$) was applied as the ultimate capacity is guaranteed by the shear capacity of the bolt. The clamping force achieved at the faying surface is equal to the bolt pretension force $F_c = F_p = 140kN$ as the complete pretension force is transformed into the clamping force at the both faying surfaces.

Due to the limited capacity of the test frame only the bottom row of the test specimen is provided with the shear connector assemblies (Figure 5.36).
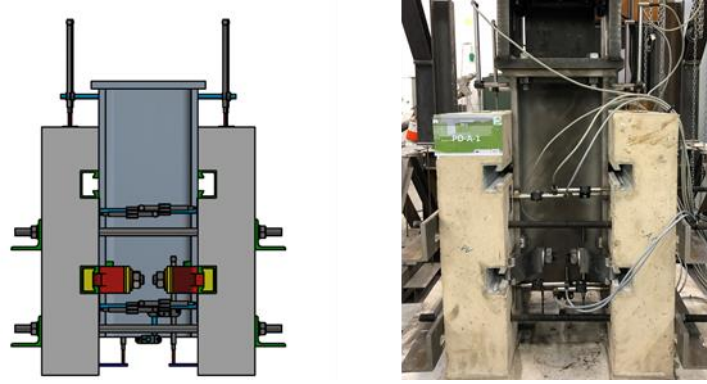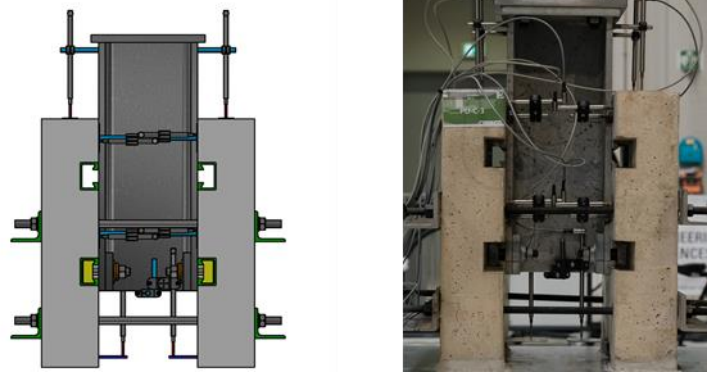
Figure 5.36 - Connector Type C test specimen

The first specimen was tested only in displacement-control mode with the displacement ratio of $v = 0.25 \frac{mm}{min}$. Based on the ultimate capacity of the first specimen $F_{u,C,1} \cong 880kN$ ($P_u \cong 220kN$), the parameters for the cycling step for later two specimens were defined. The latter two specimens were firstly cyclically loaded 25 times in harmonic manner between total force levels $F_{min} = 44kN$ and $F_{max} = 352kN$ with the force ratio of $v_F = 9.625 \frac{kN}{s}$ what gives a cycle period of $T = 64s$.
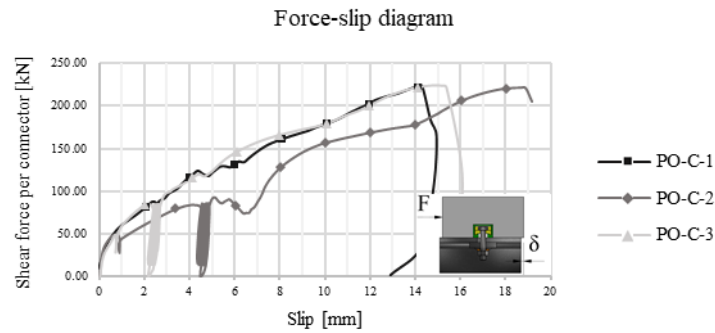
Figure 5.37 - Connector Type C force-slip curve

The initial slip capacity of the specimens is limited $F_{1,C} \cong 30 \ kN$ (Figure 5.37). This corresponds to the slip coefficient of $\mu_{1,C} \cong 0.214$ what is half of the expected value. After the slip capacity is reached the bolthole tolerance is filled and the bolt is subjected to bending by shear. The low stiffness of the M20 bolt assembly and large shear force lever arm e_b (Figure 5.38) lead to very flexible response in the bearing phase of the force-slip response.
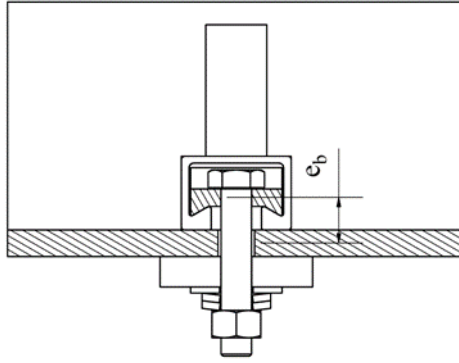
Figure 5.38 - The bolt shank support condition - Type C

Due to the high flexibility of the connector assembly the ultimate capacity of ($P_{u,m} \cong 223.1kN$) is reached at very high slip $\delta_u = 14 - 18mm$. The capacity results were very consistent with coefficient of variation of only $CV = 0.68\%$.

The maximum separation recorded at the vicinity of the shear connector during the tests was $\delta_{s,max} = 0.6mm$.

The obtained failure in all specimens was brittle, achieved by the shear of the connector bolt shank (Figure 5.39). Due to the high bolt eccentricity, firstly plastic hinges are formed under the bolt head and in the level of the flange bolt hole (lever arm e_b). After the bolt shank touches the rail lip, the failure is achieved by the shearing of the bolt shank under the rail lip.

Figure 5.39 - Push test connector Type C aftermath

If the lever arm is measured from the centre to centre of bearing plates $e_b = 30mm$:

$$P_u = F_{pl} + F_v = \frac{2M_{pl}}{e_b} + F_v = \frac{\frac{1}{6}d^3 \cdot f_{yb}}{e_b} + 0.6A_s f_{ub} \ (A_s = 314.16mm^2)$$

$$P_u = 242.24 \ kN \cong P_{u,m} = 223.1 \ kN$$

(5.4)

5.4.4 Connector Type D

The connector Type D series was also composed out of 3 test specimens. The steel parts surface treatment was hot-dip zinc galvanized (steel section and the back plates). The steel section bolt holes are enlarged round holes with $2mm$ of bolthole tolerance. The target pretension force applied was $F_p = 130kN$ what is 95% of the design pretension force for M20 HR 8.8 bolt (HS T bolt has corresponding material grade as HR).
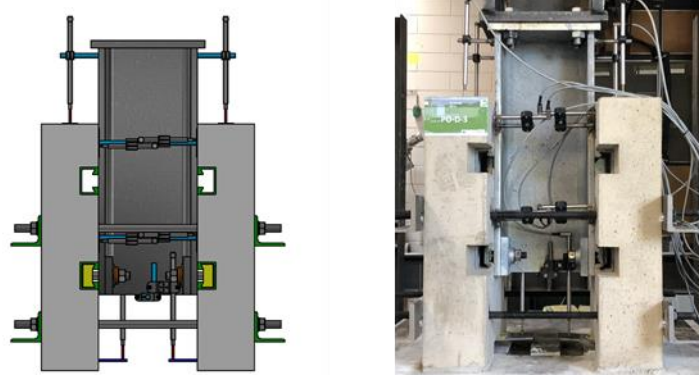
Figure 5.40 - Connector Type D test specimen

The pretension force close to the full pretension ($0.7 f_{ub} A_s$) was applied as the ultimate capacity is dominated by the shear capacity of the bolt. The clamping force achieved at the faying surface is equal to the bolt pretension force $F_c = F_p = 130kN$ as the complete pretension force is transformed into the clamping force at both faying surfaces. Due to the limited capacity of the test frame (Figure 5.40) only the bottom row of the test specimen is provided with the shear connector assemblies.

The first specimen was tested only in displacement-control mode with the displacement ratio of $v = 0.25 \frac{mm}{min}$. Based on the ultimate capacity of the first specimen $F_{u,C,1} \cong 480kN$ ($P_u \cong 120kN$), the parameters for the cycling step for later two specimens were defined. The latter two specimens were firstly cyclically loaded 25 times in harmonic manner between total force levels $F_{min} = 24kN$ and $F_{max} = 192kN$ with the force ratio of $v_F = 6\frac{kN}{s}$ what gives a cycle period of $T = 56s$.
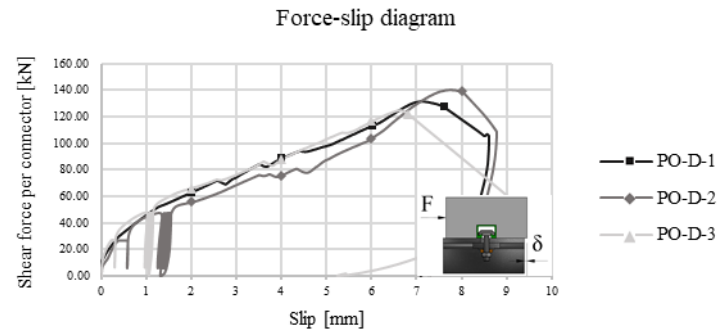
Figure 5.41 - Connector Type D force-slip curve

The initial slip capacity of the specimens is limited $F_{1,D} \cong 30\ kN$ (Figure 5.41). This corresponds to the slip coefficient of $\mu_{1,D} \cong 0.23$ what is half of the expected value. After the slip capacity is reached the bolthole tolerance is closed and the bolt is subjected to the bending by shear, however, compared to the Type C connector the lever arm is smaller due to the special geometry of the T bolt (Figure 5.42).
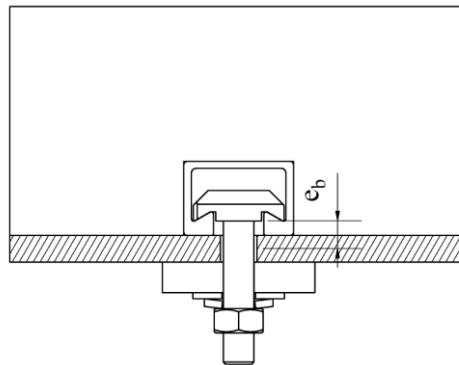
Figure 5.42 - The bolt shank support condition - Type D

On the other hand, the HS T bolt is threaded all along the shank what gives lower bending stiffness than the HR bolt that has unthreaded portion along the bolt shank. Combined, these effects lead to connector flexible response in the bearing phase of the force-slip response.

Due to high flexibility of the connector assembly the ultimate capacity of ($P_{u,m} \cong 140kN$) is reached at relatively high slip $\delta_u = 7 - 8mm$. The capacity results were consistent with coefficient of variation of $CV = 6\%$.

Figure 5.43 - Push test connector Type D aftermath

The achieved failure mode was brittle failure by shearing of the bolt shank under the T bolt head (Figure 5.43). No significant bending hinging was recorded along the bolt shank as the bolt shank eccentricity e_b is relatively low due to the special geometry of the T bolt assembly.

$$P_u = 0.6 A_s f_{ub} \; (A_s = 245 mm^2)$$

$$P_u = 137.7 \; kN \cong P_{u,m} = 140 \; kN$$

(5.5)

5.4.5 Assessment and comparison of the push test results

The results of the push test campaign placed the connectors in two distinctive groups as expected, friction type shear connectors (Type A&B) and friction-grip type shear connectors (Type C&D). Their mean force-slip curves may be observed and related in the following figure (Figure 5.44).
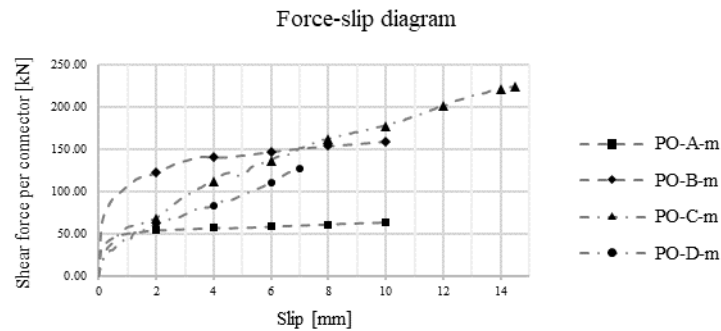
Figure 5.44 - Push test series mean force-slip curves

Connector Type A as a friction type connector has a very ductile response (note that the push tests in the case of friction connectors were stopped at the slip of $\delta = 10mm$). However, due to the complexity of its assembly, its response is inconsistent between the specimens of the test series. It acquires the ultimate capacity "fast" at the slip of $\delta_1 = 2mm$ although its capacity is very limited and accounts to only $\cong 20\%$ of the expected mean shear capacity of the applied M24 HV bolt. Compared to the expected mean shear capacity of the equivalent shear stud ($D = 25mm, f_{us} = 450MPa$) the connector capacity accounts to only 33% of the shear resistance.

Due to the inconsistency in response and very low ultimate capacity of the connector Type A, it would be very challenging to apply it as a mean of provision of shear connection within the scope of this work. Especially the geometrical constraint regarding the connector row separation (rail separation) along the beam of the proposed modular steel-concrete composite floor prevents the application of low capacity connectors (beside their ductile response and two connector per row layout). On the other hand, having in mind limitations and mechanics behind its behavior its design might be improved in order to reach useful shear capacity levels as this connector typology provides the easiest construction sequencing for the demountable steel-concrete composite floor.

Connector Type B on the other hand besides its excellent ductility provides applicable shear capacity levels. Connector Type B also reaches the ultimate capacity "fast" at the slip of $\delta_1 = 3mm$. The force-slip response may be furtherly improved by providing the rail-plate and the back-plate parts with fitted bolt holes [11]. This would not affect the sequencing of the shear connector assembly but would reduce the capacity lag due to the bolt hole tolerances (Figure 5.45). The idea shall be explored and supported by the results of the later FEA simulations of the connector behavior.
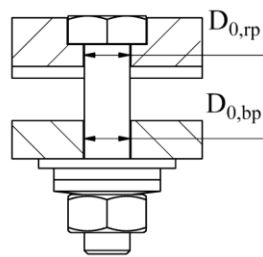
Figure 5.45 - Reduction of the bolthole tolerances

Connector Type B also exhibits considerable initial slip capacity conforming to the expected slip capacity of the friction-grip shear connectors. Its ultimate capacity is considerable regarding the expected mean shear capacity of the applied bolt (51.5%) and regarding the shear capacity of the equivalent Nelson headed stud (83.18%).
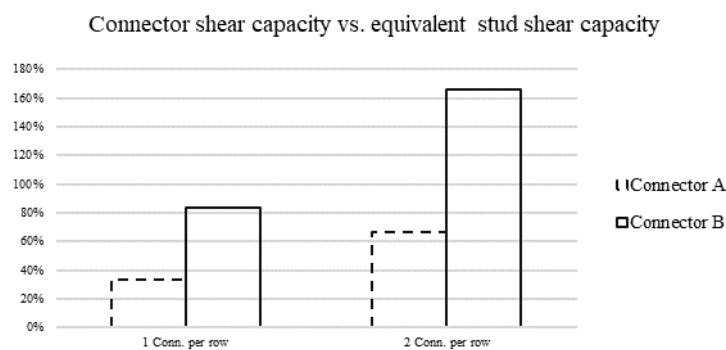
Figure 5.46 - Connector capacity vs. stud capacity

As the connector layout considers 2 connectors per row the row shear capacity surpasses the shear capacity of larger diameter equivalent headed stud (D25) in single row layout (Figure 5.46). Coupled with its significant slip capacity ($F_{1,B} \cong 75kN$), stiff response ($\delta_1 \cong 3mm$) and very high ductility ($\delta_u > 10mm$) its force-slip curve conforms closest to the sought

rigid-perfectly plastic behaviour and may be represented by trilinear force-slip curve what shall be investigated in later chapters.

Connector Type C response conforms to the friction-grip shear connector typology. It has undoubtedly highest shear capacity of all proposed connector devices ($P_{u,m} \cong 223.1 kN$). The shear capacity is provided by two mechanisms, formation of the plastic hinge beneath the bolt-head followed by the shearing of the unthreaded portion of the bolt shank. Due to the combined failure mode its capacity is 25% higher than the shear capacity of the applied bolt and twice the capacity of the equivalent (D19) Nelson headed stud.

However, it has limited slip capacity and very flexible (linear) response up to the brittle failure in shear ($\delta_u \cong 15mm$). Due to its characteristic bilinear force-slip curve it may not be classified as ductile and due to its flexibility, it would be disputable if the complete interaction composite beam behavior might be achieved.

Table 5.9 - Connector capacity vs. bolt and equivalent stud shear capacity

Connector	Bolt	$F_{v,m}$ [kN] EN 1993-1-8	$P_{u,m}/F_{v,m}$	Stud diameter D [mm]	$P_{r1,m}$ [kN] EN 1994-1-1	$P_{u,m}/P_{r,m}$
A	M24 HV	285.19	20.7%	25	176.71	33.36%
B	M24 HV	285.19	51.5%	25	176.71	83.18%
C	M20 HR	174.3	128%	19	102.07	218.6%
D	M20 HST	137.7	101.7%	19	102.07	137.16%

*Assumed ultimate strength of the stud material $f_{us} = 450 MPa$ (Nelson)

Connector Type D has similar response as the connector Type C as they are based on the same principle with slightly simpler geometry in the case of the connector Type D. Due to the connector assembly geometry the failure is reached by the shear of the threaded bolt shank. The initial slip capacity is comparable to the connector Type C while the stiffness of the following linear branch is slightly lower due to the reduced effective area of the T bolt threaded shank.

In a similar way as in case of the shear connector Type C it may not be classified as ductile due to its prominent bilinear force slip curve. Connector Type D reaches the brittle failure in shear at the slip of only $\delta_u = 6mm$ (this is not the ductile slip capacity required to classify the connector as ductile).

In previous review the comparison of the connector capacities with bolt shear capacity $F_{v,m}$ and the shear capacity of the equivalent headed stud $P_{r1,m}$ assumed that there is no failure mode related to the concrete of the floor slab (Table 5.9).

Besides the friction capacity contribution at the first faying surface (concrete slab-steel flange), the capacity contribution of the bottom faying surface ($P_{v,b}$) is transferred via connector assembly into the concrete slab through the rail channel wall. It is paramount that the concrete slab remains undamaged during the exploitation of the demountable floor so it might be reused multiple times.
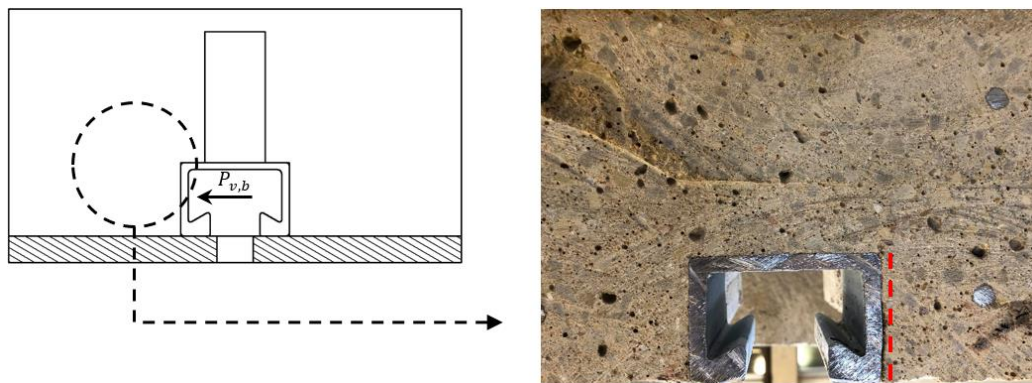
Figure 5.47 - Aftermath of the push test - Connector Type C slab

In order to assess the state of the concrete slab in the vicinity of the load introduction the concrete slab of the specimen that produced the highest shear capacity (Type C) was cut following the axis of the shear connector (Figure 5.47).

No concrete cracking was observed at the side of the load introduction proving the assumption that the load introduction through the rail channel will render the concrete related failure modes nonrelevant. This statement will be additionally supported by the later FEM results.

On the opposite side of the rail channel it was observed that the rail wall separated from the concrete slab (Figure 5.48).

Figure 5.48 - Aftermath of the push test - Connector Type C rail channel

This effect is obvious as the portion of the force $F_{v,b}$ is transferred by pulling of the rail lip at the opposite side of the load introduction followed by the local bending and shear of the rail wall and inplane compression of the rail flange what brings this portion of the force back in the zone of the load introduction. This phenomenon is not an issue for the consequent reuse of the modular slab element as it might be as well rotated and the load introduction would close the formed separation between the rail channel wall and the wall of the concrete slab socket.

Important observation was also that the rail channel inside the concrete slab was not damaged and was able to serve the same purpose as demonstrated by subsequent reassembly of the test specimen of the push series Type B (Figure 5.48).

6. Numerical analysis

6.1 Material models

6.1.1 Concrete

The uniaxial material model for the concrete material in compression was adopted according to the model for non-linear structural analysis of EN 1992-1-1 [45].
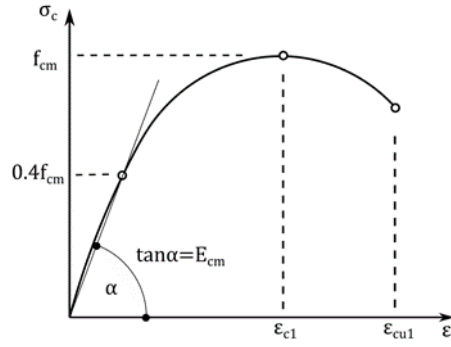
Figure 6.1 - Uniaxial stress-strain model for concrete in compression

$$\sigma_c = E_{cm}\varepsilon_c \quad \varepsilon_c \leq 0.4 f_{cm}/E_{cm}$$

$$\frac{\sigma_c}{f_{cm}} = \frac{k\eta - \eta^2}{1 + (k-2)\eta} \quad \varepsilon_c > 0.4 f_{cm}/E_{cm}$$

(6.1)

E_{cm} – secant modulus of elasticity of concrete

f_{cm} – mean compressive concrete strength

$\varepsilon_{c,1}$ – strain at the peak compressive stress

$k = 1.05 E_{cm} x |\varepsilon_{c,1}|/f_{cm}$

$\eta = \varepsilon_c/\varepsilon_{c,1}$

The relationship between the uniaxial stress and strain is considered linear with the slope coefficient equal to the secant modulus of elasticity of the concrete material (E_{cm}) up to the stress limit of $0.4 f_{cm}$. Beyond this limit the concrete behaves nonlinearly with ascending branch up to the value of mean compressive strength (f_{cm}) and corresponding strain at the ultimate stress (ε_{c1}).

After this point the concrete experiences increasing degradation, represented by the descending branch until ultimate strain concrete compressive strain (ε_{cu1}). Due to the presence of the embedded rail channel it is not expected that considerable damage related to compression will be allocated in the concrete matrix, the stress-strain relationship was not extended beyond this limit.

The uniaxial model for concrete in tension was developed using two-part stress-strain curve. The stress-strain relationship is linear elastic up to the cracking strain (ε_{cr}) followed by decaying parabolic function proposed by Wang et al. [48] beyond this limit.
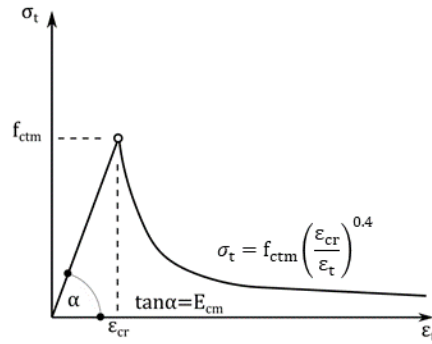
Figure 6.2 - Uniaxial stress-strain model for concrete in tension

$$\sigma_t = E_{cm}\varepsilon_c \quad \varepsilon_t \leq \frac{f_{ctm}}{E_{cm}} = \varepsilon_{cr}$$

$$\sigma_t = f_{ctm}\left(\frac{\varepsilon_{cr}}{\varepsilon_t}\right)^{0.4} \quad \varepsilon_t > \frac{f_{ctm}}{E_{cm}} = \varepsilon_{cr}$$

(6.2)

E_{cm} – secant modulus of elasticity of concrete

f_{ctm} – mean axial tensile strength of concrete

ε_{cr} – cracking strain

Based on the defined uniaxial stress-strain models appropriate CDP (Concrete Damaged Plasticity) model of the concrete material was defined considering compound stress-strain state. The recommended parameters for the definition of the model were applied (Table 6.1).

Table 6.1 - CDP model parameters

Dilatation angle	Eccentricity	$f_{b,0}/f_{c,0}$	K	Viscosity parameter
36°	0.1	1.16	0.667	0

After the onset of damage, the degradation of the concrete material is expressed as a reduced concrete material stiffness. The damage parameters d_c and d_t are the functions of the inelastic strains $\tilde{\varepsilon}_c^{in}$ and the $\tilde{\varepsilon}_t^{in}$ respectively (Figure 6.3).
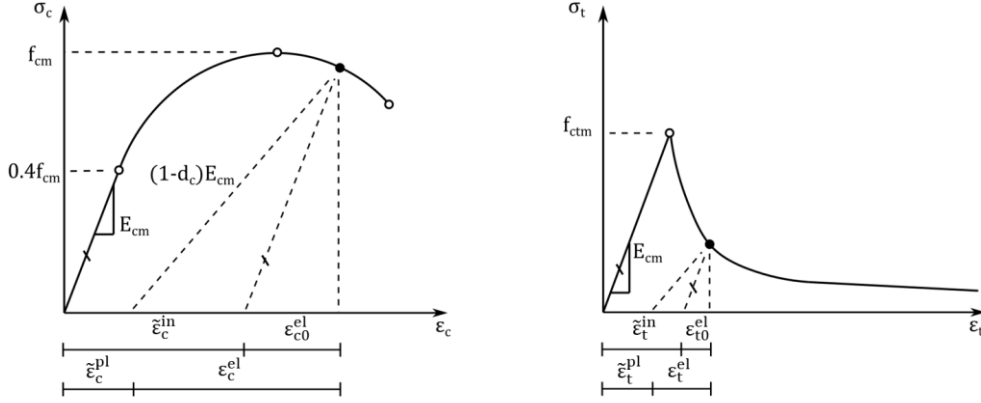
Figure 6.3 - Concrete tensile and compressive damage models

Beyond the onset of damage, the plastic strains $\tilde{\varepsilon}_c^{pl}$ and $\tilde{\varepsilon}_t^{pl}$ are then computed as:

$$\tilde{\varepsilon}_c^{pl} = \tilde{\varepsilon}_c^{in} - \frac{d_c}{1 - d_c} \cdot \frac{\sigma_c}{E_{cm}}$$

$$\tilde{\varepsilon}_t^{pl} = \tilde{\varepsilon}_t^{in} - \frac{d_c}{1 - d_c} \cdot \frac{\sigma_c}{E_{cm}}$$

(6.3)

At the onset of damage, the damage parameters d_c and d_t are nonrelevant ($d_c = d_t = 0$). Beyond this limit the damage evolution functions were defined by comparing the damaged and undamaged concrete response regarding the compressive strength f_{cm} or tensile strength f_{ctm} of the concrete material and they were provided as a function of respective compressive and tensile inelastic strains.

The damage evolution functions are defined as:

$$d_c = 1 - \frac{\sigma_c}{f_{cm}} \quad \varepsilon_c > \varepsilon_{c1}$$

$$d_t = 1 - \frac{\sigma_t}{f_{cmt}} \quad \varepsilon_c > \varepsilon_{cr}$$

(6.4)

Below are represented adopted stress-strain relationships and damage evolution functions expressed in function of the inelastic strain for the concrete class C40/50 that was adopted as a representative class that characterizes the concrete material of the test campaign (Figure 6.4). The input data regarding the concrete material for the later FE analysis is provided within the *Annex E - CDP material model of the concrete material* of the document.
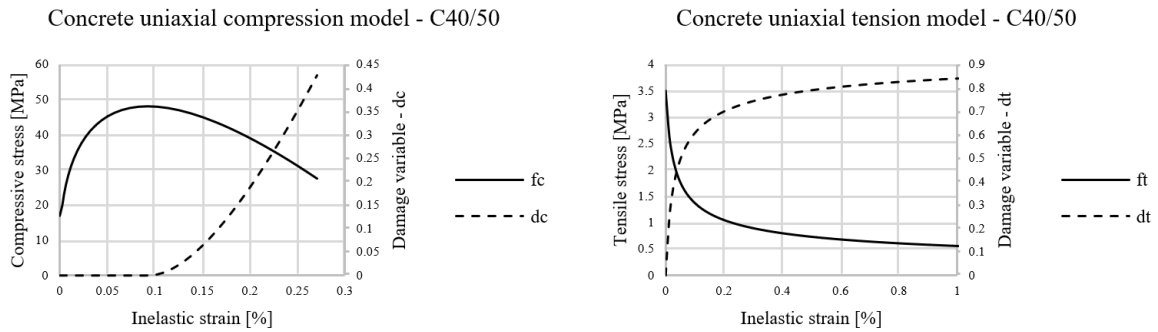
Figure 6.4 - Compressive and tensile damage models - C40/50

6.1.2 Reinforcement

As no particular tensile tests were performed in order to investigate the uniaxial tensile material behaviour of the rebar material, the behaviour of the reinforcement material B500 B was modelled applying simple bilinear stress-strain curve (EN 1993-1-5 Annex C [49]) characterized by the modulus of elasticity $E_a = 210 GPa$ up to the yield limit of $f_y = 500 MPa$. The beyond yielding behaviour was modelled as perfectly plastic (Figure 6.5).
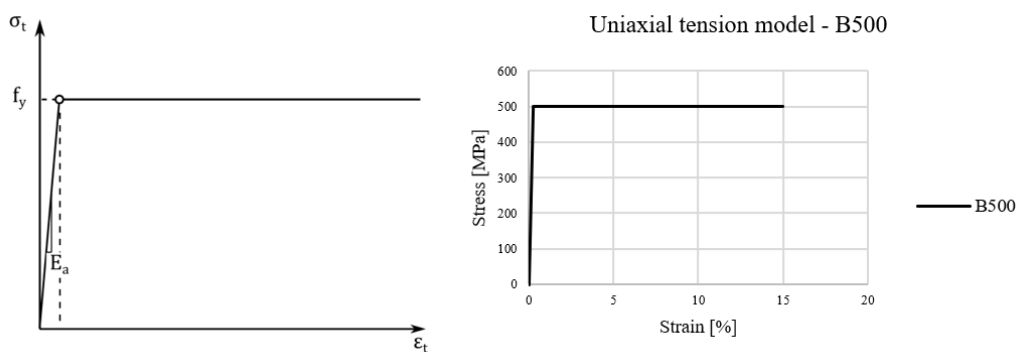
Figure 6.5 - Uniaxial tension model of reinforcement material

Based on the uniaxial tensile stress-strain model defined above, the Von-Misses yield surface is used to model the isotropic yielding of the steel material without accounting for the damage evolution of the steel material.

6.1.3 Steel connector assembly parts

6.1.3.1 Back plate and steel section material

The material of the steel section and of the back plates is declared by the producer as S355JRG. No separate tensile tests were performed in order to investigate uniaxial behaviour of the steel material. The material properties were defined according to the Table 3.1 of EN 1993-1-1 [50].
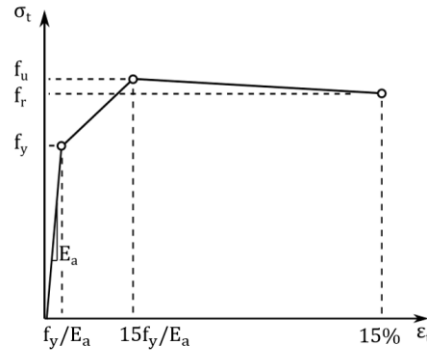
Figure 6.6 - Trilinear uniaxial stress-strain tension model

The adopted stress-strain relationship was a trilinear model (Figure 6.6). The elastic portion is defined by the modulus of elasticity ($E_a = 210GPa$) up to the yielding limit ($f_y = 355MPa$). The ultimate tensile strength of ($f_u = 490MPa$) is reached at the minimum required strain ($15f_y/E_a$). The fracture stress ($f_r = 475MP_a$) is reached with the minimum elongation of 15% (Figure 6.7).
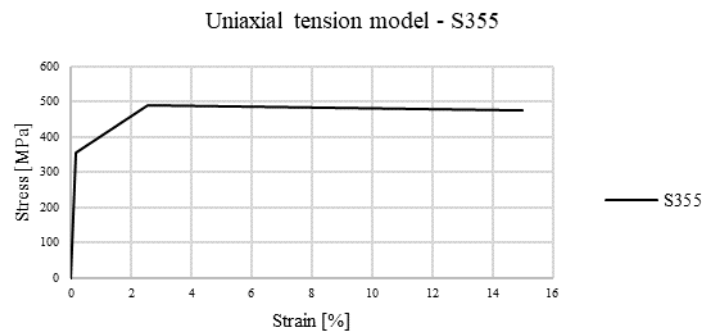
Figure 6.7 - Trilinear uniaxial stress-strain tension model - S355

Based on the uniaxial tensile stress-strain model defined above, the Von-Misses yield surface is used to model the isotropic yielding of the steel material without accounting for the damage models in a similar fashion as in the case of the reinforcement material.

6.1.3.2 Rail and anchor material

In the case of the steel materials of the rail and anchor parts, the experimental results of tensile tests were available hence the obtained stress-strain curves were applied directly in order to define uniaxial tensions stress-strain relationship of the steel material in accordance with EN 1993-1-5 Annex C (Figure 6.8).
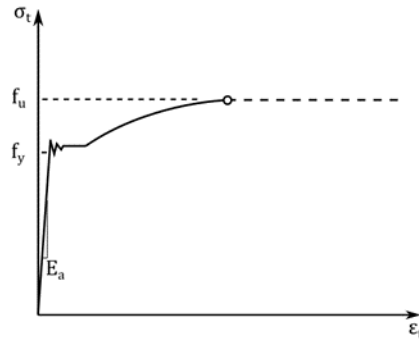
Figure 6.8 - Uniaxial tension model based on the test results

The relationship was provided up to the ultimate strength limit as beyond, due to the necking and strain localization, the experimental results do not adequately address the material behaviour. After this point the assumed response is ideal plastic behaviour (Figure 6.9).
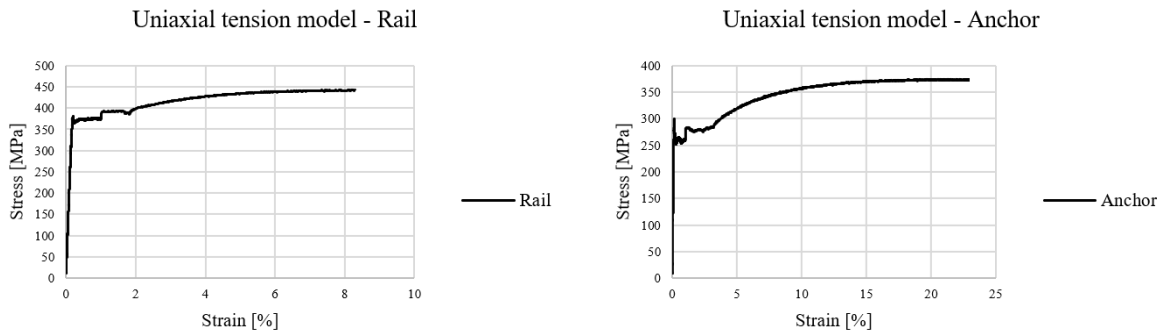
Figure 6.9 - Uniaxial tension model based on the test results - Rail and Anchor

Based on the uniaxial tensile stress-strain model defined above, the Von-Misses yield surface is used to model the isotropic yielding of the steel material without accounting for the damage models in a similar fashion as in previous two cases.

6.1.3.3 Bolt steel material

6.1.3.3.1 Ductile damage

The critical steel parts in the connector assembly that experience or may experience the significant plastic strains and failure are the bolts. For the specified steel materials of the bolt parts appropriate progressive damage material models were developed.

After reaching the ultimate tensile strength f_u of the steel material in uniaxial tensile test due to the plastic strain localization in the necking zone the true stress-strain curve may no longer represent the necking of the specimen and failure behaviour of the steel material.

In order to consider this effect, the ductile damage model for the ductile metal materials was applied (Figure 6.10). The damage model comprises damage initiation criteria based on the equivalent plastic strain at the onset of damage $\bar{\varepsilon}_0^{pl}$ and the damage evolution law that is expressed as a function of the stress triaxiality θ. As the experiments were performed in a quasi-static manner the effect of the strain rate is disregarded.
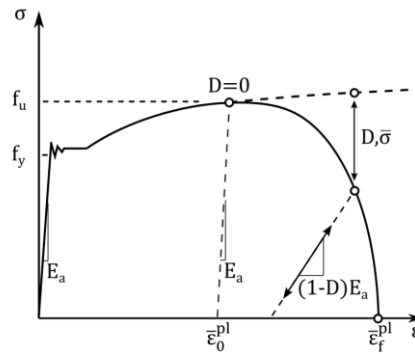
Figure 6.10 - Damage model for ductile metals

In a similar manner to the CDP model the damage parameter D evolves from the onset of damage ($D = 0$) reducing the initial material stiffness until the failure ($D = 1$).

The relationship between the equivalent plastic strain at fracture $\bar{\varepsilon}_f^{pl}$ and the stress triaxiality θ is based on the exponential function and parameters α and β.

$$\bar{\varepsilon}_f^{pl} = \alpha \cdot e^{-\beta \cdot \theta}$$

(6.5)

The previous relationship is valid as well for the uniaxial stress state.

$$\varepsilon_f^{pl} = \alpha \cdot e^{-\beta \cdot \frac{1}{3}}$$

(6.6)

The ratio between the equivalent plastic strain $\bar{\varepsilon}_f^{pl}$ and plastic strain ε_f^{pl} at fracture is then:

$$\frac{\bar{\varepsilon}_f^{pl}}{\varepsilon_f^{pl}} = e^{-\beta \cdot (\theta - \frac{1}{3})}$$

(6.7)

From the assumption that the ratio between the equivalent plastic strain $\bar{\varepsilon}_f^{pl}$ and the uniaxial plastic strain at fracture ε_f^{pl} and at the onset of the damage is the same ($\frac{\bar{\varepsilon}_f^{pl}}{\varepsilon_f^{pl}} = \frac{\bar{\varepsilon}_0^{pl}}{\varepsilon_0^{pl}}$):

$$\bar{\varepsilon}_0^{pl} = \varepsilon_0^{pl} e^{-\beta \cdot (\theta - \frac{1}{3})}$$

(6.8)

The parameter β is adopted as recommended value (β = 1.5). Taking that the onset of damage is equivalent to the start of the necking in the uniaxial tensile test, the damage initiation law is established as a function of plastic strain at the onset of necking ε_n^{pl} and the stress triaxiality θ.

$$\bar{\varepsilon}_0^{pl} = \varepsilon_n^{pl} e^{-1.5 \cdot (\theta - \frac{1}{3})}$$

(6.9)

Based on the derived relationship the damage initiation law was defined for the critical steel materials (Figure 6.11).
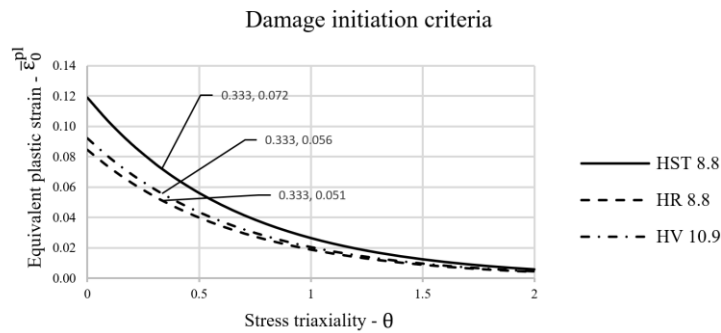
Figure 6.11 - Damage initiation law for bolt steel materials

When the damage initiation criterion is reached, the damage evolution law is defined as displacement dependent over the effective plastic displacement length $\bar{u}_{pl}$. The effective displacement length $\bar{u}_{pl}$ is dependent on the characteristic length of the finite element L_{char} and the effective plastic strain accumulated in the necking zone:

$$\bar{u}_{pl} = L_{char}(\varepsilon_{f,loc}^{pl} - \varepsilon_{n,loc}^{pl})$$

(6.10)

The effective plastic displacement length defined in this manner is hence mesh dependent. As no special means to determine the development of the plastic strains in the necking zone were considered during tensile tests, the value of the effective plastic displacement length $\bar{u}_{pl}$ was calibrated so the numerically obtained stress-strain curves match the experimental data (Table 6.2).

Table 6.2 - Ductile damage model parameters

Material	ε_n^{pl}	β	L_{char} [mm]	$\bar{u}_{pl}$ [mm]
HST 8.8	0.072	1.5	1.25	0.415
HR 8.8	0.0513	1.5	1.25	0.4
HV 10.9	0.0556	1.5	1.25	0.4

Good agreement was obtained observing the stress-strain relationship along the base length ($l_0 = 25mm$) between the experimental tensile test results and the results of the numerical model in terms of stiffness, strength and the ductility.
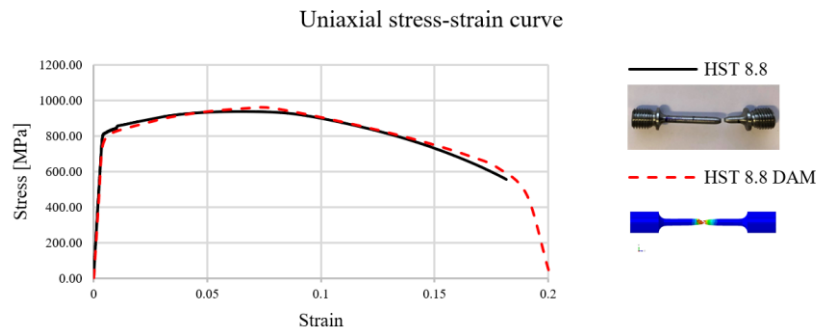
Figure 6.12 - Experimental and numerical nominal stress-strain curves - HST 8.8

In the case of the HR 8.8 bolt material during the tensile tests the necking occurred in the vicinity of the fillet transition between the grip and test diameter of the cross section hence the deformation is observed only until the necking point. However, the developed model

conforms well to the test results until the necking and in terms of the fracture elongation (A = 20%). The comparison between the test and numerical results of the tensile test assembly for the HR 8.8 and HV 10.9 materials is provided in the Figure 6.13.
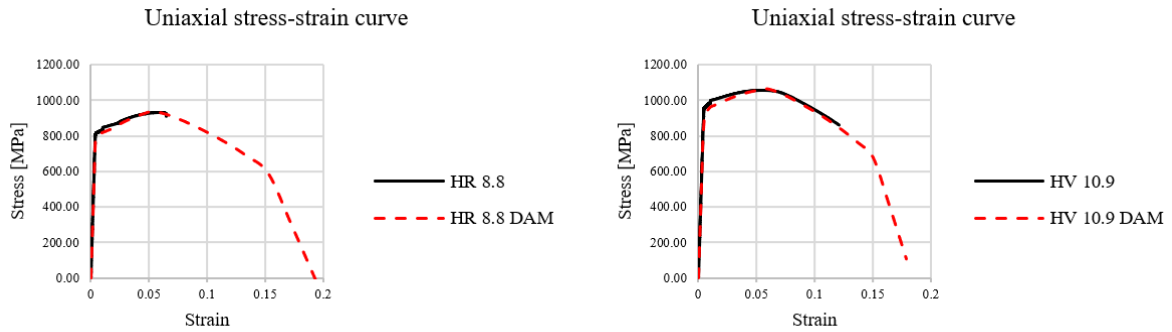
Figure 6.13 - Experimental and numerical nominal stress-strain curves – HR 8.8 & HV 10.9

6.1.3.3.2 Shear damage

After the parameters for the ductile damage model were established for the steel bolt materials the progressive shear damage model for the ductile material was built as an improvement as the overall force-slip response strongly depends on the material behaviour related to the shear.

The parameters for the progressive shear damage model were obtained comparing the force-slip response of the bolt shear tests elaborated in the chapter *5.3 Material tests* and the one obtained from the numerical model (Figure 6.14).
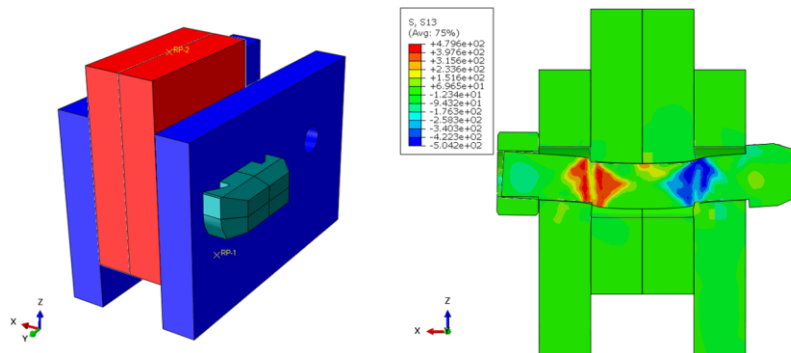
Figure 6.14 - FEA bolt shear model

The plate parts were modelled with the C3D8 elements with applied material model defined for the S355JR steel material. The bolt parts were meshed with the C3D4 finite elements with the element size of $L_e = 1.25mm$, the same type used for the modelling of the ductile damage regarding the tensile tests of the bolt steel material. The same elements were used later for the localized numerical model of the push tests.

The damage initiation law is defined as equivalent fracture strain $\bar{\varepsilon}_{f,s}^{pl}$ in function of the shear stress ratio θ_s that is the ratio between the equivalent stress q and pressure p to the maximal tangential stress τ_{max}.

$$\theta_s = (q + k_s p)/\tau_{max}$$

(6.11)

During the large deformation under the shear load of the bolt the pretension force is lost, hence it is assumed that at the bolt failure the stress state of the bolt material corresponds to the state of the pure shear ($\theta_s = 1.732$) thus the equivalent fracture strain is calibrated to the constant value of the shear stress ratio. The constant k_s is adopted as a recommended value for the dual-phase steel materials ($k_s = 0.2$).

For the damage evolution law, the displacement control shear damage evolution with the exponential decay dependent on the curve parameter α was adopted. In order to account for interaction between the ductile damage and shear damage models, the multiplicative degradation mechanism was adopted. The model parameters are presented in the Table 6.3.

Table 6.3 - Shear damage model parameters

Material	$\varepsilon_{f,s}^{pl}$	θ_s	L_{char} [mm]	$\bar{u}_{pl}$ [mm]	α
HST 8.8	0.072	1.732	1.25	0.3	1.0
HR 8.8	0.0513	1.732	1.25	0.25	1.0
HV 10.9	0.0500	1.732	1.25	0.3	0.7

Good agreement was obtained between experimental and numerical results (Figure 6.15). The numerical curve is offset in order to account for the initial deformation of the test assembly as the displacement measures were taken from the total displacement of the hydraulic jack.
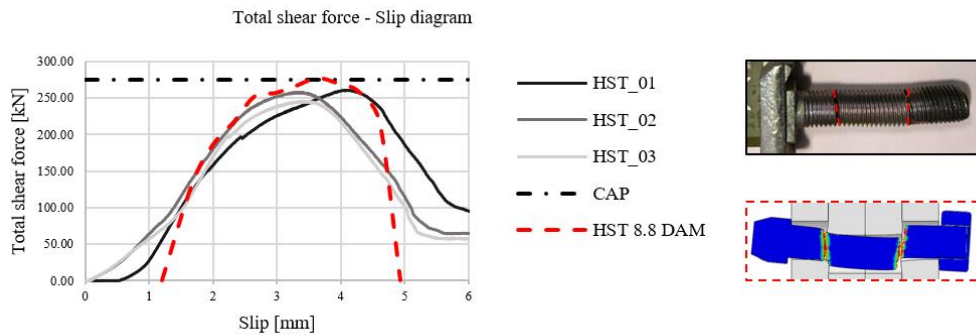
Figure 6.15 - Experimental vs. numerical bolt shear result - HST 8.8

The force delay of experimental response is due to the embedment of the parts of the threads that separated from the bolt shank during the slip. Good agreement was obtained concerning the HR 8.8 and HV 10.9 bolt materials as well (Figure 6.16). The steel material input data regarding later push test simulations is provided in the *Annex F - Steel material models*.
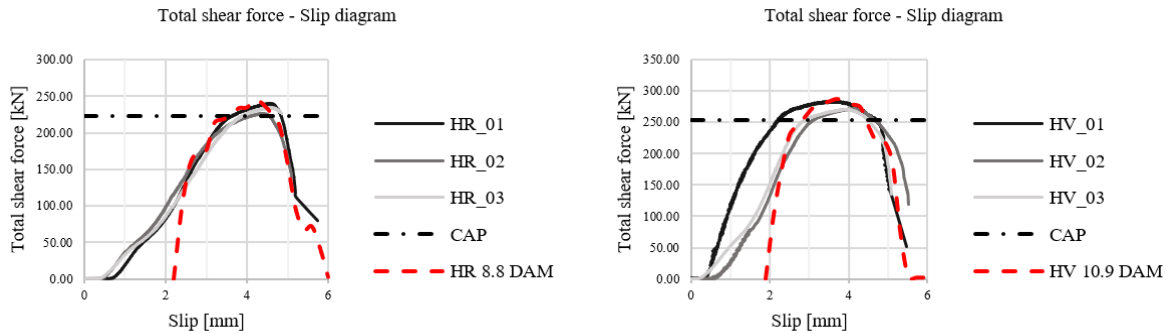
Figure 6.16 - Experimental vs. numerical bolt shear result - HR 8.8 & HV 10.9

6.2 Modelling technique and simulation sequencing

For the in-depth numerical investigation of the force-slip behavior of the proposed demountable connector devices, advance localized push FEA models were developed using Abaqus 2018 FEA software suite [51]. The material models applied were the ones developed in the previous chapter *6.1 Material models*.

Firstly, based on the principles of symmetry, the geometry of the localized FEA model was delimited (Figure 6.17) reducing the computational burden of the FE analysis. The localized push model concerns the response of the single shear connector assembly but considering the localized response of the surrounding concrete in the load introduction zone around the connector assembly. The FEA force-slip results obtained in this manner may be compared directly with the experimental force-slip results presented in the chapter *5.4 Push test results*.
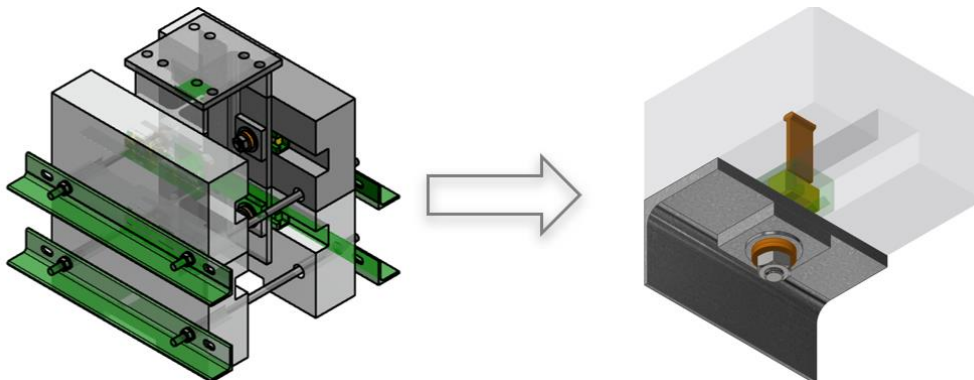
Figure 6.17 - Localization of the FEA model geometry

The displacements of the "support" face of the concrete part were coupled using coupling constraint with the displacements of the reference point RP-1 that was fixed. This way the support of the system in the direction of the load introduction was defined. The capacity per connector during the analysis is extracted then as the reaction in the direction of slip at the reference point RP-1 (Figure 6.18).

The displacements of the load introduction face of the HEB 260 were coupled to the reference point RP-2 in the similar fashion. However, the reference point RP-2 serves as a load introduction point (force or displacement load). The slip displacement was measured in the direction of the slip at the reference point RP-2.
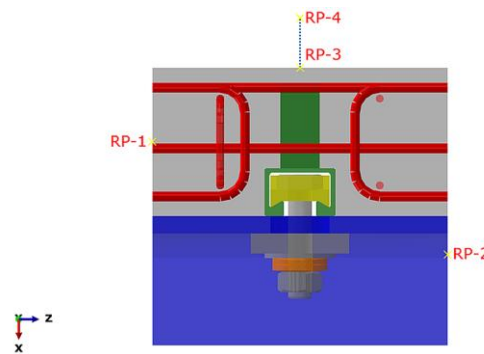
Figure 6.18 - Localized FEA model - Connector Type B

The effect of the lateral restraint assembly was introduced as the spring element between the reference points RP-3 and RP-4. The displacements of the top surface of the concrete slab were coupled with the displacements of the reference point RP-3 while the reference point RP-4 was fixed. The stiffness of the spring element conforms to the symmetric axial stiffness of the restraining threaded rod M20 8.8.

The symmetric restraint boundary conditions were applied in the XZ (web vertical midplane) and YZ (web transversal midplane) planes due to the symmetric boundary conditions.

The reinforcement was modelled as a 3D wire (line) part and meshed with the linear truss elements. In order to simulate joint response of the reinforced concrete slab, the reinforcement was constrained in the concrete matrix of the slab using embedment constraint providing the joint mechanical response of the slab and embedded reinforcement.

All parts were modelled using C3D8R solid elements except for the bolt and nut parts that were modelled using C3D4 elements with the same finite element properties described in the chapter *6.1 Material models*. The reinforcement wire part was meshed with the T3D2 truss elements.

The interaction between the parts, except between the reinforcement and the concrete slab that was modelled using embedment constraint, was modelled using surface-to-surface contact pairs. The contact property in the normal direction was modelled as "hard" with allowed separation during the analysis while the behavior in the tangential direction was modelled as "penalty" formulated frictional behavior with constant and isotropic friction defined by the coefficient of the friction μ_i.

The frictional coefficients for the concrete-steel faying surface and for the faying surface between the hot-dip galvanized plates (Table 6.4) were adopted according to the values for the friction-grip connectors explained in the chapter *3 State of the Art* and from the available literature [52].

Table 6.4 - Frictional coefficient of surface pairs

Surface pair	μ
Slab-Rail	0.45
Slab-Flange	0.45
Flange-Back plate	0.30
Steel-Steel	0.20

In order to achieve convergence of the highly nonlinear FEA model, the Abaqus/Explicit dynamic solver was used. The stable time increment of the dynamic analysis depends on the minimum size of the element in the mesh $L_{char,min}$ and on the speed of dilatation wave propagation c_d that for the linear elastic material may be expressed as:

$$c_d = \sqrt{\frac{E}{\rho}}$$

(6.12)

E – Modulus of elasticity

ρ – Density

The maximum stable time increment $\Delta_{t,max}$ is then expressed as:

$$\Delta_{t,max} = \frac{L_{char,min}}{c_d}$$

(6.13)

The maximal stable time increment $\Delta_{t,max}$ usually demands very large computational time and is not suitable for the execution of the quasi-static analyses as the one intended to recreate push tests in this case. In order to rationalize the computational time while still obtaining quasi-static response of the system, semi-automatic nonuniform mass scaling throughout the step was applied to the whole model. The increase of the mass leads to the increase of the stable time increment however it also introduces the increase of inertial forces in the model, hence the good compromise has to be achieved between the actual time demand for the execution of the simulation and the validity of the obtained results regarding minimization of the inertial effects.

In order to reduce further the inertial effects by reducing accelerations in the system during the analysis, the loads (temperature and monotonic displacement loads) were variated throughout the step adhering to the "smooth step" amplitude function (Figure 6.19).
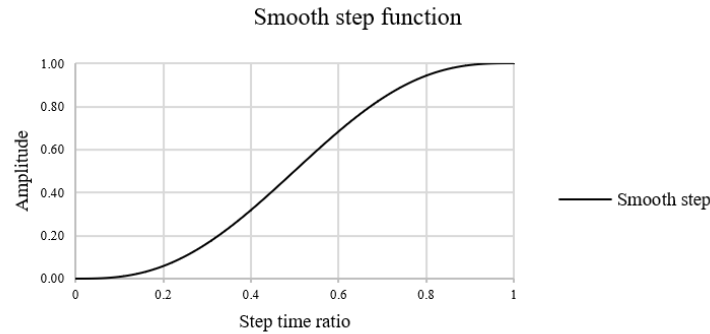
Figure 6.19 - Smooth step curve

The analysis is performed in several steps (Figure 6.20). In the first step (0-1) the pretension force in the bolt part is applied as the temperature difference ($\Delta T < 0$). The intensity of the temperature difference ΔT_i is calibrated so the obtained pretension force agrees with the designated pretension force F_p from the actual push tests. The pretension force introduces the clamping action between the faying surfaces.

In the following step (1-2), using the rising smooth step amplitude, the mean force value of the cycling stage is introduced in the force-controlled mode. When the mean force of the

cycling stage is reached, the cycling step is initiated. The cycling step is composed out of 25 harmonic cycles where the load is variated between 5% and 40% of the ultimate force per connector obtained in the first test $(P_{u,1})$.
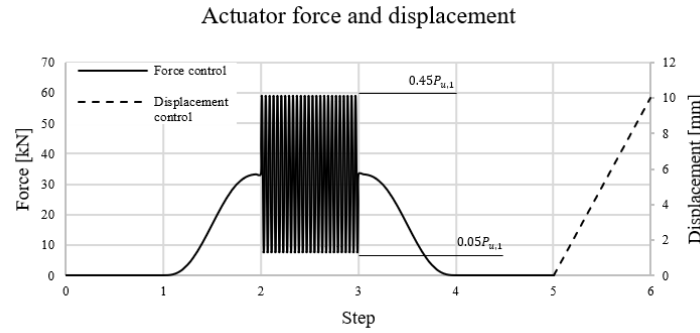
Figure 6.20 - Simulation load sequencing - Connector Type B

After the cycling step (2-3), in the following step (3-4) the system is deloaded following the decaying smooth step function. In order to terminate the kinetic effects in the system, the system is relaxed in the following step (4-5). In the slip step (5-6) the displacement-controlled load is variated along the step in linear order adhering to the procedure of the actual experimental load sequencing.
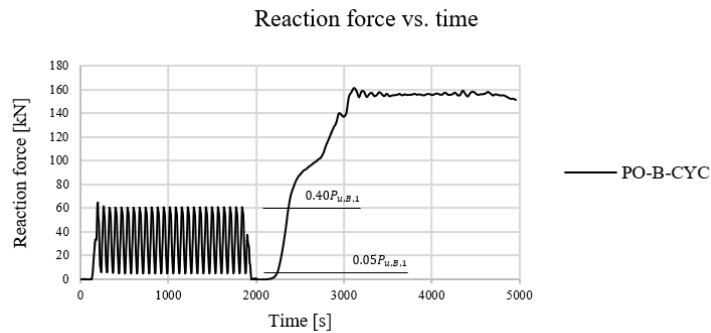
Figure 6.21 - Simulation reaction force - Connector Type B

The validity of the simulation results obtained with the target time increment ($\Delta t = 0.025 s$) was approved by the good response in the cycling step regarding force response (reaction) that is particularly sensitive to inertial effects (Figure 6.21). During the cycling step the reaction completely matched the designated force load applied with the harmonic function at the reference point RP-2 (Figure 6.20 & Figure 6.21).
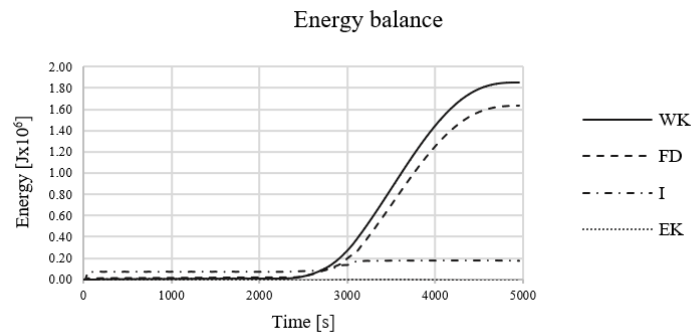
Figure 6.22 - Simulation energy balance - Connector Type B

The validity of the results was also confirmed by observing the energy balance of the whole model as the kinetic energy was negligible during the whole analysis compared to the all other energy contributions (Figure 6.22). The good response of the model is also observed in the level of artificial strain energy (hourglass effect) that was kept at the level of 5% relative to the total internal energy (I).

It may be observed that after the activation of the second faying surface in the case of the connector Type B, the external work (WK) generated in the model is "spent" on the sliding in the displacement-controlled step expressed by the friction dissipation energy contribution (FD). These results correspond to the stable stress-strain state of the assembly accompanied by the sliding action at the faying surfaces.

6.3   Numerical analyses results

6.3.1   Connector Type A

After the pretension step (I), the force-slip behaviour of the connector Type A exhibits significant flexibility in the initial force-slip response (Figure 6.23). The numerical results provide more flexible response in the initial stage compared to the experimental results due to the precise modelling of the tolerances of the complicated clamp assembly.
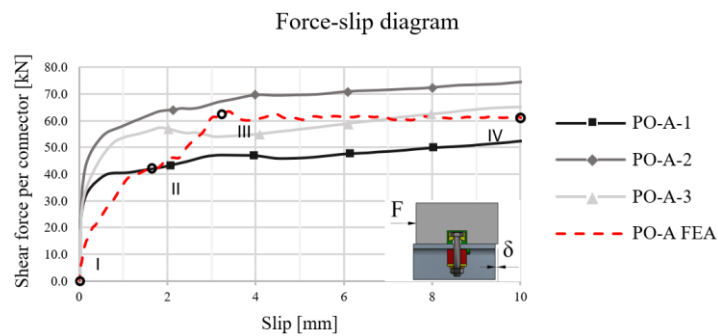
Figure 6.23 - Experimental vs. numerical force-slip results - Connector Type A

Due to the tolerances within the connector assembly the slip capacity is reached only with substantial deformation (II) until the clamp element is blocked inside the rail what prevents the free rotation of the clamp assembly under the shear load.

After the clamp tail is blocked inside the rail channel socket (II) the clamp element has two supports in the direction of the shear load (bolt and the rail channel lip at the clamp tail) and the additional frictional capacity is developed at the second faying surface (flange-clamp). The stronger activation of the secondary capacity contribution mechanism is manifested with double-curvature bending state of the bolt due to the shear action of the bolt (II).
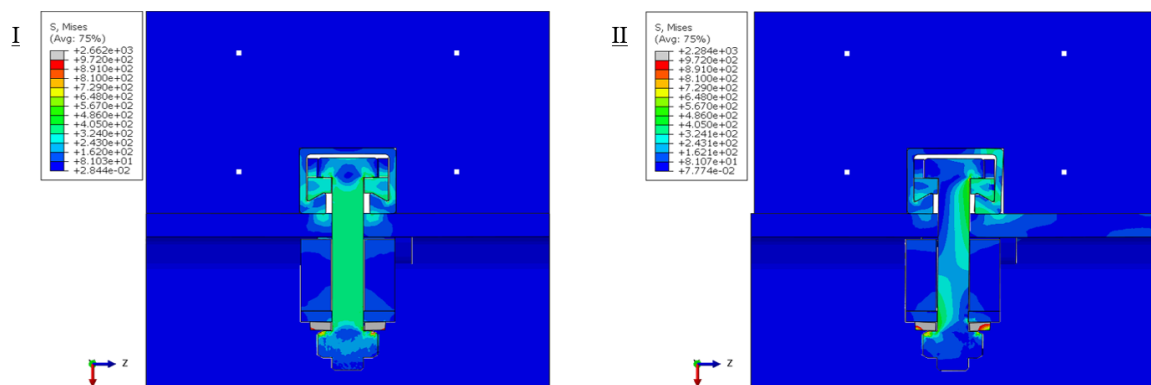
Figure 6.24 - Stress field development - Connector Type A

The reaction is increased until the friction capacity is reached at the both faying surfaces producing the sliding under the constant reaction force (capacity). This state is characterized by the constant stress and deformation state of the connector assembly (III-IV).
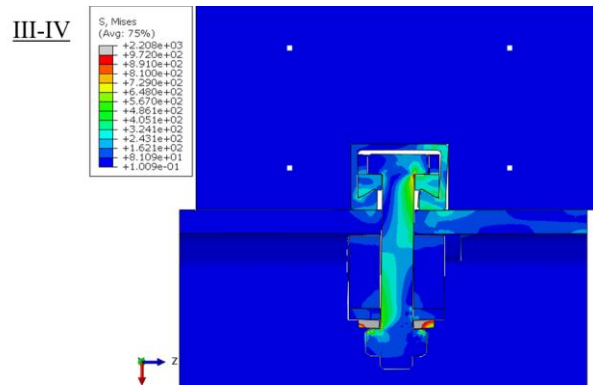
Figure 6.25 - Stable stress state - Connector Type A

When the sliding state is reached, the damage evolution parameter *D* is negligible across the whole model (concrete and bolt parts). These results support the assumption that the concrete slab element remains undamaged when the ultimate capacity P_u of the connector is reached and that due to the provision of the substantial elastic reserve of the bolt material there shall be no pretension (clamping force) loss during the loading due to the plasticity of the bolt material (Figure 6.26).
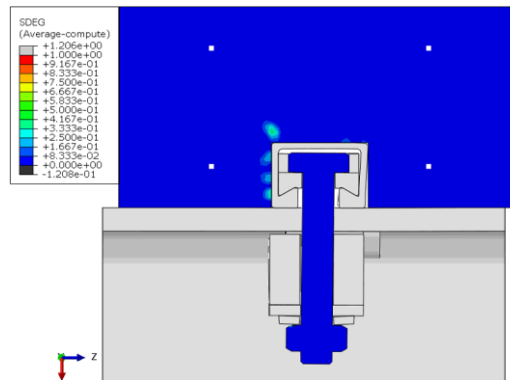
Figure 6.26 - Damage parameter at the stable stress state - Connector Type A

The numerical results in terms of the slip at the ultimate capacity δ_u and the ultimate capacity P_u of the shear connector Type A is matched well with the results of the experimental campaign (Figure 6.23). However, due to the uncertainty of the pretension application, low developed capacity of the shear connector Type A and complicated and resource intensive manufacture, it is concluded that it is not suitable for the proposed application.

6.3.2   Connector Type B

The numerically obtained force-slip curve per shear connector matches well with the experimentally obtained force slip results (Figure 6.27). The pretension bolt assembly is firstly preloaded to the desired pretension force by applying the negative temperature difference ΔT to the bolt part. The high strength M24 HV 10.9 pretension bolt is axially loaded producing the clamping force at the friction interfaces (I).
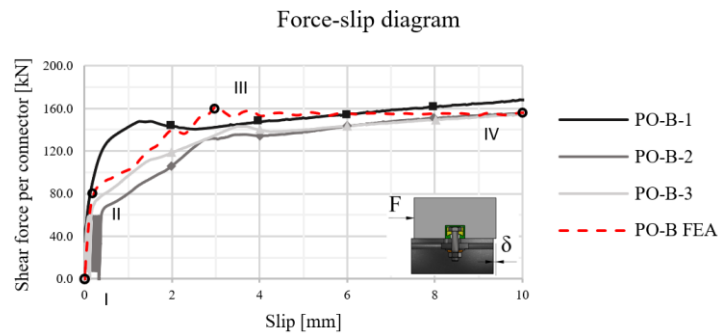
Figure 6.27 - Experimental vs. numerical force-slip results - Connector Type B

The slip displacement introduced at the load application surface of the steel section initiates reaction at the support due to the frictional capacity at the first faying surface (concrete slab-steel section flange). The increase of the resistance is immediate until the reaching of the slip capacity at the first faying surface (II). Until this point the second faying surface is not activated. This is proven by the almost axial stress state in the bolt shank at the slip capacity of the shear connector (Figure 6.28).
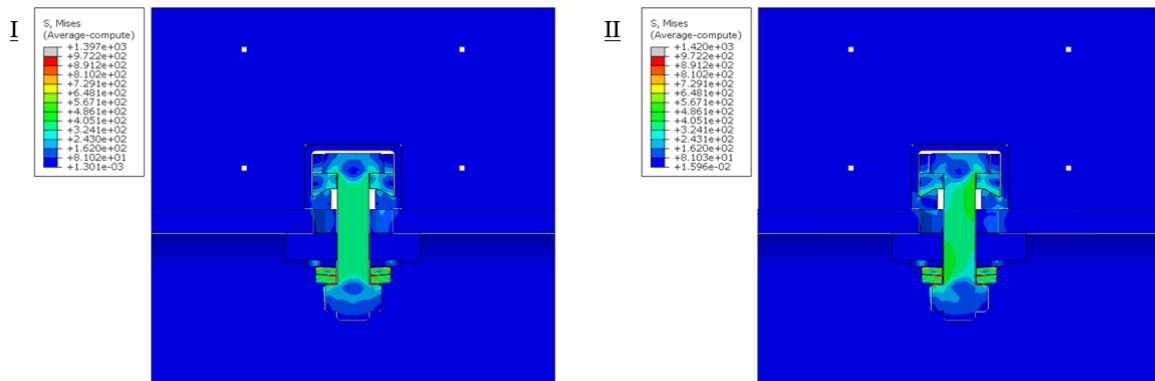
Figure 6.28 - Stress field development - Connector Type B

The additional slip displacement activates the bottom faying surface (steel section flange-back plate). The additionally generated frictional force is transmitted via the bolt shank by bending

of the bolt in shear (II-III). This stress state of the bolt shank is consequence of the combined actions effects of the pretension force, the shear and moment generated by the frictional capacity at the second faying surface by the same pretension force (M-V-P). This region is distinct with the finite stiffness branch of the force-slip curve that is related to the bending stiffness of the bolt and its boundary conditions within the connector assembly. When the slip capacity is reached at the second faying surface (III) as well, the system response is attributed to the sliding of the steel section flange, clamped between the two faying surfaces until the long-slotted bolt hole tolerance is closed (III-IV). Due to the allocation of the substantial elastic reserve of the bolt material regarding the target pretension force F_p, the reached stable stress state of the bolt did not consider yielding of the bolt shank material (Figure 6.29) what would deload the pretensioned bolt and reduce the total capacity by reducing the frictional contributions of the two faying surfaces.
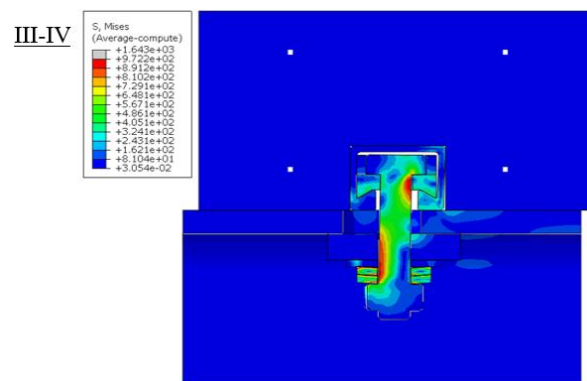
Figure 6.29 - Stable stress state - Connector Type B

The damage variable D of the concrete slab at the ultimate capacity (stable stress state) related to the tensile failure of the concrete material is limited to the load introduction zone and develops only to the extent of the first reinforcement bars while the bolt remained undamaged.
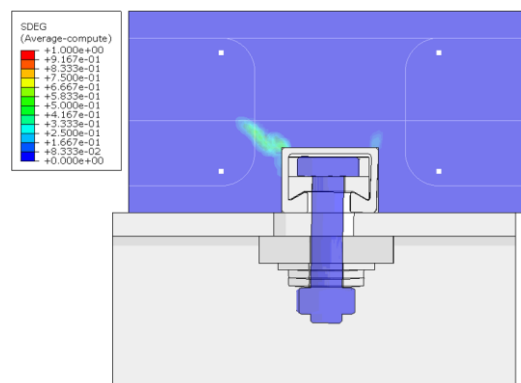
Figure 6.30 - Damage parameter at the stable stress state - Connector Type B

6.3.3   Connector Type C

The numerically obtained force-slip behaviour of the connector Type C push test simulation matches well with experimental push test data (Figure 6.31). After the pretension step (I) where the bolt shank is axially loaded, the slip displacement applied at the load introduction surface of the steel section closes the connector assembly tolerances while the friction generated capacity originates from the first faying surface.
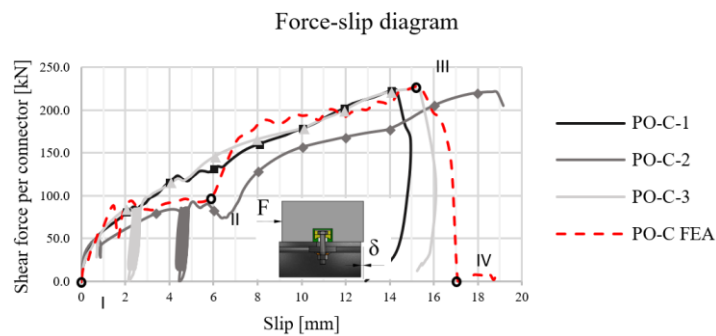
Figure 6.31 - Experimental vs. numerical force-slip results - Connector Type C

After the closure of the assembly tolerances (II) the system regains stiffness (Figure 6.32). The large diameter circular bolthole bears on the unthreaded shank of the M20 HR 8.8 bolt and the connector response is dominated by the shear action of the bolt (II). Due to the shear force (reaction) distribution partially via the wall of the embedded rail channel, the rail wall opposite to the load introduction zone separates from the concrete slab rail channel socket.
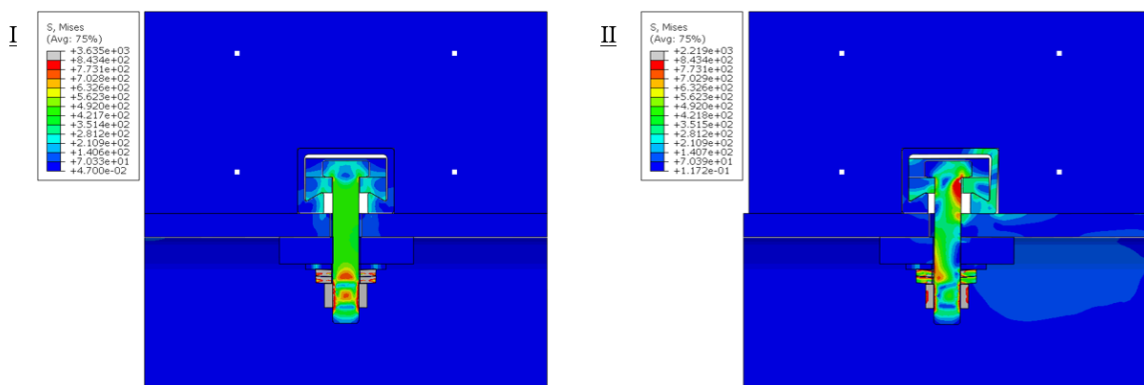
Figure 6.32 - Stress field development - Connector Type C

Due to the large lever arm e_b of the bolt shank the increase of the shear load generates the plastic hinging at the bolt shank supports (III). The slip is rapidly increased until the bolt shank gets into the contact with the rail lip at the side of the load introduction.

When the bolt shank contacts the rail lip, the shear introduction from the flange bolt hole has direct support in the form of the rail lip and the load is transferred via this shear plane. The increase of displacement shears off the bolt at this particular location in a brittle manner (IV).
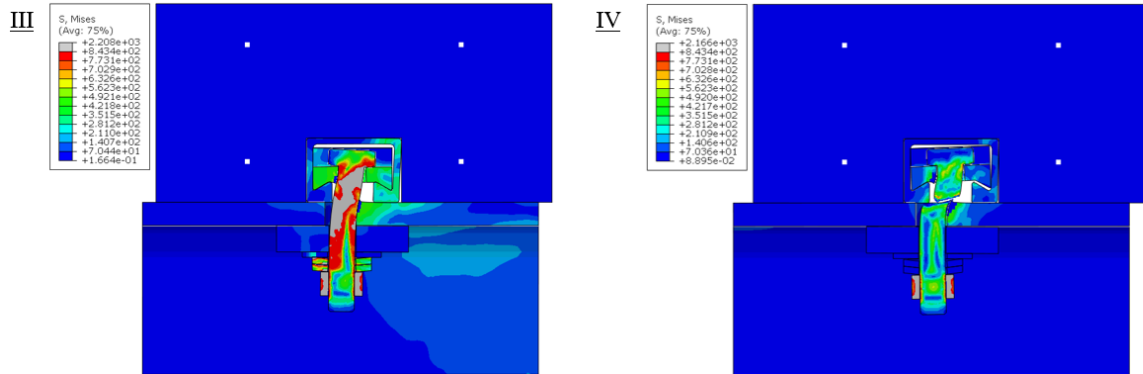
Figure 6.33 - Plastic hinging followed by the shear failure - Connector Type C

The obtained fractured bolt shape matches well with the fractured shape obtained during the course of the push tests (Figure 6.34). The obtained ultimate capacity F_u matches well with the combined shear failure load produced by the double-curvature hinging of the bolt shank $M_{pl,b}$ followed by the shear of the unthreaded bolt shank F_v of the M20 HR 8.8 pretension bolt.
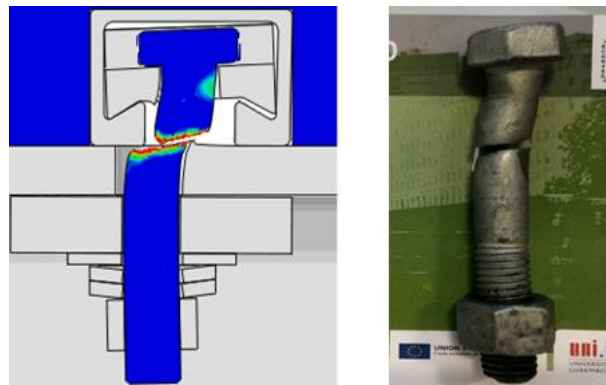
Figure 6.34 - Bolt shear failure shape - FEA vs. experimental result (Connector Type C)

The obtained capacity per shear connector in the case of the connector Type C was the highest achieved of all shear connector typologies ($P_u \cong 220 kN$). It was particularly important to check the damage state of the concrete surrounding the load introduction zone at the point of the maximum shear capacity P_u. In the numerical model limited distribution of the damage parameter D related to the concrete failure in tension was observed but only to the extent of the first reinforcement bars (Figure 6.35). This was confirmed by performing a section cut of the slab test specimen through the axis of the shear connector where no cracking at the load introduction zone could be observed. At the same time, the separation of the rail wall at the

opposite side of the load introduction zone is evident just like in the case of the numerical
analysis (Figure 6.35).
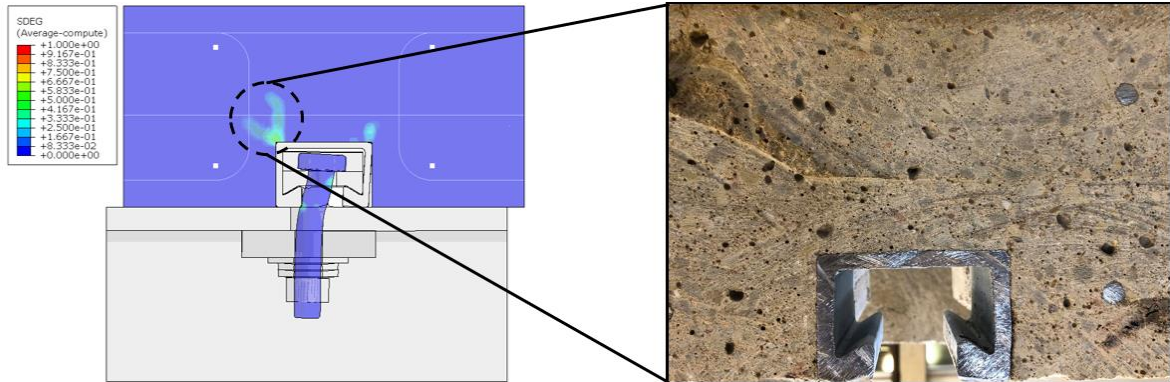
Figure 6.35 - Concrete damage state at the load introduction zone

The state of the concrete slab in the case of connector Type C after the actual push test and at
the ultimate reaction point of the numerical model supports the assumption that the concrete
remains intact even when the high concentrated shear loads are introduced at the load
introduction zone of the connector assembly.

6.3.4 Connector Type D

The numerically obtained force-slip model matches well the experimentally obtained force-
slip results in terms of stiffness, strength and ductility (Figure 6.36). In the pretension step (I)
the pretension (clamping) force is introduced via temperature difference $\Delta T < 0$ what produces
axial stress state in the HS T bolt (Figure 6.37).
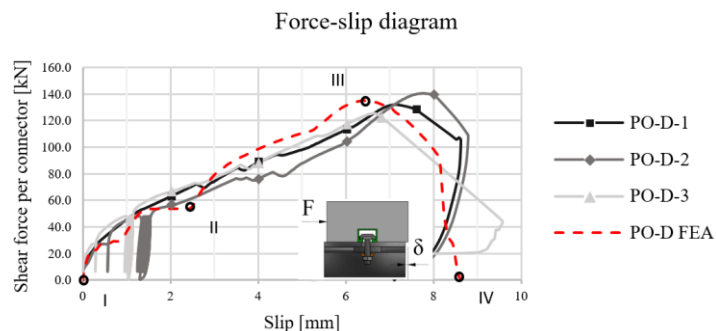
Figure 6.36 - Experimental vs. numerical force-slip results - Connector Type D

When the slip (shear) load is applied, the initial response is flexible due to the assembly
tolerances, lower stiffness and larger lever arm of the bolt shank supports. When the assembly
tolerances are covered the system restores its stiffness (II).
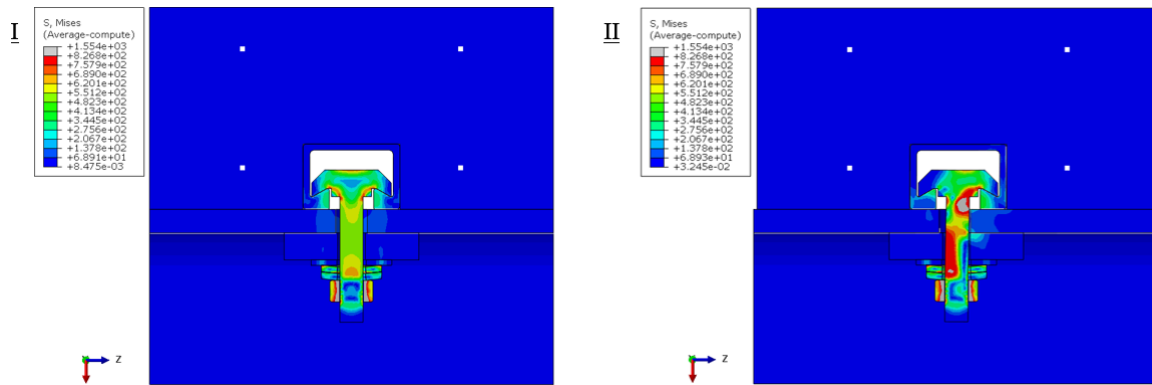
Figure 6.37 - Stress field development - Connector Type D

At this moment (II) the section flange achieves the contact with the bolt shank. Only in the case of the connector Type D, the threaded portion of the shank was modelled with the diameter that corresponds to the effective shear area A_s but the actual bolthole tolerance of $2mm$ was respected by the model by designating the same clearance between the bolt shank and the bolt hole surfaces during the analysis. The following response is dominated by the shear action of the bolt. The reaction (capacity) increases almost linearly until the brittle failure of the bolt shank in shear (Figure 6.38). The sequence of the force-slip behaviour corresponds to the typical response of the friction-grip shear connector typologies.

The separation of the embedded rail wall opposite to the load introduction zone is equivalent to the same phenomena that occurred during the push test and that was later observed on the push test specimen after the test completion.
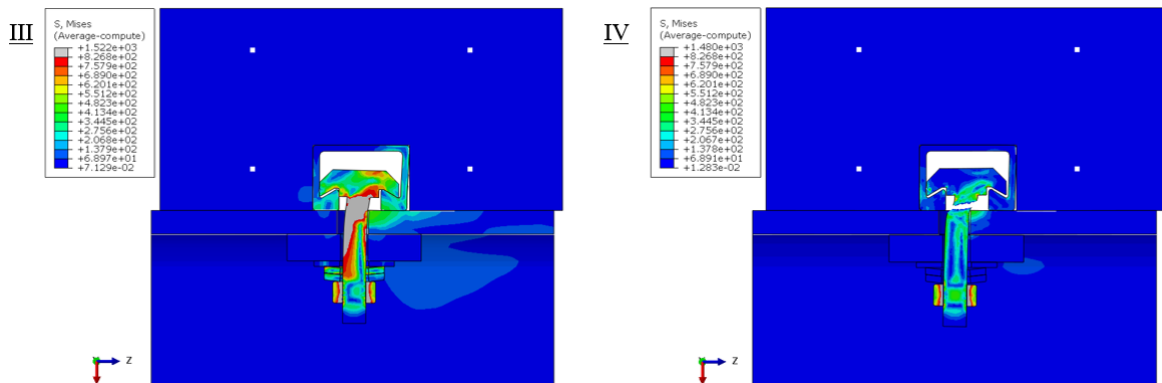
Figure 6.38 - Shear failure sequence - Connector Type D

The obtained fractured bolt shape of the numerical analysis matches well with the deformed shape obtained at the end of the push tests (Figure 6.39). The obtained ultimate capacity matches well with the shear capacity $P_{u,b}$ of the threaded bolt derived using the material properties of the HS T 8.8 bolt material obtained from the tensile tests.
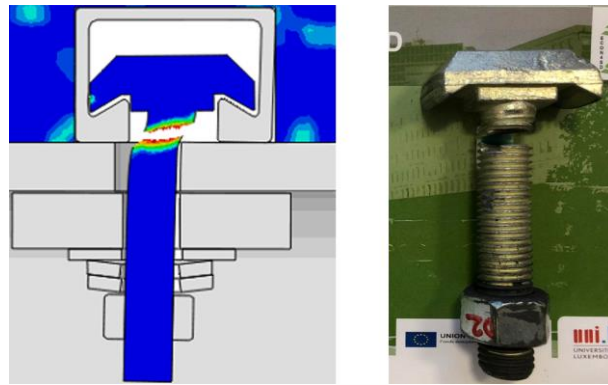
Figure 6.39 - Bolt shear failure shape - FEA vs. experimental result

Obtained results prove the experimental observations that the obtained two-phase force-slip relationship besides strength does not have sufficient stiffness and the ductility to fulfil the previously set behavioural requirement. On the other hand, the observed damage in the concrete still could be neglected. The slab element remains intact at the ultimate shear capacity P_u.

7. Connector Type B behaviour and design model

The connector Type B fulfils in the best way the pre-set mechanical requirements in terms of stiffness, strength and ductility for the application in the demountable steel-concrete composite floor system.

The force-slip response may be improved further by reducing the execution tolerances regarding the boltholes of the rail-plate and the back-plate parts of the connector assembly discussed in the chapter *5.4.5 Assessment and comparison of the push test results*. The designation of the relevant boltholes as "fitted" would not impair the execution and the assembly of the shear connection as the ease of the installation of the connector is achieved by the application of slotted holes at the top flange and the possibility to slide the connector along the rail channel socket.
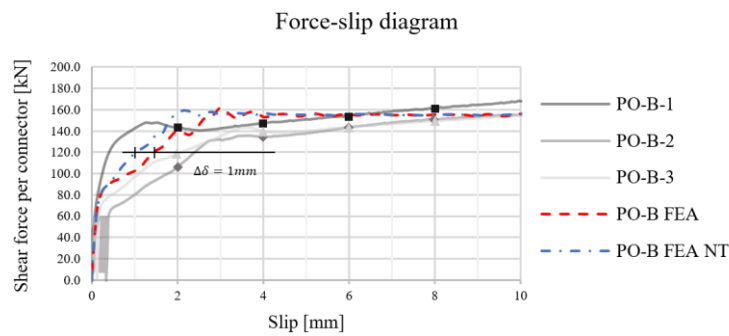
Figure 7.1 - Improvement of the force-slip behavior - Fitted boltholes

On the other hand, the mechanical improvement is evident (Figure 7.1). The activation of the second faying surface happens without force "lagging" and the ultimate capacity of the system is reached faster in terms of slip. The bolthole tolerances that added up in the force-slip response ($\Delta D = 0.5mm$) now are deducted and the ultimate capacity is reached at the slip of $2mm$ instead of $3mm$ stiffening the response of the shear connector. In the following chapters the force-slip behaviour of the connector Type B will consider the application of the fitted boltholes in the mentioned connector parts.

The behaviour of the shear connector Type B may be modelled quite well with the trilinear force-slip mechanical model (Figure 7.2). The first region (I) is characterized by the slip capacity of the first faying surface $P_{1,m}$. The slip capacity is the function of the applied pretension F_p and the coefficient of friction at the first faying surface μ_1.

The second, finite stiffness force-slip region may be defined by the transversal stiffness of the connector assembly k_B and the slip at the ultimate capacity δ_1 when the sliding is achieved at the both faying interfaces.
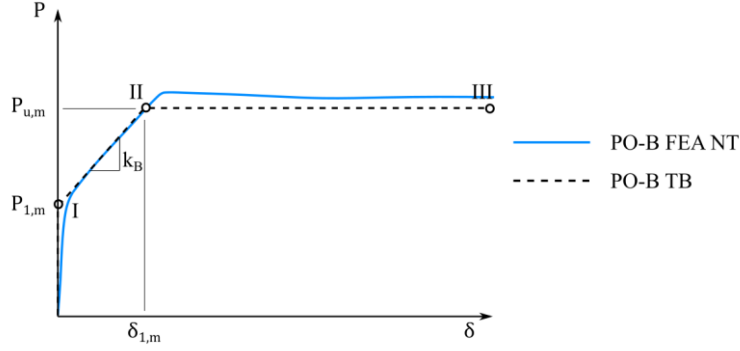
Figure 7.2 - FEA force-slip results vs. mechanical model - Connector Type B

The final force-slip branch is defined only with the ultimate capacity of the shear connector $P_{u,m}$ until the closing of the long-slotted bolt hole tolerance. The relevant points of the connector force-slip model are defined in the following table (Table 7.1).

Table 7.1 - Force-slip behavior model - Connector Type B

Point	F	δ
I	$P_{1,m} = F_p \mu_1$	0
II	$P_{u,m} = F_p(\mu_1 + \mu_2)$	$\delta_{1,m} = (P_{u,m} - P_{1,m})/k_B$
II	$P_{u,m} = F_p(\mu_1 + \mu_2)$	$(L_0 + D_0 - D)/2$

The transversal stiffness coefficient, due to the complexity of the boundary conditions is extracted from the numerical analysis and has a value of $k_B = 41.08 \frac{kN}{mm}$.

The main parameters that affect the force-slip response of the shear connector are the applied pretension force F_p and the properties of the faying surfaces μ_i. The increase of the pretension force would lead to overall increase in the slip capacity and the ultimate capacity of the shear connector.

The similar effect might be achieved by increasing the frictional coefficients μ_i at the relevant faying surfaces. The easiest solution is better control of the frictional properties of the second faying surface μ_2 (flange-backplate). The slip capacity would remain the same but the

contribution of the second faying surface would be increased, however this would mean larger slip δ_1 at the ultimate capacity and higher bending effects in the bolt (Figure 7.3).
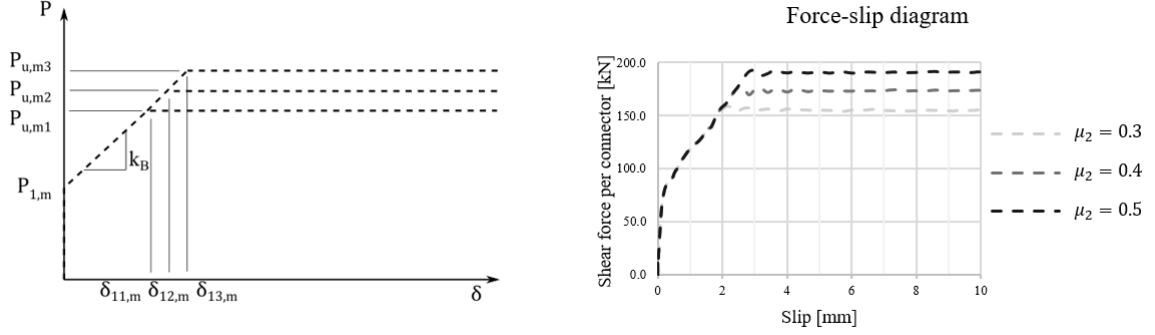
Figure 7.3 - Increase of the frictional properties of the second faying surface μ_2

The increase of the capacity achieved either by increase of the pretension force F_p or by improvement of the frictional properties of the faying surfaces μ_i in the final term must not produce the yielding of the bolt material at the ultimate capacity $P_{u,m}$ as it would render the force-slip model invalid and would decrease drastically the capacity of the shear connector [36].

The force-slip behaviour of the shear connectors (headed studs) in their entire complexity is not explicitly defined by the current code for the design of steel-concrete composite structures EN 1994-1-1 but rather is defined by their characteristic capacity $P_{u,k}$ while their ductility and stiffness are indirectly proven regarding the detailing requirements, ratio of the height of the shear connector over its diameter $\frac{h_{sc}}{d}$, degree of shear connection η etc.

Based on the experimental and numerical results of the connector Type B behaviour, it is assumed that it has sufficient strength and ductility ($\delta_{u,k} > 6mm$) and that the finite stiffness of the second force-slip region is sufficient that in the unpropped condition of the composite beam (as predefined in the chapter *4 Structural concept*) and under the full degree of shear connection ($\eta = 1.00$) the connector behaviour may be defined as rigid ideally plastic and could be as well defined only by its characteristic capacity $P_{u,k}$ (Figure 7.4).
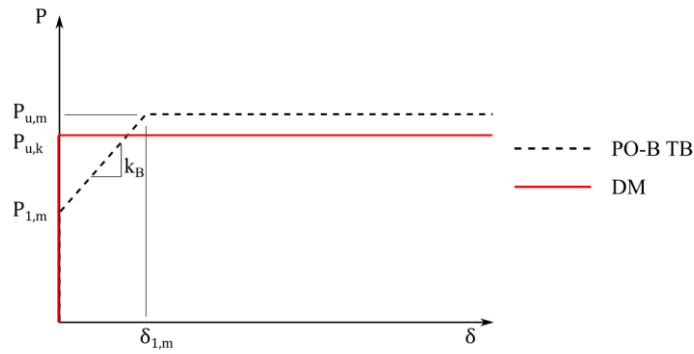
Figure 7.4 - The connector behavior and design model

Based on the experimental results of the connector Type B, due to the small scatter of the results ($\delta < 10\%$) from the mean value, in accordance with the EN 1994-1-1 Annex B the characteristic capacity of the connector $P_{u,k}$ was defined at the slip of $\delta = 6mm$ as:

$$P_{u,k} = 0.9 P_{u,m}$$

$$P_{u,k} = 0.9 \cdot 145 kN = 130.5 kN$$

(7.1)

Considering the influence of the long-term concrete behaviour (creep and shrinkage) on the connector response, the two should not have adverse effect. Higher compressive stress concentrations in the concrete matrix distributed by the embedded rail are introduced through the M-V-P action of the bolt by activation of the second faying surface ($P_{v,b} = P_u - P_1$). However, in the exploitation load range the connector capacity is provided by the slip capacity of the first faying surface (rigid response), due to this fact no permanent compressive stresses are generated that could induce concrete creep in the vicinity of the load introduction zone.
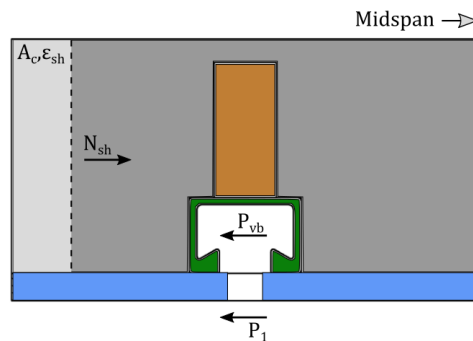
Figure 7.5 - Long-term effects on connector response

On the other hand, as the concrete solid slab modules are prefabricated the majority of the shrinkage is completed before the assembly of the demountable composite floor. Even if

present (curing of the joints between the slab elements) it produces shear action in the opposite direction of the one induced by the floor load (simply supported condition) relaxing the connector load, hence the long-term effects of the concrete material are present only globally what may be taken into account by applying the creep coefficient obtained in accordance with EN 1992-1-1 [45] in the simplified method (modular ratio) in accordance with EN 1994-1-1 [8]. The explanation of the method is given in detail by Hanswille et al. [37].

In the following chapter, based on the mean force-slip trilinear behaviour response of the connector Type B, the assumptions regarding implications of the connector behaviour on the beam (floor) response will be proven.

8. Implications of the connector Type B behaviour on the demountable secondary composite beam response

8.1 Load sequencing and the modelling technique

The simply supported composite beam that represents the main bearing element of the demountable composite floor may be sequenced in several ways (Figure 8.1). If the beam is propped in the construction stage and the load (including self-weight) is applied after the initiation of the shear connection, the complete response of the beam is composite. If the shear connection is stiff and strong enough (the connector device poses sufficient stiffness and the degree of shear connection is higher than $\eta > 0.5$ as per EN 1994-1-1) the initial response is characterized by the complete interaction composite behaviour and the stiffness of the composite beam k_{bII} is directly dependent on the idealized moment of inertia of the composite cross section $I_{i,0}$.
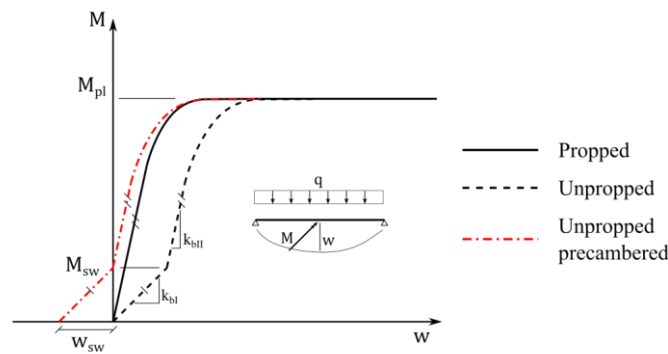
Figure 8.1 - Sequencing of the composite beam

The advantage of this method of sequencing is that it provides immediately high stiffness of the system (lower deformations), however the drawback is that the shear connection is loaded immediately as the longitudinal shear force $V_{L,i}$ is affine to the distribution of the vertical shear T_z and proportional to the properties of the idealized composite cross section ($I_i, A_{c,i}, z_{c,i}$).

The unpropped sequencing allows for the self-weight of the steel section and the slab to be assigned to the steel beam in the execution stage (the steel beam serves as a formwork support). This methodology of the sequencing allows for correspondingly lower load of the shear connection but as the self-weight of the floor is applied on the steel beam characterized by the stiffness k_{bI} that is lower than the stiffness of the composite beam, the deformations are higher.

The chosen sequencing of the proposed demountable steel-concrete composite flooring system is unpropped with the precamber that is equal to the self-weight deflection of the steel section beam w_{sw} in the execution stage. This sequencing pattern allows for two important consequences. Firstly, after the placement of the modular one-way solid slab elements the system is brought to the zero-deflection state. This allows for easy placement of the demountable shear connector assemblies along the beam and initiation of the shear connection via pretension of the high strength pretension bolts. The second benefit is that applying unpropped sequencing the loading of the shear connection is offsetted, hence the finite stiffness shear connection behaviour stage would not affect the stiffness of the composite beam in the range of exploitational loads (SLS) while the substantial ductility would allow for uniform distribution of the longitudinal shear force along the half-span of the beam when reaching plastic moment capacity of the composite cross section at the midspan.
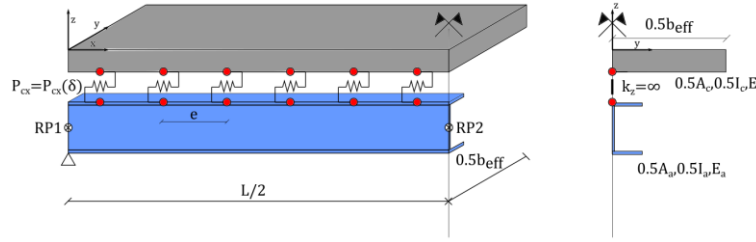
Figure 8.2 - Beam model definition

To prove the expressed assumptions the special FEA composite beam model was developed (Figure 8.2). The geometry of the model was defined considering the principles of symmetry, hence only the quarter of the beam was modelled.

The nodal displacements of the nodes that reside on the support face of the steel section were coupled to the reference point RP-1. The nodal displacements of the complete composite cross section at the midspan of the composite beam respect the X-symmetry boundary conditions. The appropriate boundary conditions were defined in these points in order to recreate simply supported condition of the composite beam.

$$RP-1 \quad U_x \neq 0 \quad U_y = U_z = 0 \quad R_x = R_z = 0 \quad R_y \neq 0$$

$$Midspan\ cross-section\ nodes\ (X-Symm) \quad U_x = R_y = R_z = 0$$

(8.1)

The concrete slab and steel section part were meshed in the same manner and the same material models were applied as in the chapter *6 Numerical analysis* except that the concrete material was modelled as C30/37 concrete class and the steel section material was designated as S235. The reinforcement was modelled using linear truss elements with bilinear material model for B500 B reinforcement steel and it was tied to the concrete matrix applying the embedment constraint (Figure 8.3).
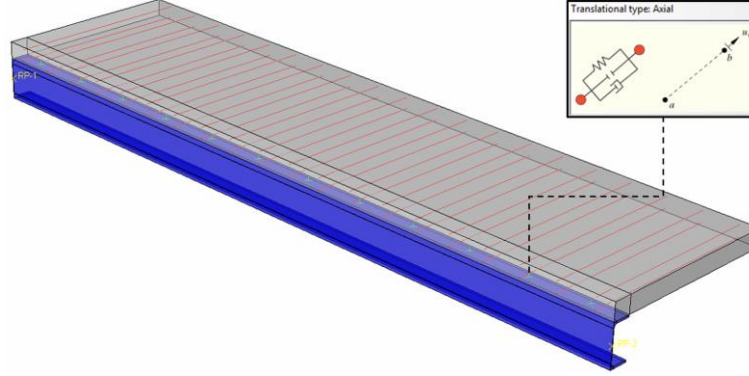
Figure 8.3 - Composite beam FEA model

The fastener connector elements were spread uniformly along the length of the beam (equidistantly) and placed at the mid position of the steel section top flange as in the push tests. The mechanical properties of the connector device were defined based on the trilinear force-slip curve of connector Type B adopted in the previous chapter. The modelled force-displacement behaviour follows the following principle:

$$F_1\ (Shear\ force) - U_1\ (Slip)\quad (Nonlinear - Elastic\ acc.to\ TB)$$

$$F_3\ (Separation\ force) - U_3\ (Uplift)\quad (Rigid)$$

(8.2)

The mean capacity values ($P_{1,m}$ and $P_{u,m}$) and the derived lateral stiffness of the connector assembly k_B were used for the derivation of the connector force-slip model (Figure 8.4). The behaviour in the direction perpendicular to the slab-steel section interface (uplift) was set as rigid as observed in the experimental results (no uplift).

The number of fastener elements (connectors) was defined so the obtained degree of shear connection is always full ($\eta \geq 100\%$).

For the purpose of the comparison, additional connector property was modelled as completely rigid, both in the longitudinal and perpendicular direction of the steel section flange. The composite beam behavior achieved in this manner is very close to the idealized composite beam behavior as its response does not depend on the properties of the shear connection.
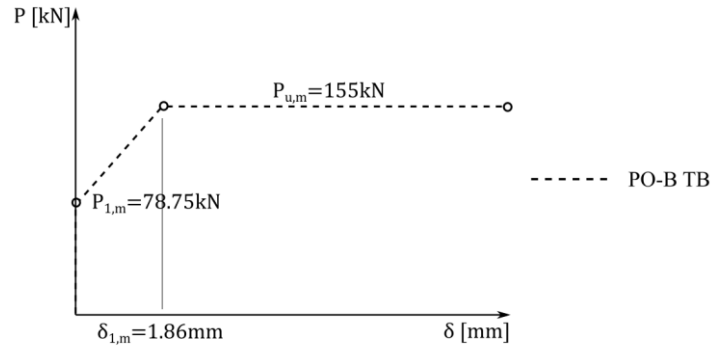
Figure 8.4 - Properties of the shear connector Type B

To allow for the load transfer between the concrete slab and the steel section, the surface-to-surface contact interaction was defined between the bottom surface of the concrete slab and the top surface of the steel section top flange.

The analysis is performed in several steps in order to recreate the actual sequencing of the demountable composite floor (Figure 8.5). In the precamber step, the negative self-weight load is applied in the system via the steel section, while the concrete slab and the steel section are tied. The non-composite response is achieved by lowering the modulus of elasticity of concrete using the predefined field variable. Afterwards, the concrete part and the steel section are recalled in the strain-free state but with preserved deformed shape. The system is precambered and it is ready for the subsequent loading (I).
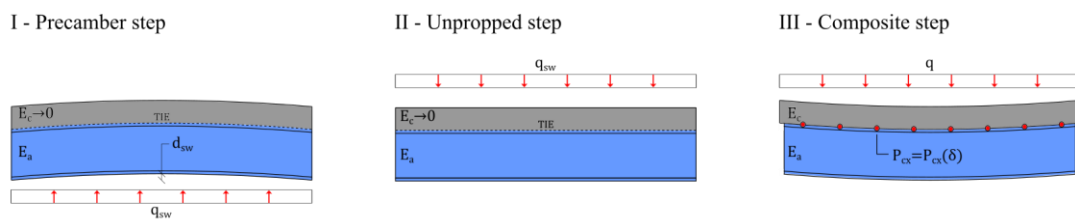
Figure 8.5 - FEA model sequencing

In the following step, the self-weight load of the composite floor is applied on the top flange of the steel section. In the similar manner the unpropped response is achieved by lowering the modulus of elasticity of the concrete using the field variable. The achieved deflection negates the one accumulated in the precambering step and the floor is brought in zero-deflection state (II). The concrete part is again recalled in strain-free state while the stress-strain field of the steel section is preserved conforming to the unpropped system response.

Finally, as in the actual sequencing of the demountable floor, the shear connection is initiated, the stiffness of the concrete is set to the nominal value and the exploitation load is applied on the composite system (III). In this manner the actual sequencing of the proposed floor system is completely respected by the numerical model.

8.2 Parametric study

The parametric study was performed on a set of secondary composite beam systems recommended by Arcelor-Mittal conceptual design guide for steel structures in buildings [6] applying the design solutions considered in the previous chapters.

The relevant moment-deflection curves (Figure 8.6) are plotted regarding the method of the load sequencing (propped, unpropped and unpropped with precamber) and the type of shear connection (rigid or nonlinear-elastic in accordance with trilinear model TB).
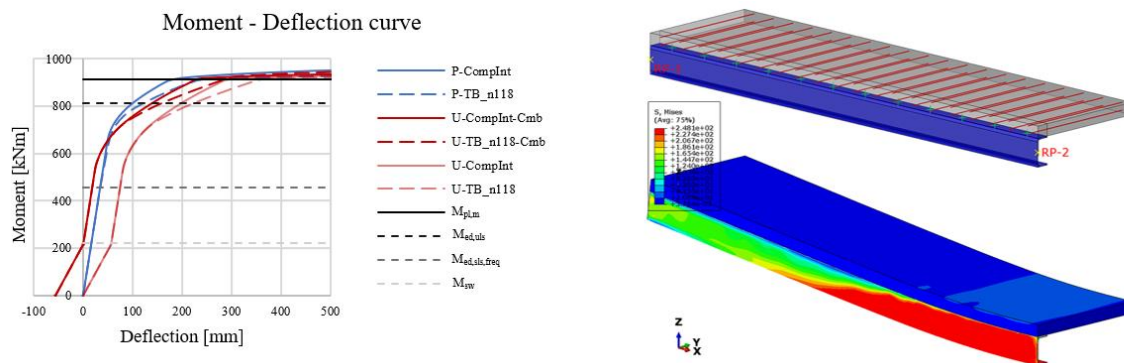
Figure 8.6 - Moment-deflection curves regarding construction sequencing - HEA 340

The plastic moment capacity obtained from the model is almost equal to the mean plastic bending capacity $M_{pl,m}$ derived using the plastic method ([37], [38], [8]). The slightly higher capacity obtained by the model is generated due to the exact position of the centre of compressive forces in the concrete what gives slightly higher lever arm of the internal forces.

As the sections increase, hence the lever arm and the axial capacity of the steel section, this effect is drastically reduced to only 2%.

Until the frequent combination load level $M_{ed,sls,freq}$ the maximum difference in the deflection between the complete interaction theory and the unpropped response of the model is $\Delta_w = 3.87\%$, hence the stiffness in the elastic stage of the composite response could be modelled precise applying the complete interaction elastic theory. The beneficial effect of the shear connection load offset by unpropping is confirmed as in the propped system this difference is almost twice higher ($\Delta_w = 6.5\%$) at the same load level.

This is proven also by observing the distribution of the connector slip along the half-span of the beam (Figure 8.7). Up to the frequent combination load level (50% of the plastic moment capacity) all the connectors behave rigid-like and the slip is equal to zero. The same conclusion is made by observing the distribution of the longitudinal shear (Figure 8.8). Up to the same load level the longitudinal shear is linearly distributed along the half span affine to the distribution of the vertical shear (elastic distribution).
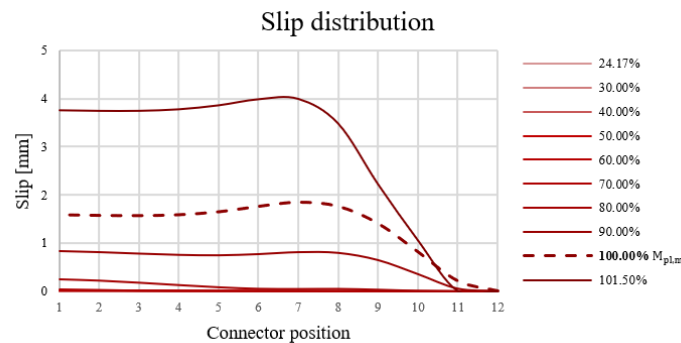
Figure 8.7 - Slip evolution - HEA 340

As the load is increased, the longitudinal shear force starts to be redistributed due to the start of the nonlinear force-slip behavior of the first (and later consecutive) shear connector and due to the yielding of the steel material at the half span of the composite beam. Due to the substantial ductility of the shear connector Type B, the longitudinal shear force is uniformly distributed along the half-span of the composite beam when the plastic moment capacity $M_{pl,m}$ is reached (Figure 8.8).

9. Summary and outlook

The composite steel-concrete floors offer high stiffness and strength with the efficient expenditure of the consumed virgin materials. At the same time, they preserve high execution tolerance, flexibility and recyclability inherited from their steel-structure counterparts in the construction of the floor systems in buildings.

This research proved that they may be designed in a manner where additional property of demountability and modularity is added to their gross value without omitting the previously stated advantages. Following the 3R principle and the principles of the circular economy through the reuse of critical components of such designed demountable steel-concrete composite floor (steel section and modular elements of the concrete slab) the system allows for reduction of the consumption of the virgin materials and generated waste compared to its contemporary counterparts what furtherly increases the sustainability and competitiveness of the steel-concrete composite structures. The flexibility of the system is further enhanced by adhering of its geometry to the standard architectural grids (*Chapters 1&2*).

Within the scope of this work, having in mind the advantages and the disadvantages of similar and mechanically equivalent solutions regarding the current state of the art, four demountable connector devices have been developed in order to allow execution of the modular and demountable steel-concrete composite floor system. Two were based completely on the frictional behaviour (Type A and B) like frictional dumping elements while the latter two were developed as friction-grip connector devices (Type C and D). All connectors allowed for demountability, flexibility and ease of execution of the shear connection. Due to the application of the pretension force through the rail channel and not through the thickness of the concrete slab, the usual pretension loss problems due to the creep of the surrounding concrete were mitigated (*Chapters 3&4*).

The connector device Type B provided the best response in terms of initial stiffness, strength and the ductility regarding its force-slip behaviour compared to the friction-based connector Type A and the friction-grip connectors Type C and D. The connector Type B exhibited as well high initial stiffness what allowed for predictability of the composite beam behaviour in the elastic region (complete interaction theory) under the exploitational loads if the full degree of shear connection is employed. The sufficient strength allowed for the successful design of the shear connection for usual floor spans in buildings with acceptable longitudinal spacing

between connector devices (rails). The exceptional ductility of the connector ($\delta_{u,k} \geq 6mm$) allowed for efficient utilization of the connector strength (uniform distribution of the longitudinal shear coupled with the equidistant spacing of the shear connectors) along the half span of the composite beam. Under the highest connector failure load no damage in the concrete slab was recorded at the load introduction zone during the experimental campaign nor at the peak capacity in the numerical simulations. This strongly supports the assumption that the modular concrete slab elements along with the steel section may be reused in the future projects after certain refurbishment as retreatment of the faying surfaces (*Chapters 5,6,7 and 8*).

If the necessary design measures are employed as precise designation and control of the pretension force F_p and the number of the disc springs in the connector assembly regarding the target pretension force F_p, its mechanical properties are predictable and adhere to the proposed trilinear force-slip curve. Based on the established force-slip model the steel-concrete composite beams may be designed applying the same clauses and design principles of EN 1994-1-1 [8] for ductile shear connectors.

Further experimental work is required in order to experimentally verify the conclusions regarding the behaviour model of the shear connector Type B and the response of the demountable composite beam. In the first case the variating response regarding the pretension force F_p and the properties of the faying surfaces is to be verified on the improved geometry of the shear connector device (fitted boltholes). In the second case the detailing of the joints between the modular slab elements firstly have to be solved. The behaviour of the demountable steel-concrete composite beam has to be verified regarding the plastic theory (bending capacity) and the theory of the complete interaction (stiffness) when utilizing the connector Type B in full degree of shear connection layout ($\eta \geq 1.00$).

Additionally, the mechanical behaviour of the proposed demountable shear connector would be strongly influenced by the pretension relaxation during the accidental fire event. Special care regarding the passive protection of the connector assembly has to be considered in order to offset pretension loss due to thermic expansion of pretension bolt assembly in case of fire.

Lastly, the environmental and financial impacts of the proposed demountable floor system achieved employing the connector Type B assembly has to be compared with its contemporary peers and its feasibility proven through the LCA and LCCA analyses.

10. Bibliography

[1] "Institute of Civil and Environmental Engineering (INCEEN)." [Online]. Available: https://wwwfr.uni.lu/recherche/fstc/research_unit_in_engineering_sciences_rues/research_areas/institute_of_civil_and_environmental_engineering_inceen.

[2] "Eco-Construction for Sustainable Development (ECON4SD)." [Online]. Available: https://econ4sd.uni.lu/.

[3] "Volet FEDER - Portail des Fonds européens / Luxembourg." [Online]. Available: http://www.fonds-europeens.public.lu/fr/programmes/ice-2014-2020/ice-volet-feder/index.html.

[4] "Closing the loop: The why and who of the Circular Economy." [Online]. Available: http://sustainablebrandsmadrid.com/blog/circular-economy-closing-the-loop/.

[5] "Home." [Online]. Available: http://orbilu.uni.lu/.

[6] SCI, "Steel buildings in Europe: Multi-storey steel buildings Part 2: Concept Design," 2008.

[7] SSEDTA, "Structural Steelwork Eurocodes Development of A Trans-national Approach," 2001.

[8] CEN, "EN 1994-1-1: Design of composite steel and concrete structures - Part 1-1: General rules and rules for buildings," 2004.

[9] G. Hanswille, "Composite Bridge Design for Small and Medium Spans Working Item : New types of shear connection," 2002.

[10] "Worldsteel." [Online]. Available: https://www.worldsteel.org/.

[11] CEN, "EN 1090-2: Execution of steel structures and aluminium structures - Part 2: Technical requirements for steel structures," 2008.

[12] L. N. Dallam, "Static and fatigue properties of high-strength bolt shear connectors," 1970.

[13] A. S. Kozma, "Demountable Composite Beams: Analytical calculation approaches for shear connections with multilinear load-slip behaviour," 2020.

[14] M. Pavlović, "Resistance of bolted shear connectors in prefabricated steel-concrete composite decks," 2013.

[15] L. Wang, M. D. Webster, and J. F. Hajjar, "Experimental Investigation of Deconstructable Steel-Concrete Shear Connections in Sustainable Composite Beams," *Struct. Congr. 2017*, no. 2006, pp. 34–47, 2017.

[16] L. N. Dallam, "High Strength Bolt Shear Connectors - Pushout Tests," *ACI J.*, vol. 65, no. 9, pp. 767–769, 1968.

[17] K. Roik and G. Hanswille, "Beitrag zur Ermittlung der Tragfähigkeit von Reib-Abscherverdüblungen bei Stahlverbundträgerkonstruktionen," *Stahlbau*, vol. 2, pp. 41–

46, 1984.

[18] W. T. Marshall, H. M. Nelson, and H. K. Banerjee, "An experimental study of the use of high-strength friction-grip bolts," *Struct. Eng.*, vol. 49, no. 4, 1971.

[19] K. Sattler, "Betrachtungen über die Verwendung hochzugfester Schrauben bei Stahlträger-Verbundkonstruktionen," in *IABSE*, 1960, pp. 333–350.

[20] N. Newmark, C. Siess, and I. Viest, "Tests and Analysis of Composite Beams with Incomplete Interaction," in *Society for Experimental Stress Analysis*, 1951, pp. 75–92.

[21] D. J. Dedic and F. W. Klaiber, "High-Strenght Bolts as Shear Connectors in Rehabilitaion Work," *Concr. Int.*, vol. 6, no. 7, 1984.

[22] S. S. M. Lee and M. A. Bradford, "Sustainable composite beams with deconstructable bolted shear connectors," in *Research and Applications in Structural Engineering, Mechanics and Computation*, 2013, pp. 1373–1378.

[23] N. Hawkins, "Strength in shear and tension of cast-in-place anchor bolts," in *American Concrete Institute (ACI)*, 1987, pp. 233–255.

[24] D. Lam and X. Dai, "Demountable Shear Connectors for Sustainable Composite Construction," *Proc. 2013 World Congr. Adv. Struct. Eng. Mech.*, pp. 93–100, 2013.

[25] M. Pavlović, Z. Marković, M. Veljković, and D. Bucrossed D Signevac, "Bolted shear connectors vs. headed studs behaviour in push-out tests," *J. Constr. Steel Res.*, vol. 88, pp. 134–149, 2013.

[26] M. Spremic, Z. Markovic, M. Veljkovic, and D. Budjevac, "Push-out experiments of headed shear studs in group arrangements," *Adv. Steel Constr.*, vol. 9, no. 2, pp. 139–160, 2013.

[27] CEN, "EN 1990: Basis of structural design," 2005.

[28] CEN, *Eurocode 3: Design of steel structures - Part 1-8: Design of joints*. 2005.

[29] CEN, "ENV 1994-1-1:1994. Eurocode 4: Design of composite steel and concrete structures - Part1-1: General rules and rules for buildings," 1992.

[30] Roik and Bürkner, "Reibwert zwischen Stahlgurten und aufgespannten Betonfertigteilen," *Bauingenieur*, vol. 53, pp. 37–41, 1978.

[31] A. A. Bagon, "A new type of urban bridge, prefabricated and demountalbe," *Demountable Concr. Struct. - A Chall. Precast Concr.*, pp. 293–305, 1985.

[32] AISC, *Specification for Structural Steel Buildings*. 2010.

[33] T. Sano, K. Shirai, Y. Suzui, and Y. Utsumi, "Loading tests of a brace-type multi-unit friction damper using coned disc springs and numerical assessment of its seismic response control effects," *Bull. Earthq. Eng.*, vol. 17, no. 9, pp. 5365–5391, 2019.

[34] DIN, "DIN 6796: Conical spring washers for bolt/nut assemblies." 1987.

[35] G. P. Davet, "Using Belleville Springs To Maintain Bolt Preload," 1997.

[36] S. Ramhormozian, G. C. Clifton, G. A. MacRae, and G. P. Davet, "Stiffness-based approach for Belleville springs use in friction sliding structural connections," *J. Constr. Steel Res.*, vol. 138, pp. 340–356, 2017.

[37] G. Hanswille, M. Schäfer, and M. Bergmann, *Eurocode 4 DIN EN 1994-1-1 Bemessung und Konstruktion von Verbundtragwerken aus Stahl und Beton*. Ernst, Wilhelm & Sohn, 2020.

[38] R.P. JOHNSON, *Composite Structures of Steel and Concrete*, 3rd ed. Blackwell Publishing Ltd, 2004.

[39] DIBt, "ETA-09/0339," 2018.

[40] CEN, "EN 14399-4: High-strength structural bolting assemblies for preloading – Part 4: System HV – Hexagon bolt and nut assemblies," 2006.

[41] ISO, "Plain washers — Large series — Part 1: Product grade A." 2000.

[42] CEN, "EN 14399-3: High-strength structural bolting assemblies for preloading - Part 3: System HR - Hexagon bolt and nut assemblies." 2015.

[43] CEN, "EN 12390-3: Testing hardened concrete: Compressive strength of test specimens." 2001.

[44] CEN, "EN 12390-13: Determination of the modulus of elasticity under pressure (secant module)." 2014.

[45] CEN, "EN 1992-1-1: Design of concrete structures - Part 1-1 : General rules and rules for buildings Eurocode." 2004.

[46] CEN, "EN ISO 6892-1: Metallic materials - Tensile testing - Part 1: Method of test at room temperature." 2009.

[47] "One Source for Asset Protection Solutions | MISTRAS Group." [Online]. Available: https://www.mistrasgroup.com/. [Accessed: 04-Mar-2022].

[48] T. Wang and T. T. C. Hsu, "Nonlinear finite element analysis of concrete structures using new constitutive models," *Comput. Struct.*, vol. 79, no. 32, pp. 2781–2791, 2001.

[49] CEN, "EN 1993-1-5: Design of steel structures - Part 1-5: Plated structural elements." 2006.

[50] CEN, "Eurocode 3: Design of steel structures - Part 1-1: General rules and rules for buildings," 2005.

[51] D. Systèmes, *Abaqus 6.12 Abaqus/CAE User's Manual*. 2012.

[52] D. T. Langill, "Coefficient of Friction for Zinc," *American Galvanizers Association*, 1994. [Online]. Available: https://galvanizeit.org/knowledgebase/article/coefficient-of-friction-for-zinc.

11. Annexes

11.1 Annex A - Geometry of custom-built connector assembly parts

<u>Clamp - L</u>

Clamp - R

QTY	PART NUMBER	DESCRIPTION	MATERIAL	MASS	TOTAL
5	CLMP_R	CLAMP - RIGHT DRILL	S355	2.74 kg	13.71 kg

PARTS LIST

A-A (1 : 2)

B-B (1 : 2)

C-C (1 : 2)

Clamp_Rigth - 1:2

CLMP_R

Half cylinder

*The diameter of the cylinder may be reduced from nominal value of Ø30 by 0.3mm

PARTS LIST

QTY	PART NUMBER	DESCRIPTION	MATERIAL	SURFACE TREATMENT	MASS	TOTAL
10	CLMP_HC	Sliding Half Cylinder	S355	SA 2.5	0,22 kg	2,21 kg

			Date	Name	Sliding Half Cylinder – 1:1	
		Drawn	5/7/2019	jovan.fodor		
		Checked				
		Standard				
					CLMP_HC	1
						A4
State	Changes	Date	Name			

Sliding nut

PARTS LIST					
QTY	PART NUMBER	DESCRIPTION	MATERIAL	MASS	TOTAL
10	CLMP_NUT_T	Nut	S355	0.286 kg	2,86 kg

			Date	Name	
		Drawn	5/7/2019	jovan.fodor	Sliding Nut - 1:1
		Checked			
		Standard			
					CLMP_NUT_T

CLMP_NUT_T — 1 — A4

Rail plate - M24

Rail plate - M20

11.2 Annex B - Layout of the concrete slab

Long rail slab – PO-A
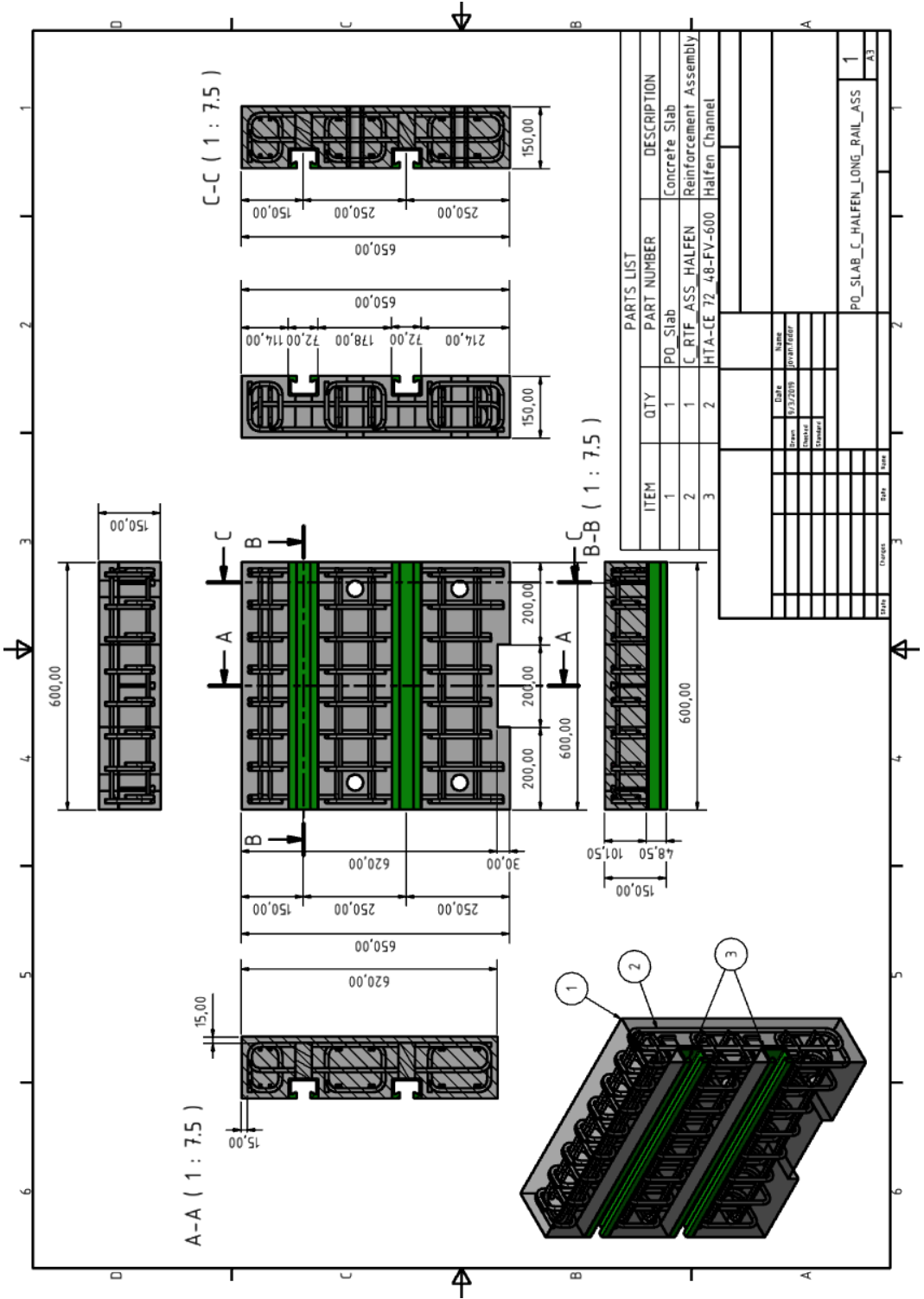
Short rail slab – PO-B-C-D
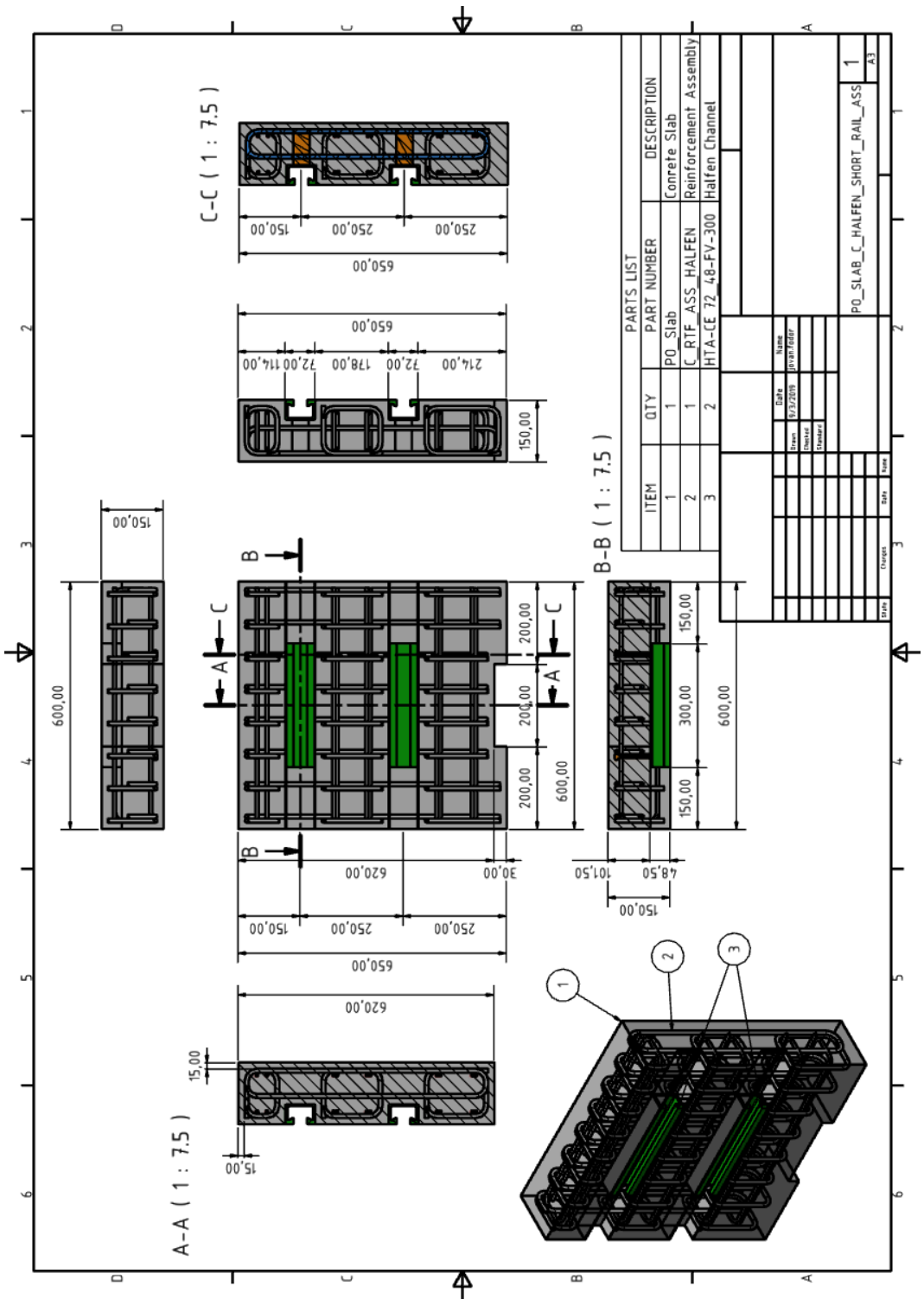
11.3 Annex C - Concrete compression test results

Test parameters

Test:	Universal Zug- / Druckversuch
UTM type:	4000kN
Load cell:	4000 kN
Extensometer:	XHead
Clamping device:	no
Test area:	Lower test area
Sample dimensions:	D = 150 mm
Length data:	Le = 150 mm; Lc = 300 mm
Test rates:	V0 = 50 mm/min; V1 = 0.6 MPa/s
Rate switch points:	F0 = 10 kN
End of test criterions:	Force = 4000 kN; dF = 1 kN

Universal Zug- / Druckversuch
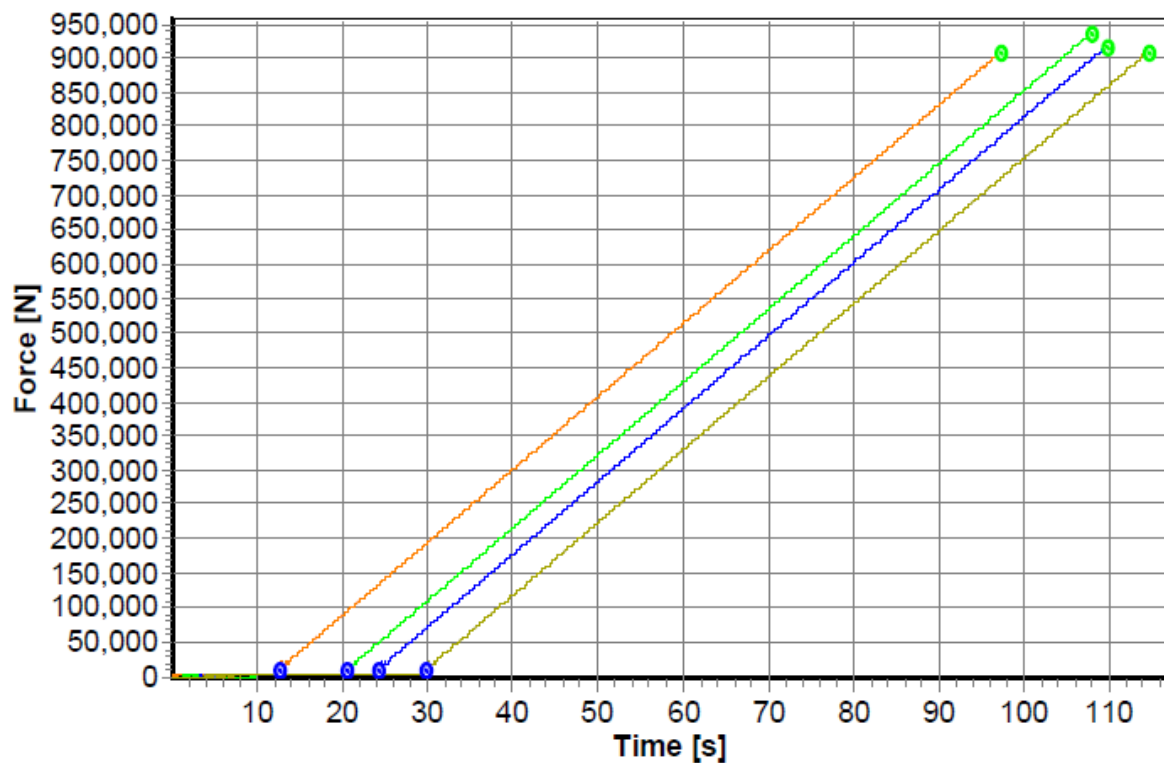
Test results

	Date	Time	FH N	RH N/mm2	Rho kg/m3	D mm	h mm	m g
1	27.01.20	10:38	908308.00	51.40	2332.36	150.00	296.00	12200.00
2	27.01.20	11:51	937300.00	53.04	2347.37	150.00	297.00	12320.00
3	27.01.20	12:29	916244.00	51.85	2328.32	150.00	297.00	12220.00
4	27.01.20	13:22	908492.00	51.41	2340.96	150.00	296.00	12245.00

Test parameters

Test:	Prüfung von Festbeton - Teil 13: E-Modul unter Druckbelastung
UTM type:	4000kN
Load cell:	4000 kN
Extensometer:	XHead
Clamping device:	no
Test area:	Lower test area
Sample dimensions:	D = 150 mm
Length data:	Le = 200 mm
Test rates:	V0 = 50 mm/min; V1 = 0.6 MPa/s
Rate switch points:	F0 = 10 kN
End of test criterions:	dF = 1 kN

Prüfung von Festbeton - Teil 13: E-Modul unter Druckbelastung
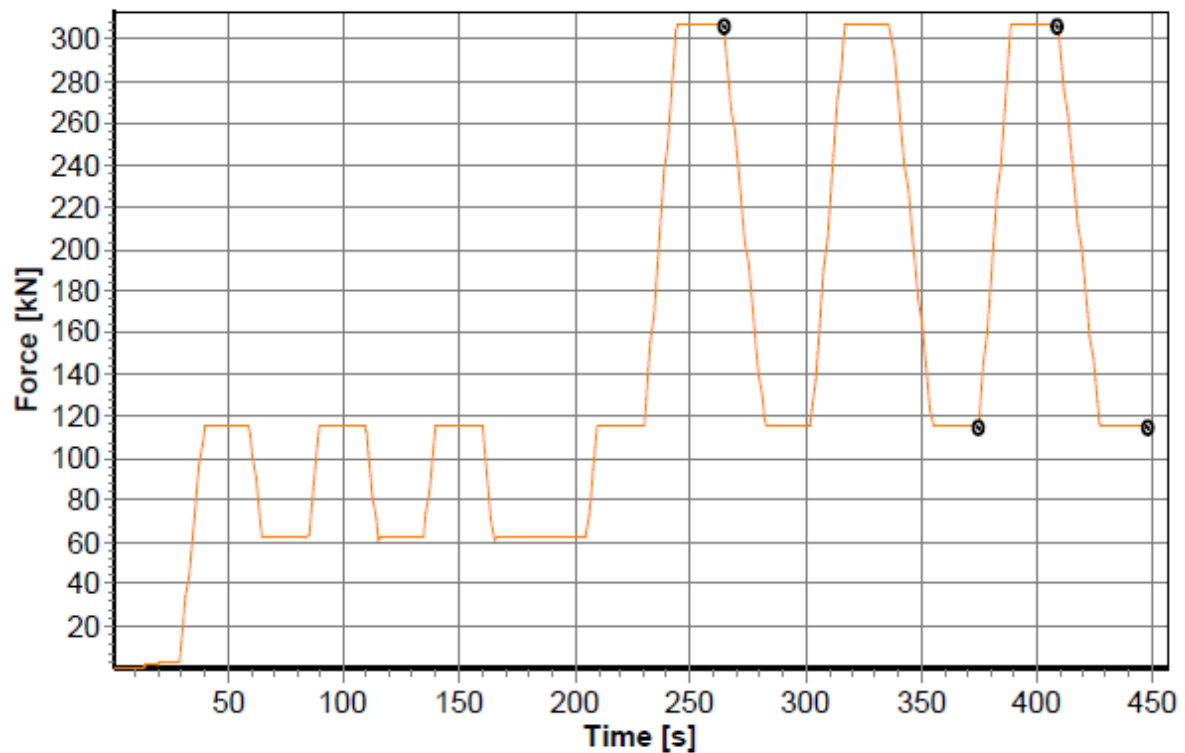
Test results

	Date	Time	Fmax N	A2b %	A3b %	Ec,0 MPa	Ec,S MPa
1	27.01.20	13:09	307032.00	0.0077	0.0076	41945.91	39103.48

11.4 Annex D - Steel tensile test results

<u>Rail (HTA)</u>

Nominal tensile test results

<u>Anchor (AT)</u>

Nominal tensile test results

<u>M24 HV 10.9 (HV)</u>

Nominal tensile test results

M20 HR 8.8 (HR)

Nominal tensile test results

M20 HST 8.8 (HST)

Nominal tensile test results
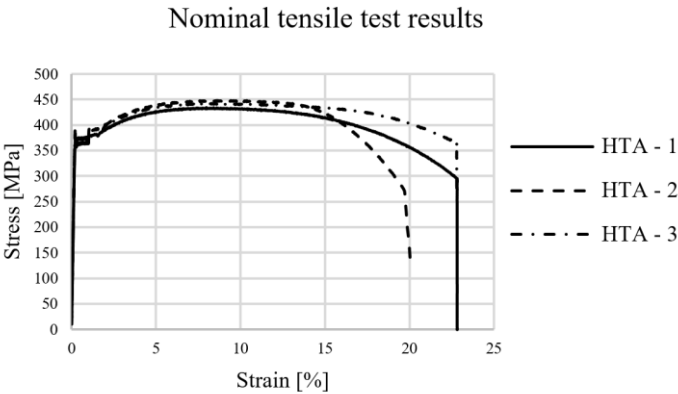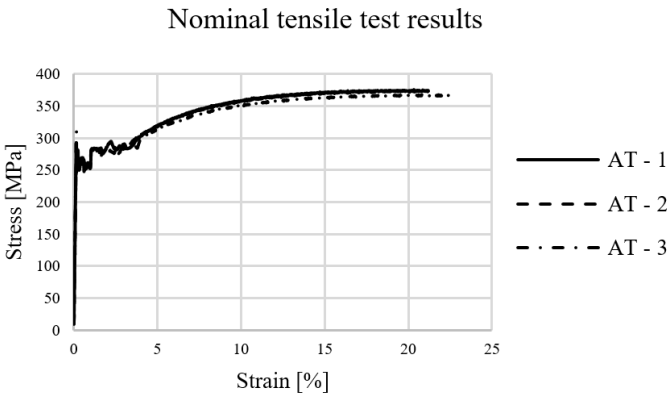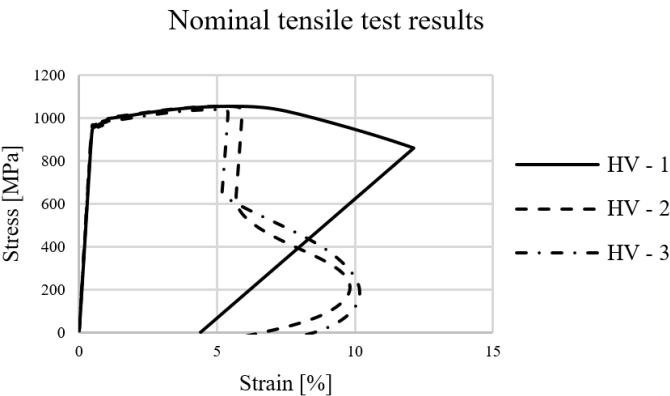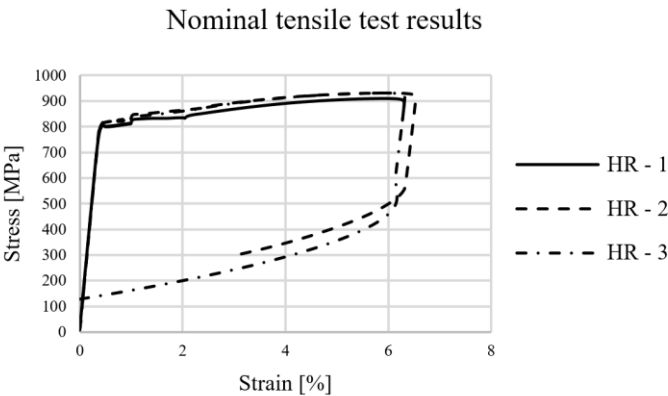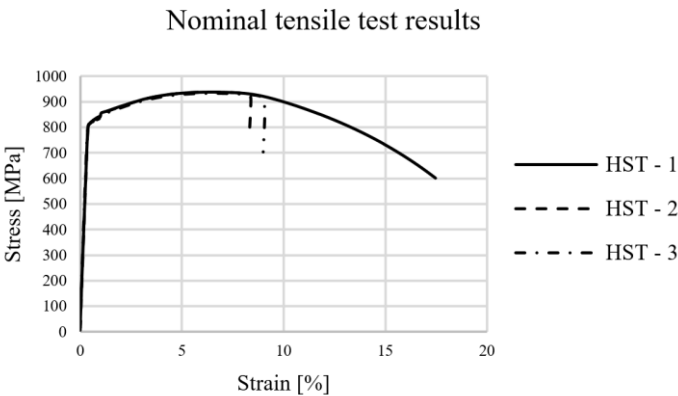
11.5 Annex E - CDP material model of the concrete material

<div style="display: flex;">
<div style="width: 50%;">

```
*Material, name=M1_ C_40_50_CDP
              *Density
              2.5e-09,
              *Elastic
            35028.8, 0.2
     *Concrete Damaged Plasticity
       36.,  0.1,  1.16, 0.667,   0.
     *Concrete Compression Hardening
            16.998,        0.
         20.0448, 2.75823e-05
         22.9646, 4.41622e-05
         25.7531, 6.44818e-05
         28.4057, 8.86718e-05
         30.9175, 0.000116869
         33.2836, 0.000149216
         35.4988, 0.000185864
         37.5574, 0.000226969
         39.4538, 0.000272696
         41.1819, 0.000323219
         42.7352, 0.000378719
         44.1072, 0.000439386
         45.2909, 0.000505421
         46.2787, 0.000577036
          47.063, 0.000654452
         47.6355, 0.000737902
         47.9877, 0.000827634
         48.1104, 0.000923907
          47.994, 0.00102699
         47.6284, 0.00113719
         47.0028, 0.00125479
          46.106, 0.00138013
         44.9258, 0.00151355
         43.4496, 0.00165541
         41.6639, 0.00180609
         39.5544, 0.00196601
         37.1058,  0.0021356
         34.3019, 0.00231532
         31.1257, 0.00250566
         27.5586, 0.00270715
     *Concrete Tension Stiffening
           3.50035,        0.
         2.65303, 0.000124241
         2.25606, 0.000235549
         2.01103, 0.000342509
         1.83949, 0.000447361
         1.71028, 0.000550995
         1.60817, 0.000653845
         1.52468, 0.000756154
         1.45466, 0.000858068
         1.39477, 0.000959683
         1.34273, 0.00106106
         1.29693, 0.00116226
         1.25619, 0.00126329
         1.21962,  0.0013642
         1.18654,   0.001465
         1.15642, 0.00156571
```

</div>
<div style="width: 50%;">

```
1.12882,  0.00166633
1.10342,  0.00176688
1.07992,  0.00186737
1.05809,   0.0019678
1.03775,  0.00206817
1.01872,   0.0021685
1.00086,  0.00226879
0.984067, 0.00236903
0.968225, 0.00246924
0.953249, 0.00256941
0.93906,  0.00266955
0.925591, 0.00276966
0.912781, 0.00286974
0.900576,  0.0029698
0.88893,  0.00306983
0.8778,   0.00316983
0.867148, 0.00326981
0.85694,  0.00336977
0.847146, 0.00346971
0.837737, 0.00356962
0.828688, 0.00366951
0.819977, 0.00376939
0.811582, 0.00386925
0.803485, 0.00396908
0.795667,  0.0040689
0.788113, 0.00416871
0.780808, 0.00426849
0.773738, 0.00436826
0.76689,  0.00446801
0.760253, 0.00456775
0.753816, 0.00466747
0.747569, 0.00476718
0.741502, 0.00486687
0.735607, 0.00496654
0.729876,  0.0050662
0.724301, 0.00516585
0.718875, 0.00526548
0.713591,  0.0053651
0.708443, 0.00546471
0.703425,  0.0055643
0.698532, 0.00566387
0.693759, 0.00576344
0.6891,   0.00586299
0.684551, 0.00596253
0.680107, 0.00606206
0.675765, 0.00616157
0.671521, 0.00626107
0.66737,  0.00636056
0.66331,  0.00646003
0.659337, 0.00655949
0.655448, 0.00665894
0.65164,  0.00675838
0.64791,  0.00685781
0.644256, 0.00695722
0.640674, 0.00705662
0.637163, 0.00715601
```

</div>
</div>

0.63372, 0.00725539
0.630344, 0.00735476
0.62703, 0.00745411
0.623779, 0.00755346
0.620587, 0.00765279
0.617454, 0.00775211
0.614377, 0.00785142
0.611354, 0.00795072
0.608384, 0.00805
0.605465, 0.00814928
0.602596, 0.00824854
0.599776, 0.00834779
0.597003, 0.00844704
0.594275, 0.00854627
0.591592, 0.00864548
0.588952, 0.00874469
0.586354, 0.00884389
0.583797, 0.00894307
0.58128, 0.00904225
0.578802, 0.00914141
0.576362, 0.00924057
0.573958, 0.00933971
0.57159, 0.00943884
0.569258, 0.00953796
0.566959, 0.00963707
0.564694, 0.00973617
0.562461, 0.00983526
0.56026, 0.00993434
0.55809, 0.0100334
*Concrete Compression Damage
0., 0.
0., 2.75823e-05
0., 4.41622e-05
0., 6.44818e-05
0., 8.86718e-05
0., 0.000116869
0., 0.000149216
0., 0.000185864
0., 0.000226969
0., 0.000272696
0., 0.000323219
0., 0.000378719
0., 0.000439386
0., 0.000505421
0., 0.000577036
0., 0.000654452
0., 0.000737902
0., 0.000827634
0., 0.000923907
0.00233452, 0.00102699
0.00993462, 0.00113719
0.0229384, 0.00125479
0.0415817, 0.00138013
0.0661141, 0.00151355
0.0968001, 0.00165541
0.13392, 0.00180609
0.177772, 0.00196601
0.228672, 0.0021356

0.286956, 0.00231532
0.352982, 0.00250566
0.427132, 0.00270715
*Concrete Tension Damage
0., 0.
0.242066, 0.000124241
0.355477, 0.000235549
0.425479, 0.000342509
0.474484, 0.000447361
0.511397, 0.000550995
0.540568, 0.000653845
0.56442, 0.000756154
0.584424, 0.000858068
0.601535, 0.000959683
0.616401, 0.00106106
0.629486, 0.00116226
0.641125, 0.00126329
0.651572, 0.0013642
0.661022, 0.001465
0.669628, 0.00156571
0.677511, 0.00166633
0.684769, 0.00176688
0.691483, 0.00186737
0.697718, 0.0019678
0.703531, 0.00206817
0.708967, 0.0021685
0.714068, 0.00226879
0.718866, 0.00236903
0.723392, 0.00246924
0.72767, 0.00256941
0.731724, 0.00266955
0.735572, 0.00276966
0.739232, 0.00286974
0.742718, 0.0029698
0.746045, 0.00306983
0.749225, 0.00316983
0.752268, 0.00326981
0.755184, 0.00336977
0.757983, 0.00346971
0.760671, 0.00356962
0.763256, 0.00366951
0.765744, 0.00376939
0.768142, 0.00386925
0.770456, 0.00396908
0.772689, 0.0040689
0.774847, 0.00416871
0.776934, 0.00426849
0.778954, 0.00436826
0.780911, 0.00446801
0.782807, 0.00456775
0.784646, 0.00466747
0.78643, 0.00476718
0.788163, 0.00486687
0.789847, 0.00496654
0.791485, 0.0050662
0.793078, 0.00516585
0.794628, 0.00526548

11.6 Annex F - Steel material models

*Material, name=M2_B_500
*Density
7.83e-09,
*Elastic
210000., 0.3
*Expansion
1.2e-05,
*Plastic
501.19,0.
*Material, name=M3_Anchor_Mistras
*Density
7.83e-09,
*Elastic
213215., 0.3
*Expansion
1.2e-05,
*Plastic
293.857,   0.
281.124, 0.000108045
278.217, 0.000176221
278.502, 0.000223066
277.097, 0.000281765
278.503, 0.000309805
280.803, 0.000347097
281.881, 0.000388005
276.814, 0.000490168
273.154, 0.000557308
271.901, 0.000617539
271.116, 0.000664647
270.542, 0.000725332
272.497, 0.000772221
271.894, 0.000819541
269.903, 0.000877245
268.223, 0.000930399
268.701, 0.000976636
266.223, 0.00104285
263.984,   0.0011143
260.425, 0.00116581
259.673, 0.00122066
261.803, 0.00127039
260.422, 0.00131361
257.237, 0.00139393
253.542,   0.0014615
253.275, 0.00149404
255.403, 0.00154101
255.717, 0.00160059
255.727, 0.00164909
256.549, 0.00168068
255.399, 0.00174295
255.161, 0.00179025
255.268, 0.00184727
256.395, 0.00188287
255.606, 0.00193843
256.489, 0.00199523
255.881, 0.00203501
257.282,   0.0020931

257.498, 0.00213488
256.436, 0.00219637
257.837, 0.00223282
255.775, 0.00226982
258.644, 0.00231628
258.357, 0.00238292
259.77, 0.00242641
258.942, 0.00248545
259.202, 0.00252654
260.714, 0.00256185
261.388, 0.00261291
260.74, 0.00265901
260.546, 0.00271435
261.358, 0.0027506
261.727, 0.00280902
261.518, 0.00285023
262.847, 0.00289789
262.466, 0.00294645
262.349, 0.00298423
263.014, 0.00305212
263.583, 0.00310897
262.547, 0.00314915
264.082, 0.00321681
263.867, 0.00325312
263.061, 0.00330327
264.349, 0.00334157
264.541, 0.0033963
263.749, 0.00343444
264.513, 0.00349548
264.273, 0.0035364
264.075, 0.00359769
264.174, 0.00363243
265.017, 0.00368565
264.156, 0.00374082
265.062, 0.00378039
264.285, 0.00383135
264.575, 0.00389895
264.649, 0.00392946
264.915, 0.00400426
263.296, 0.00402895
263.43, 0.00409537
263.979, 0.00414193
263.248, 0.00419202
264.191, 0.00423867
264.322, 0.00430028
263.975, 0.0043315
264.483, 0.0043909
263.899, 0.00443873
264.717, 0.00448147
263.564, 0.00454863
263.33, 0.00459631
265.434, 0.00465338
262.874, 0.00470309
263.12, 0.00474572
262.821, 0.00479565
260.481, 0.00485246
261.789, 0.00490369
261.302, 0.00494413

262.674, 0.00499243
260.405, 0.00506294
260.459, 0.00510685
261.613, 0.00515302
261.537, 0.00519381
260.398, 0.00525569
261.33, 0.00530618
260.562, 0.00535971
259.642, 0.0054073
257.947, 0.00546442
255.324, 0.00552144
256.81, 0.00557457
256.66, 0.00562384
255.956, 0.0056709
258.69, 0.00570541
256.811, 0.00575807
257.462, 0.00580779
257.578, 0.00586073
258.279, 0.00592354
257.704, 0.00597079
257.034, 0.00601609
258.667, 0.00605191
257.362, 0.00611588
257.708, 0.00615233
259.098, 0.006205
258.078, 0.00625695
258.089, 0.00630513
257.927, 0.00636809
258.613, 0.0064087
257.611, 0.00646287
260.806, 0.00649074
258.511, 0.00654486
260.507, 0.0066037
259.512, 0.00665448
259.105, 0.0067014
260.754, 0.00674677
260.567, 0.00679244
261.079, 0.00684574
259.626, 0.00689782
260.816, 0.00694218
260.609, 0.00698423
259.805, 0.00703148
261.024, 0.00707429
261.381, 0.0071191
261.43, 0.00717476
260.602, 0.00724132
261.627, 0.00728571
261.387, 0.00734588
260.164, 0.00738138
261.271, 0.00742684
261.793, 0.00749142
261.572, 0.00751678
260.783, 0.00758469
260.998, 0.0076378
262.164, 0.00767839
262.251, 0.00772758
260.942, 0.00778211
261.051, 0.00783181

261.618, 0.00786917
261.857, 0.00792038
261.991, 0.00797567
262.174, 0.00801911
261.362, 0.0080724
261.944, 0.00811739
261.708, 0.00818049
261.832, 0.00823293
261.577, 0.00828089
261.326, 0.00832319
262.466, 0.00837647
261.719, 0.00842841
262.72, 0.00847972
261.517, 0.00852101
262.539, 0.00856904
262.265, 0.00860874
262.777, 0.0086671
262.349, 0.00871906
286.913, 0.0102824
284.065, 0.0124461
280.957, 0.0146201
281.777, 0.0167746
285.405, 0.0188979
283.991, 0.0211322
285.391, 0.0233862
290.913, 0.0253693
291.082, 0.0274848
292.502, 0.0296123
301.776, 0.0314219
305.688, 0.0329202
308.794, 0.0343367
312.256, 0.0358075
315.597, 0.0372535
318.356, 0.0387643
321.278, 0.0402642
325.062, 0.0417536
327.659, 0.0432389
330.404, 0.0447321
333.81, 0.0462411
335.633, 0.0477405
339.112, 0.049259
341.155, 0.0507486
344.352, 0.0522498
346.059, 0.0537799
348.776, 0.0552762
350.199, 0.056784
353.312, 0.0582908
354.557, 0.0598107
357.309, 0.0613307
358.858, 0.0628296
361.21, 0.0643477
361.978, 0.0658444
365.265, 0.0673442
367.61, 0.06887
368.35, 0.0703595
370.861, 0.0718771
372.174, 0.0733947
374.124, 0.0748924

375.256,	0.0764449		441.467,	0.16578
377.009,	0.0779179		441.502,	0.167349
378.579,	0.0794803		441.905,	0.168911
380.972,	0.0809661		442.252,	0.170485
380.73,	0.0824872		443.473,	0.1721
384.191,	0.0840029		444.943,	0.173631
384.77,	0.0855341		444.769,	0.175262
386.258,	0.0870508		445.504,	0.176824
387.185,	0.0885979		445.744,	0.178453
388.946,	0.0901025		447.922,	0.180012
390.462,	0.0916079		448.16,	0.181621
392.01,	0.0931425		449.186,	0.183204
393.352,	0.0946544		449.711,	0.184802
395.08,	0.0961704		450.854,	0.186432
395.841,	0.0976929		450.533,	0.188025
397.763,	0.0992195		452.165,	0.189627
398.328,	0.100723		452.56,	0.191245
400.433,	0.102271		453.526,	0.192853
401.112,	0.103798		453.913,	0.194487
402.34,	0.105348		455.202,	0.196077
403.629,	0.106868		455.393,	0.197734
404.944,	0.108394		457.135,	0.199356
405.173,	0.109933		457.071,	0.200995
406.814,	0.111443		456.422,	0.202602
409.234,	0.112997		457.809,	0.203731
409.662,	0.11455		458.331,	0.203764
410.73,	0.116049		458.336,	0.203776
412.292,	0.117603		458.434,	0.203798
413.546,	0.119144		*Material, name=M4_Rail_Mistras	
413.449,	0.120688		*Density	
414.82,	0.122201		7.83e-09,	
416.019,	0.123748		*Elastic	
417.624,	0.125316		211746., 0.3	
418.735,	0.126861		*Expansion	
418.5,	0.128402		1.2e-05,	
419.03,	0.129942		*Plastic	
420.816,	0.131472		339.97,	0.
421.443,	0.133032		347.182,	2.3191e-05
423.397,	0.134544		352.892,	3.64974e-05
423.941,	0.136137		359.617,	5.50526e-05
425.584,	0.137664		364.931,	8.32931e-05
426.506,	0.139217		369.776,	0.000113432
426.686,	0.140782		374.497,	0.000137662
427.314,	0.142338		379.547,	0.000158502
428.165,	0.143898		378.228,	0.000214132
428.463,	0.145448		371.883,	0.000317332
430.051,	0.147026		369.785,	0.000360357
430.63,	0.148563		368.032,	0.000410607
432.784,	0.150129		366.343,	0.000479296
432.746,	0.151674		366.942,	0.000542601
432.995,	0.153244		365.299,	0.000602283
434.374,	0.154814		366.842,	0.000630844
435.235,	0.156376		366.983,	0.000685526
435.678,	0.157951		366.864,	0.000726998
436.743,	0.159511		368.055,	0.000784183
437.132,	0.161068		367.974,	0.000823375
439.235,	0.16263		368.52,	0.000870549
439.312,	0.164213		367.958,	0.000935765

369.601, 0.000966195	375.32, 0.00383679
369.195, 0.0010266	375.372, 0.00387955
369.28, 0.00107335	375.22, 0.00393733
369.828, 0.00111006	375.738, 0.00398709
371.014, 0.00116063	374.724, 0.00403222
370.368, 0.0012123	375.985, 0.00406903
371.259, 0.00125537	376.297, 0.00412065
371.812, 0.00130945	375.865, 0.00417824
370.224, 0.00135174	375.74, 0.00422744
372.341, 0.00140521	376.149, 0.00426748
371.549, 0.00144393	376.892, 0.00432874
372.534, 0.0015006	376.789, 0.00438269
372.213, 0.00154375	375.561, 0.00443218
372.256, 0.00159893	375.883, 0.00448956
373.94, 0.0016423	376.47, 0.00451282
373.186, 0.00169356	375.822, 0.00457628
373.471, 0.00173659	375.881, 0.00462388
373.331, 0.00178954	375.977, 0.00467613
373.618, 0.00185005	375.957, 0.00470844
373.994, 0.00189182	377.128, 0.00477106
373.506, 0.00194128	376.973, 0.00481338
375.881, 0.00197975	376.831, 0.00486839
374.259, 0.00204444	375.197, 0.00492182
374.264, 0.00209182	376.417, 0.00496494
375.146, 0.00215221	376.679, 0.00502278
375.742, 0.00219537	375.361, 0.00507435
374.851, 0.00225562	377.546, 0.00511916
375.397, 0.00228346	376.103, 0.00516705
375.92, 0.0023335	377.254, 0.00520776
374.112, 0.00237967	377.601, 0.00526271
375.81, 0.00243592	376.802, 0.00532711
375.187, 0.00247668	377.006, 0.00537058
375.582, 0.00253378	376.554, 0.00541459
374.576, 0.00258915	376.968, 0.00545529
374.546, 0.00264284	378.075, 0.00552197
375.372, 0.00268964	378.463, 0.0055657
374.424, 0.00274543	376.829, 0.00561933
376.096, 0.00277782	377.541, 0.00565897
375.47, 0.00283845	378.245, 0.00571575
374.549, 0.0028875	377.934, 0.0057551
374.717, 0.00293524	378.165, 0.0058114
373.695, 0.00298795	377.317, 0.00586043
375.559, 0.00303655	377.806, 0.0058986
374.712, 0.00308684	377.748, 0.0059451
375.296, 0.00315623	377.38, 0.00600942
375.202, 0.00318835	377.849, 0.0060551
374.296, 0.00323372	377.605, 0.00611287
374.604, 0.00328488	378.46, 0.00616153
375.807, 0.00333776	377.637, 0.00619867
374.429, 0.00338019	379.333, 0.00624691
374.945, 0.00343588	378.528, 0.00630002
374.399, 0.00349261	377.955, 0.00635019
373.874, 0.00353348	378.133, 0.00640303
374.775, 0.00358904	377.501, 0.00646405
373.716, 0.00363502	378.92, 0.00650269
374.17, 0.00368974	378.629, 0.0065446
374.929, 0.00373825	378.133, 0.00660371
374.699, 0.00376784	377.663, 0.00666737

377.968, 0.00670525	462.794, 0.0538196
378.334, 0.00674255	463.918, 0.0555141
378.147, 0.0067999	465.663, 0.0572174
378.689, 0.00684344	466.408, 0.0589448
377.964, 0.00688856	467.95, 0.0606673
379.94, 0.00694004	468.584, 0.0623697
377.215, 0.00699713	470.953, 0.0641037
378.985, 0.00704852	471.303, 0.0658647
378.434, 0.00709401	472.485, 0.0676066
379.06, 0.00714011	472.055, 0.0693537
378.744, 0.00721114	474.697, 0.0711515
377.993, 0.00724434	474.835, 0.0728755
377.956, 0.00729948	476.912, 0.0746925
378.631, 0.00734054	477.834, 0.0764525
378.186, 0.00739648	478.666, 0.0782556
378.466, 0.00744673	478.534, 0.0800623
377.799, 0.00749467	479.905, 0.0818785
379.196, 0.00754674	480.978, 0.0836783
377.761, 0.00759115	481.608, 0.0855055
379.107, 0.00763871	482.203, 0.0873293
377.963, 0.00769603	483.031, 0.0891874
379.487, 0.00774199	484.678, 0.0910152
378.285, 0.00778647	484.372, 0.0928733
378.613, 0.00783874	484.492, 0.0947303
379.018, 0.00788724	486.621, 0.0965831
377.482, 0.00794785	486.963, 0.098444
378.854, 0.00798265	487.381, 0.100323
377.061, 0.00805002	487.806, 0.102215
378.793, 0.00807713	487.763, 0.104124
378.534, 0.00813166	489.677, 0.105993
396., 0.00835456	490.222, 0.10788
396.83, 0.0105071	490.792, 0.109802
398.22, 0.0125612	491.718, 0.111707
398.941, 0.0144858	492.945, 0.113647
396.268, 0.0157336	492.713, 0.11556
400.831, 0.0167715	492.166, 0.117503
407.23, 0.018074	494.577, 0.119427
411.214, 0.0195794	493.662, 0.121383
415.339, 0.0211864	494.914, 0.12334
418.622, 0.0227657	494.461, 0.125316
422.057, 0.0243314	495.618, 0.127256
424.967, 0.025926	495.735, 0.129238
427.758, 0.0274916	497.896, 0.131186
430.916, 0.029131	497.754, 0.133191
433.85, 0.0307251	497.575, 0.135153
437.036, 0.0323482	498.986, 0.137159
439.581, 0.0339333	498.323, 0.139119
442.039, 0.0355572	499.55, 0.141138
444.441, 0.0372	500.31, 0.143154
445.941, 0.0388261	499.778, 0.145172
448.912, 0.0404704	500.742, 0.147185
450.42, 0.0421212	500.778, 0.149236
452.538, 0.0437552	500.551, 0.151313
454.342, 0.0454196	500.23, 0.153342
456.282, 0.0471037	499.207, 0.155391
458.257, 0.0487507	498.69, 0.157437
459.481, 0.0504397	497.692, 0.159499
460.664, 0.0521443	497.706, 0.161574

```
      496.875,    0.16365
      495.206,   0.165684
      495.406,    0.16774
      492.211,   0.169777
      491.83,   0.171865
      491.06,   0.173885
      489.469,   0.175925
      487.275,   0.177953
      483.65,   0.180057
      481.351,   0.182048
      478.989,   0.184102
      476.469,   0.186113
      473.778,   0.188177
      471.308,   0.190195
      467.783,   0.192196
      465.819,   0.194217
      461.299,    0.19624
      458.595,   0.198276
      455.1,   0.200316
      449.262,    0.202326
*Material, name=S355
*Density
7.83e-09,
*Elastic
210533., 0.3
*Plastic
      355.6,        0.
      502.425, 0.0226545
      546.25,  0.137167
*Material, name=HST_88
*Damage Initiation, criterion=DUCTILE
      0.11903,       0.,        0.
      0.10245,     0.1,      0.
      0.0881793,     0.2,       0.
      0.0758967,     0.3,       0.
     0.0721951, 0.333333,       0.
      0.0653249,     0.4,       0.
      0.0562256,     0.5,       0.
      0.0483939,     0.6,       0.
      0.041653,     0.7,       0.
      0.035851,     0.8,       0.
      0.0308573,     0.9,       0.
      0.0265591,      1.,       0.
      0.0228596,     1.1,       0.
      0.0196755,     1.2,       0.
      0.0169348,     1.3,       0.
      0.0145759,     1.4,       0.
      0.0125456,     1.5,       0.
      0.0107981,     1.6,       0.
      0.00929404,     1.7,       0.
      0.00799945,     1.8,       0.
      0.00688519,     1.9,       0.
      0.00592614,      2.,       0.
*Damage Evolution, type=DISPLACEMENT,
degradation=MULTIPLICATIVE
      0.415,
*Damage Initiation, criterion=SHEAR, ks=0.2
      0.072, 1.732,   0.
```

```
*Damage Evolution, type=DISPLACEMENT,
degradation=MULTIPLICATIVE,
softening=EXPONENTIAL
      0.3,1.
*Density
7.83e-09,
*Elastic
213072., 0.3
*Plastic
      826.857,          0.
      834.355, 0.000715191
      837.658,   0.0014404
      842.951,   0.00216069
      847.875,   0.00288639
      849.217,   0.00360775
      864.707,   0.00426551
      868.201,   0.00496467
      870.645,   0.00570709
      872.921,   0.00641119
      875.699,   0.00721372
      878.087,   0.00786451
      880.977,   0.00862452
      883.552,   0.00929191
      886.385,   0.0100109
      889.185,   0.0107584
      892.091,   0.0115054
      895.052,   0.0122493
      897.891,    0.012992
      936.418,   0.0237761
      938.708,   0.0245167
      941.015,   0.0252611
      942.922,   0.0258821
      945.08,   0.0266299
      947.161,    0.027374
      949.334,    0.028124
      951.312,  0.0288733
      953.069,   0.0294991
      955.031,   0.0302543
      956.953,   0.0310078
      958.536,    0.03164
      960.336,    0.032402
      962.126,   0.0331216
      963.886,   0.0338853
      965.553,   0.0346532
      967.03,   0.0352935
      968.68,   0.0360649
      969.982,   0.0367084
      971.612,    0.037488
      972.835,   0.0381392
      974.428,   0.0389228
      975.615,   0.0395803
      977.001,   0.0403679
      978.219,   0.0410269
      979.556,   0.0418198
      980.732,   0.0424864
      982.089,    0.043288
      983.086,   0.0439644
      984.13,   0.0446408
```

Left column:

```
985.353,   0.045452
986.305,   0.0461314
987.358,   0.0468129
988.522,   0.0476392
989.437,   0.0483314
990.367,   0.0490275
991.243,   0.0497277
992.179,   0.0504299
993.087,   0.0511381
993.931,   0.0518532
 994.69,   0.0525735
995.477,   0.053294
996.424,   0.054024
997.166,   0.0547595
997.869,   0.0554983
998.667,   0.0562415
999.352,   0.0569968
  1000.,   0.0576058
1000.72,   0.0583702
 1001.3,   0.0591464
1001.87,   0.059768
1002.54,   0.0605556
1003.23,   0.0613511
1003.73,   0.0619956
1004.24,   0.0626466
1004.84,   0.0634729
1005.34,   0.0641424
1005.76,   0.0648182
1006.31,   0.0656735
1006.63,   0.0663718
1006.97,   0.067079
1007.37,   0.067792
1007.69,   0.0685184
1007.92,   0.0692597
 1008.1,   0.07001
1008.32,   0.0705787
1008.37,   0.0713515
1008.45,   0.0721353
*Material, name=HR_88
*Damage Initiation, criterion=DUCTILE
0.0845348,    0.,     0.
0.0727598,    0.1,    0.
0.0626249,    0.2,    0.
0.0539017,    0.3,    0.
0.0512729, 0.333333,     0.
0.0463937,    0.4,    0.
0.0399314,    0.5,    0.
0.0343693,    0.6,    0.
0.0295819,    0.7,    0.
0.0254614,    0.8,    0.
0.0219148,    0.9,    0.
0.0188623,    1.,     0.
0.0162349,    1.1,    0.
0.0139735,    1.2,    0.
0.0120271,    1.3,    0.
0.0103518,    1.4,    0.
0.0089099,    1.5,    0.
0.00766882,   1.6,    0.
```

Right column:

```
0.00660062,    1.7,    0.
0.0056812,     1.8,    0.
0.00488986,    1.9,    0.
0.00420874,    2.,     0.
*Damage Evolution, type=DISPLACEMENT,
   degradation=MULTIPLICATIVE
0.4,
*Damage Initiation, criterion=SHEAR, ks=0.2
0.0512, 1.732,   0.
*Damage Evolution, type=DISPLACEMENT,
   degradation=MULTIPLICATIVE,
   softening=EXPONENTIAL
0.25,1.
*Density
7.83e-09,
*Elastic
216582., 0.3
*Plastic
827.138,        0.
828.539, 0.000512729
831.394, 0.00102546
831.192, 0.00153819
835.378, 0.00205092
835.118, 0.00256365
837.54, 0.00307638
841.295, 0.0035891
845.16, 0.00410183
857.435, 0.00461456
859.186, 0.00512729
860.088, 0.00564002
861.003, 0.00615275
862.574, 0.00666548
863.704, 0.00717821
865.463, 0.00769094
866.659, 0.00820367
868.396, 0.0087164
870.155, 0.00922913
871.913, 0.00974186
872.935, 0.0102546
874.652, 0.0107673
875.701,   0.01128
877.242, 0.0117928
878.757, 0.0123055
880.134, 0.0128182
881.368, 0.013331
882.706, 0.0138437
884.19, 0.0143564
885.59, 0.0148691
887.565, 0.0153819
889.25, 0.0158946
891.01, 0.0164073
892.696, 0.0169201
893.961, 0.0174328
897.009, 0.0179455
901.197, 0.0184583
903.799, 0.018971
906.217, 0.0194837
908.035, 0.0199964
```

910.279,   0.0205092
912.144,   0.0210219
913.91,   0.0215346
915.676,   0.0220474
917.982,   0.0225601
919.745,   0.0230728
921.539,   0.0235855
923.282,   0.0240983
925.377,   0.024611
927.121,   0.0251237
928.745,   0.0256365
930.499,   0.0261492
932.163,   0.0266619
934.201,   0.0271747
935.81,   0.0276874
937.318,   0.0282001
938.922,   0.0287128
940.446,   0.0292256
942.361,   0.0297383
943.875,   0.030251
945.302,   0.0307638
946.784,   0.0312765
948.555,   0.0317892
949.927,   0.0323019
951.396,   0.0328147
952.716,   0.0333274
953.979,   0.0338401
955.604,   0.0343529
956.89,   0.0348656
958.18,   0.0353783
959.445,   0.0358911
960.935,   0.0364038
962.207,   0.0369165
963.357,   0.0374292
964.493,   0.037942
965.938,   0.0384547
966.974,   0.0389674
968.092,   0.0394802
969.195,   0.0399929
970.13,   0.0405056
971.407,   0.0410183
972.445,   0.0415311
973.442,   0.0420438
974.387,   0.0425565
975.52,   0.0430693
976.48,   0.043582
977.257,   0.0440947
978.331,   0.0446074
979.179,   0.0451202
979.931,   0.0456329
980.947,   0.0461456
981.668,   0.0466584
982.508,   0.0471711
983.274,   0.0476838
984.059,   0.0481966
984.611,   0.0487093
985.439,   0.049222
986.145,   0.0497347

986.803,   0.0502475
987.369,   0.0507602
*Material, name=HV_109
*Damage Initiation, criterion=DUCTILE
0.0920667,   0.,   0.
0.0792425,   0.1,   0.
0.0682047,   0.2,   0.
0.0587043,   0.3,   0.
0.0558413, 0.333333,   0.
0.0505273,   0.4,   0.
0.0434892,   0.5,   0.
0.0374315,   0.6,   0.
0.0322176,   0.7,   0.
0.02773,   0.8,   0.
0.0238674,   0.9,   0.
0.0205429,   1.,   0.
0.0176814,   1.1,   0.
0.0152185,   1.2,   0.
0.0130987,   1.3,   0.
0.0112742,   1.4,   0.
0.00970376,   1.5,   0.
0.0083521,   1.6,   0.
0.00718872,   1.7,   0.
0.00618739,   1.8,   0.
0.00532554,   1.9,   0.
0.00458373,   2.,   0.
*Damage Evolution, type=DISPLACEMENT,
degradation=MULTIPLICATIVE
0.4,
*Damage Initiation, criterion=SHEAR, ks=0.2
0.05, 1.732,   0.
*Damage Evolution, type=DISPLACEMENT,
degradation=MULTIPLICATIVE,
softening=EXPONENTIAL
0.3, 0.7
*Density
7.83e-09,
*Elastic
212610., 0.3
*Plastic
972.179,   0.
976.45, 0.000555524
980.624, 0.00111447
985.509,   0.0016739
987.471,   0.0022328
990.626, 0.00278971
995.532, 0.00333368
1008.58, 0.00383788
1010.25,   0.0044387
1011.4,   0.00489444
1012.95,   0.00548455
1014.43,   0.00605586
1015.97,   0.00660927
1017.57,   0.00714877
1019.49,   0.00781715
1021.16,   0.00834673
1022.78,   0.00887678
1024.44,   0.00940438

1026.1,	0.00993086	1107.56,	0.0423927
1028.13,	0.0105902	1108.26,	0.0428505
1029.72,	0.0111125	1109.07,	0.043466
1031.36,	0.011633	1109.95,	0.0440846
1032.91,	0.0121566	1110.55,	0.0445567
1034.99,	0.0128083	1111.34,	0.0451899
1036.62,	0.0133253	1111.93,	0.0456682
1038.2,	0.0138455	1112.71,	0.0463175
1040.29,	0.0144907	1113.27,	0.0468156
1041.96,	0.0150067	1113.83,	0.0473155
1043.53,	0.0155209	1114.53,	0.0479926
1045.58,	0.0161678	1115.06,	0.0485088
1047.14,	0.0166813	1115.58,	0.049033
1048.69,	0.0171973	1116.03,	0.0495642
1050.71,	0.0178382	1116.52,	0.0501067
1052.29,	0.0183538	1117.07,	0.0506625
1053.87,	0.0188713	1117.49,	0.0512316
1055.8,	0.0195154	1117.85,	0.0518083
1057.44,	0.0200317	1118.27,	0.052401
1058.98,	0.0205499	1118.59,	0.0530066
1060.89,	0.021194	1118.76,	0.0534202
1062.39,	0.0217092	1119.03,	0.0540534
1063.88,	0.0222244	1119.24,	0.0547066
1065.7,	0.022873	1119.34,	0.0551527
1067.21,	0.0233911	1119.41,	0.0558413
1068.59,	0.02391		
1070.34,	0.0245575		
1071.8,	0.0250791		
1073.12,	0.0255973		
1074.51,	0.0261202		
1076.24,	0.0267746		
1077.65,	0.0272984		
1078.94,	0.0278281		
1080.26,	0.0283553		
1081.95,	0.0290181		
1083.1,	0.0295498		
1084.4,	0.0300794		
1085.64,	0.0306166		
1086.81,	0.0311509		
1088.31,	0.0318223		
1089.49,	0.0323633		
1090.6,	0.0328676		
1091.69,	0.033406		
1092.83,	0.0339516		
1094.,	0.0345023		
1095.2,	0.035128		
1096.11,	0.035606		
1097.21,	0.0361599		
1098.22,	0.0367205		
1099.26,	0.0372835		
1100.38,	0.0378504		
1101.3,	0.038425		
1102.27,	0.0390016		
1103.22,	0.0395815		
1104.2,	0.0401635		
1105.14,	0.0407518		
1105.86,	0.0411912		
1106.65,	0.041794		